Université de Montréal

Développement d'une nouvelle méthode par échographie musculosquelettique à la détermination de la cinématique intervertébrale lombaire et application au complexe articulaire de l'épaule

Development of a new musculoskeletal ultrasound method for determining lumbar intervertebral kinematics and its application for the shoulder joint complex

Par Mohammad Reza Effatparvar

Programme en sciences biomédicales

Faculté de médecine

en extension à l'Université du Québec à Trois-Rivières

Thèse présentée

en vue de l'obtention du grade de Philosophiae Doctor (Ph.D.)

en sciences biomédicales

Septembre 2025

Université de Montréal

Département d'anatomie, Université du Québec à Trois-Rivières

Cette thèse intitulée

Développement d'une nouvelle méthode par échographie musculosquelettique à la détermination de la cinématique intervertébrale lombaire et application au complexe articulaire de l'épaule

Présentée par

Mohammad Reza Effatparvar

A été évaluée par un jury composé des personnes suivantes

Guillaume Desroches
Président-rapporteur

Stéphane Sobczak
Directeur de recherche

Felipe Verdugo Ulloa
Membre du jury

Florent Moissenet
Examinateur externe

Résumé

La détermination précise de la cinématique 3D de la colonne lombaire est essentielle pour le diagnostic des restrictions de mouvements et de l'instabilité vertébrale, ainsi que pour l'élaboration de stratégies de réadaptation efficaces. Les modalités d'imagerie conventionnelles telles que la tomodensitométrie (CT) et l'imagerie par résonance magnétique (IRM) permettent une analyse anatomique et cinématique précise, mais présentent certaines limites, notamment l'exposition aux rayonnements ionisants, un coût élevé et une applicabilité restreinte pour les évaluations dynamiques in-vivo. À l'inverse, l'imagerie par ultrasons constitue une alternative non ionisante, plus économique et de plus en plus accessible, bien que son application à l'analyse cinématique rachidienne soit restée limitée en raison de défis techniques.

Cette thèse examine le développement, la faisabilité et la validation d'une méthode basée sur l'échographie pour la reconstruction 3D et la mesure de la cinématique articulaire. Bien que développée principalement pour la colonne lombaire, la faisabilité de cette méthode a également été testée sur le complexe articulaire de l'épaule afin de démontrer son potentiel d'application à d'autres articulations. La thèse débute par (1) une revue systématique de la littérature, dans laquelle 183 articles ont été examinés et seulement 9 répondaient aux critères d'inclusion, chacun rapportant des résultats cinématiques partiels (flexion-extension, rotation axiale ou déplacements linéaires). Les études ne rapportaient pas d'évaluations cinématiques 3D ce qui a mis en évidence la nécessité de développements supplémentaires dans ce domaine.

Pour combler cette lacune, (2) un nouvel algorithme de reconstruction 3D à partir d'images échographiques a été développé et validé sur six colonnes lombaires cadavériques (T12–S2) dont les tissus mous ont été conservés. Les reconstructions ont été comparées à des modèles cinématiques obtenues par CT-Scan, et la fidélité intra-opérateur a été évaluée en répétant l'ensemble du processus de segmentation et de reconstruction trois fois chez deux spécimens. Les résultats ont montré une excellente fidélité (ICC = 0,966 ± 0,014 pour le CT-Scan et ICC = 0,930 ± 0,012 pour l'échographie) et une faible erreur moyenne de reconstruction entre les spécimens (0.23 ± 0.17). Toutes les différences se situaient dans les limites d'accord (Bland & Altman). L'effet de l'épaisseur du paquet adipeux postérieur

sur l'erreur de reconstruction a également été évalué et s'est avéré faible, indiquant la robustesse de la méthode face à la variabilité morphologique.

Sur la base de ce cadre validé, (3) une seconde étude in-vitro a été menée afin d'évaluer la capacité de la méthode à mesurer la cinématique intervertébrale discrète. Sept colonnes lombaires cadavériques (T12–S2) ont été isolées. Des marqueurs techniques (TMs) ont été fixés sur chaque vertèbre, imagés par échographie et CT-Scan (Gold standard), puis soumis à dix positions discrètes, comprenant quatre positions de flexion-extension, quatre positions d'inclinaison latérale (droite et gauche, en amplitudes partielle et complète), et deux positions de rotation axiale complète (droite et gauche). Des reconstructions 3D ont été générées et des systèmes de référence anatomiques (ARF) ont été définis pour calculer les amplitudes de mouvement intervertébrales à l'aide des angles d'Euler. La fidélité intra-opérateur est restée élevée (ICC 2,1 = 0,89 ± 0,01 pour l'échographie ; ICC = 0,91 ± 0,01 pour le CT) et la différence moyenne de ROM entre les modalités était de –0,23° ± 0,20° ($p = 0,57$), avec la majorité des valeurs dans les limites d'accord (95 %).

La quatrième phase de la thèse (4) a porté sur l'application in-vivo de la méthode développée. Cinquante-six participants en bonne santé, âgés de 20 à 60 ans et sans antécédent de lombalgie, ont été recrutés. Une sonde échographique suivie a été utilisée pour acquérir des images du mur postérieur de la colonne lombaire lors de la flexion complète et en position de rectitude. Les murs postérieurs des vertèbres L4, L5 et la partie postérieure du sacrum jusqu'à S2 ont été segmentés à partir des images échographiques afin de reconstruire des modèles 3D. Des repères anatomiques ont été définis et les ROM intervertébrales 3D ont été déterminées. Une excellente fidélité intra-observateur journalière (ICC 2,1 = 0,91 ± 0,02) et inter-journalière (ICC 2,1 = 0,92 ± 0,01) a été observée.

Des différences significatives liées à l'âge ont été relevées pour la flexion entre les groupes 20–30 et 40–50 ans (1,64 ± 2,12°, $p = 0,02$), 20–30 et 50–60 ans (2,17 ± 2,39°, $p = 0,00$), ainsi que 30–40 et 50–60 ans (1,70 ± 2,71°, $p = 0,21$). Pour la translation proximodistale, des différences significatives ont été observées entre les groupes 20–30 et 40–50 ans (0,44 ± 0,57 mm, $p = 0,03$), 20–30 et 50–60 ans (0,58 ± 0,65 mm, $p = 0,00$), et

30–40 et 50–60 ans (0,43 ± 0,78 mm, $p = 0,04$). Concernant la translation antéro-postérieure, des différences significatives ont été relevées entre les groupes 20–30 et 50–60 ans (0,92 ± 0,83 mm, $p = 0,00$) et 30–40 et 50–60 ans (0,66 ± 0,95 mm, $p = 0,00$). La flexion était fortement corrélée à la translation proximodistale ($\rho = 0,86$, $p = 0,00$) et à la translation antéro-postérieure ($\rho = 0,61$, $p = 0,00$). Aucune différence significative liée au sexe n'a été observée.

Enfin, pour évaluer la transférabilité de la méthode développée, une étude de faisabilité a été réalisé pour déterminer la cinématique de l'articulation de l'épaule et comparer les valeurs de ROM obtenues avec celles issues de modèles CT. Pour cela, une épaule humaine cadavérique a été isolée. Des TMs ont été fixés sur les segments osseux. Les os et les TMs ont été segmentés à partir d'images CT et échographiques pour générer des modèles 3D. L'épaule a été soumise à des mouvements discrets, et les TMs ont été numérisés. Les ARF ont été définis à partir de repères anatomiques obtenus par palpation virtuelle. La cinématique articulaire a été calculée et les ROM ont été rapportées en angles d'Euler. Les modèles 3D et les valeurs de ROM ont été comparés entre l'échographie et le CT. Le modèle 3D échographique a montré une erreur moyenne de reconstruction de 0,66 ± 0,06 mm par rapport au CT, indiquant des volumes légèrement plus importants pour les modèles échographiques. Les ROM issues de l'échographie étaient également légèrement surestimées (0,43 ± 0,72°) par rapport au CT. L'analyse de Bland–Altman a confirmé l'accord entre les deux méthodes. Malgré une légère surestimation par l'échographie, un fort accord a été observé pour les mesures de ROM, indiquant la possibilité d'extraire des données morphologiques adéquates et démontrant la faisabilité de l'utilisation de données échographiques pour la détermination de la cinématique de l'épaule.

En conclusion, cette thèse démontre que la reconstruction 3D basée sur l'échographie est une technique valide, fiable et pratique pour évaluer la cinématique intervertébrale lombaire et potentiellement celle d'autres articulations. La méthode développée a montré un fort accord avec les modèles par CT-Scan, une robustesse face aux variations des tissus mous et une applicabilité avérée en contexte cadavérique et in vivo. Avec l'intégration croissante de la segmentation basée sur l'intelligence artificielle, cette

méthode présente un fort potentiel pour des applications cliniques et de futures recherches nécessitant une analyse des mouvements rachidiens en temps réel et non invasive.

Mots-clés : Colonne lombaire, Cinématique intervertébrale, Reconstruction 3D, Imagerie par ultrasons, Validation in-vitro, Application in-vivo

Abstract

Accurate determination of lumbar spine 3D kinematics is essential for diagnosing motion restrictions and spinal instability, as well as for developing effective rehabilitation strategies. Conventional imaging modalities such as Computed Tomography (CT) and Magnetic Resonance Imaging (MRI) allow for precise anatomical and kinematic analysis but have limitations, including exposure to ionizing radiation, high cost, and restricted applicability for dynamic in-vivo assessments. In contrast, ultrasound imaging offers a non-ionizing, cost-effective, and increasingly accessible alternative, though its application in spinal kinematics has remained limited due to technical challenges.

This thesis investigates the development, validation and feasibility of an ultrasound-based method for 3D reconstruction and joint kinematic measurement. Although primarily developed for the lumbar spine, the method's feasibility has also been tested on the shoulder joint to demonstrate its potential for application to other joints. The thesis begins with (1) a systematic literature review, where 183 articles were screened and only 9 met the inclusion criteria, each reporting partial kinematic outcomes (flexion-extension, axial rotation, or linear displacements). None of the studies performed full 3D kinematic measurements, highlighting the need for further development in this field. To address this gap, (2) a novel ultrasound-based 3D reconstruction algorithm was developed and validated on six cadaveric lumbar spines (T12-S2) with preserved soft tissues. The reconstructions were compared to CT-derived models, and intra-operator reliability was evaluated by repeating the entire segmentation and reconstruction pipeline three times for two specimens. The results showed excellent reliability (ICC = 0.966 ± 0.014 for CT and ICC = 0.930 ± 0.012 for ultrasound) and low reconstruction errors across specimens (0.23 ± 0.17). All differences fell within the Bland–Altman limits of agreement. The effect of posterior fat pad thickness on reconstruction error was also evaluated and found to be weak, indicating the method's robustness across varying body types.

Building on this validated framework, (3) a second in-vitro study was conducted to evaluate the method's ability to measure discrete intervertebral kinematics. Seven cadaveric lumbar spines were isolated (T12-S2). Technical markers (TMs) were glued on each

vertebra, imaged with ultrasound and CT, and subjected to ten discrete movements including mid and full flexion, extension, right and left side bending and full right and left axial rotations. 3D reconstructions were generated, and anatomical reference frames (ARF) were defined to calculate intervertebral ROM using Euler angles. The intra-operator reliability remained high (ICC 2,1 = 0.89 ± 0.01 for ultrasound; ICC = 0.91 ± 0.01 for CT), and the mean ROM difference between modalities was –0.23° ± 0.20° (p = 0.57), with most values falling within the 95% limits of agreement, confirming measurement agreement.

The fourth phase of the thesis (4) focused on in-vivo application of the developed method. Fifty-six healthy participants with no low back pain aged between 20 to 60 were recruited. A tracked ultrasound probe was used to acquire images of the posterior aspect of the lumbar spine during full lumbar flexion and standing posture. The L4 to S2 vertebrae were segmented from ultrasound images to reconstructed 3D models. Anatomical reference frames were defined, and 3D intervertebral ROM were measured. Excellent within-day (ICC 2,1 = 0.91 ± 0.02) and between-day (ICC 2,1 = 0.92 ± 0.01) reliability was observed. Significant age-related differences were found in flexion between the 20–30 vs 40–50 age groups (1.64 ± 2.12°, $p = 0.02$), 20–30 vs 50–60 groups (2.17 ± 2.39°, $p = 0.001$), and 30–40 vs 50–60 groups (1.70 ± 2.71°, $p = 0.21$). Concerning proximodistal translation, significant differences were found between the 20–30 vs 40–50 groups (0.44 ± 0.57mm, $p = 0.03$), 20–30 vs 50–60 groups (0.58 ± 0.65mm, $p<0.01$, and 30–40 vs 50–60 groups (0.43 ± 0.78mm, $p = 0.04$). As for anteroposterior translation, significant differences were detected between the 20–30 vs 50–60 groups (0.92 ± 0.83mm, $p<0.01$ and between the 30–40 vs 50–60 groups (0.66 ± 0.95mm, $p < 0.01$). Furthermore, flexion was strongly correlated with proximodistal ($r_s = 0.86$, $p<0.01$) and anteroposterior ($r_s = 0.61$, $p = p<0.01$) translations. No significant differences were observed between sexes in any motion variable.

Finally, to evaluate the transferability of the developed method, a feasibility study was conducted to determine shoulder joint kinematics and compare the ROM values with those obtained using CT-based models. For this purpose, a shoulder was isolated from a human cadaver. TMs were affixed to the bony segments. Bones and TMs were segmented from CT and ultrasound images to generate 3D models. The shoulder underwent discrete

motions, and TMs were digitized. ARFs were defined from anatomical landmarks based on virtual palpation. Joint kinematics was calculated, and ROMs were reported as Euler angles. The 3D models and ROM values were compared between ultrasound and CT. The ultrasound 3D model showed a mean reconstruction error of 0.66±0.06 mm compared to the CT scan, indicating larger volumes for the ultrasound models. The ROMs from ultrasound were also slightly overestimated (0.43±0.72°) compared to CT-Scan. Bland-Altman analysis confirmed agreement between the two methods. Regardless of the slight overestimation for ultrasound, high agreement was observed for the ROM measurements between the two imaging methods. This agreement indicates the possibility of adequate morphological data extraction and highlights the feasibility of using ultrasound-based data for shoulder kinematic determination.

In conclusion, this thesis demonstrates that ultrasound-based 3D reconstruction is a valid, reliable, and practical technique for assessing intervertebral lumbar spine kinematics and may be for other joints. The developed method showed strong agreement in comparison to CT based model, was robust to soft tissue variations, and proved its applicability in both, cadaveric and in-vivo contexts. With the growing integration of artificial intelligence–based segmentation, this method holds strong potential for future clinical and research applications requiring real-time, non-invasive spine motion analysis.

Keywords: Lumbar spine, Intervertebral kinematics, 3D reconstruction, Ultrasound imaging, In-vitro validation, In-vivo application

Table of Contents

Table of Figures

List of Abbreviations

2D - Two-Dimensional

3D - Three-Dimensional

AL - Anatomical Landmark

ARF - Anatomical Reference Frame

BMI - Body Mass Index

CAM - Computer-Assisted Frame

CT - Computed Tomography

DICOM - Digital Imaging and Communications in Medicine

ISB - International Society of Biomechanics

LBP - Lower Back Pain

MRI - Magnetic Resonance Imaging

MSU - Musculoskeletal Ultrasound

ROM - Range of Motion

FE – Flexion and Extension

SB – Side Bending

AR – Axial Rotation

PD – Proximodistal

ML – Mediolateral

AP - Anteroposterior

TRF - Technical Reference Frame

TM – Technical Marker

SC - sternoclavicular

AC - acromioclavicular

GH - glenohumeral

PSIS - Posterior Superior Iliac Spines

MD – Mean Difference

SD – Standard Deviation

UP – Upper Limit

LL – Lower Limit

ICC – Intraclass Correlation Coefficients

MDC - Minimal Detectable Change

SCC - Spearman Correlation Coefficients

UQTR - Université du Québec à Trois-Rivières

FRQNT - Fonds de recherche du Québec—Nature et Technologie

NSERC - Natural Sciences and Engineering Research Council of Canada

Acknowledgement

First and foremost, I would like to express my deepest gratitude to my research supervisor, Professor Stéphane Sobczak. His unwavering support, insightful guidance, and continuous encouragement throughout my doctoral journey have been instrumental in shaping both my academic path and professional growth. I am sincerely thankful for the trust he placed in me and the freedom he allowed in pursuing my ideas.

I would also like to acknowledge the contributions of my collaborators and the members of the research team. Their input, technical assistance, and collaboration have significantly enriched the quality of this project. Special thanks go to my dear friends, Marc-Olivier Saint-Pierre and Félix-Antoine Lavoie, for their warm welcome to the laboratory, their invaluable assistance in data collection, their guidance in deepening my understanding of the project, and their thoughtful contributions to revising the article, as well as to Hugo Lacombe, a young student of remarkable intelligence and capability, whose work in creating the kinematic measurement interface greatly accelerated the progress of this research.

I extend my sincere appreciation to the individuals who generously donated their bodies to science. Their contribution made the in-vitro component of this study possible, and their gesture is recognized with the utmost respect.

A special thank you goes to my wife, Sanaz, whose love, patience, and strength have been the foundation of my perseverance. Her infinite support and understanding during the most challenging moments have been beyond words. This thesis would not have been possible without her presence and belief in me.

Lastly, I would like to thank my daughter, Deniz. Her arrival into our lives brought not only joy but an incredible source of energy, purpose, and inspiration. Though she is too young to read this, her mere presence filled my heart with hope and gave me the strength to keep going when I needed it the most. This thesis is, in part, for her future.

Introduction

The accurate assessment of lumbar spine kinematics is fundamental to understanding how mobility restrictions emerge and evolve, particularly with age or musculoskeletal dysfunctions. Segmental motion of the spine plays a critical role in daily movements such as bending, lifting, and walking, and alterations in intervertebral kinematics are often among the first biomechanical indicators of reduced functional capacity (Lin et al., 2020). Reliable and accessible methods for evaluating such motion are therefore essential for clinical diagnostics, rehabilitation planning, and biomechanical research (Breen & Breen, 2018).

Several methods have been developed to assess spinal motion, ranging from manual clinical tests and motion capture systems to advanced imaging techniques. Manual assessments are commonly used in clinical practice but are limited by their subjective nature and inability to capture vertebral-level motion in three dimensions (3D) (Roach et al., 2013). Optical motion capture systems offer high precision in whole-body kinematics but rely on skin-mounted markers, which are prone to soft tissue artefacts (Heneghan & Balanos, 2010). To reduce these artefacts, some experimental studies have attached motion-capture markers to intracortical bone pins inserted directly into the vertebrae or adjacent bones, providing a more accurate representation of skeletal motion; however, the invasive nature of this approach renders it unsuitable for routine clinical or large-scale in-vivo applications (Cuesta-Vargas, 2015). Surface-based methods such as rasterstereography estimate spinal posture and curvature from back-surface topography and provide radiation-free assessments of global spinal alignment (Mohokum et al., 2015). However, because the spine is reconstructed indirectly from surface geometry and model-based assumptions, these techniques mainly describe overall posture and deformity and only approximate individual vertebral motion, offering limited access to true intervertebral kinematics (Betsch et al., 2013). In parallel, wearable systems using inertial measurement units or magneto-inertial sensors enable out-of-laboratory monitoring of trunk and spinal motion during daily activities, including walking and sports tasks (Papi et al., 2017). Nonetheless, their accuracy remains constrained by soft-tissue artefacts, sensor movement

relative to the underlying bone, magnetic disturbances and drift, and the difficulty of resolving motion at the level of individual vertebrae rather than larger trunk segments (Agostini et al., 2017).

Medical imaging has long served as the standard method for evaluating intervertebral motion. Conventional radiographs and fluoroscopy allow for the capture of spinal movements but remain confined to two-dimensional (2D) evaluations and expose patients to ionizing radiation (Pearson et al., 2011). Computed tomography (CT) and magnetic resonance imaging (MRI) enable high-resolution 3D reconstruction of vertebral segments; however, CT also involves radiation exposure, and MRI is often costly, time-consuming, and restricted to static, supine imaging (Daniel et al., 2023). More recently, biplanar radiography systems have offered a compromise, allowing a 3D measurement in standing posture (Melhem et al., 2016). Nonetheless, accessibility remains limited, and it still involves radiation exposure.

Ultrasound imaging has emerged as a non-ionizing, cost-effective, and portable alternative. Its potential has already been demonstrated in various musculoskeletal contexts, including fracture assessment (Wu et al., 2021b), joint navigation (Mhaskar et al., 2023), and surgical guidance (Dixon et al., 2022). Beyond bone-focused applications, major developments have also concerned musculotendinous structures, where ultrasound is widely used to quantify muscle architecture (e.g., fascicle length, pennation angle) and tendon mechanical properties, including with elastography, thereby supporting diagnosis, monitoring, and biomechanical analysis of muscle–tendon function (Drakonaki, 2012; Leitner et al., 2019; Van Hooren et al., 2020). This imaging method has also been used for spine kinematics determination. However, all the applications so far have remained limited to 2D measurements and fail to capture the full complexity of intervertebral motion. The primary reason for this limitation is the lack of validated 3D reconstruction techniques tailored to the spine.

Recent developments in ultrasound imaging, have made it possible to generate 3D bone models from sequential 2D images (Forbes et al., 2021). These approaches could provide a framework for establishing anatomical reference frames directly on vertebrae, thereby enabling 3D kinematic analysis. Despite these promising prospective, the

application of 3D ultrasound-based kinematic analysis of lumbar spine motion has not been previously documented in the literature. There remains a critical gap in both the methodological validation of ultrasound-based reconstruction and its application to real human movement. Addressing this gap could offer a non-ionizing, more accessible, and dynamic alternative to conventional imaging for spinal mobility evaluation, particularly valuable in contexts that require frequent or radiation-free monitoring.

The overarching objective of this thesis was to develop, validate, and apply an ultrasound-based method for determining 3D intervertebral kinematics of the lumbar spine. Through a series of in-vitro and in-vivo studies, this work aimed to establish the feasibility, reliability, and clinical utility of ultrasound imaging for assessing spinal motion.

This thesis has been structured around five main objectives:

- (1) Systematic Review: Reviewing the literature on ultrasound-based spinal motion analysis to identify methodological gaps and evaluate the current limitations preventing clinical adoption.
- (2) Development: Developing an algorithm for 3D reconstruction of ultrasound images and validating it against 3D reconstructions generated from CT images.
- 3) In-vitro Validation: Applying the developed ultrasound-based 3D reconstruction technique to measure the 3D kinematics of the entire lumbar spine and validating the kinematic outputs against CT-based ground truth data.
- (4) In-vivo Application: Applying the validated method in a human participant study to evaluate intervertebral range of motion (ROM) at L4–S1 during lumbar flexion, examining age-related changes and assessing measurement reliability.
- (5) Transferability of the method: Assessing the feasibility of applying the developed approach to the shoulder joint complex to determine 3D kinematics and to compare these results with those obtained from CT scans.

Based on these objectives, chapter 1 provides a comprehensive review of the relevant literature and introduces the general methodology applied throughout the thesis. It covers anatomical considerations, conventional and alternative imaging modalities, and the technical challenges in determining spine kinematics.

Chapter 2 reports the results of a systematic review that reveals the absence of validated 3D ultrasound methods for intervertebral motion analysis, highlighting the need for new imaging pipelines and reconstruction strategies.

Chapter 3 describes the development of a in-vitro 3D ultrasound-based reconstruction algorithm. This includes imaging and manual segmentation and comparing the 3D models with the CT-derived models to assess accuracy in surface geometry.

Chapter 4 presents in-vitro kinematic results under controlled motion conditions. Intervertebral ROM in flexion-extension, side bending, and axial rotation were quantified using ultrasound-based models and validated against CT. Agreement analyses, including Bland–Altman plots and intraclass correlation coefficients, were used to quantify the method's validity and reliability, respectively.

Chapter 5 shifts to the in-vivo application. Lumbar spine motion (L4–S1) was measured during voluntary lumbar flexion in a cohort of healthy adults aged 20 to 60 years. The data were used to analyze age-related and sex-related differences in intervertebral mobility and to evaluate within- and between days reliability. Additionally, correlations between primary and coupled motions were assessed to confirm biomechanical consistency.

Finally, Chapter 6 presents a feasibility study on the transfer of the developed method to the shoulder joint complex. The kinematics of the entire shoulder complex were determined using both ultrasound and CT images. Reconstruction errors and agreement analyses between the two imaging modalities were conducted to evaluate the transferability of the kinematic measurement method to other joints.

In summary, this thesis introduces a novel methodology for determining lumbar spine 3D intervertebral kinematics using ultrasound imaging. It validated a practical method for mobility assessment that could complement or eventually replace more invasive and expensive imaging systems in both clinical and research settings.

Chapter 1 – Litterature review

This literature review is divided into three sections. The first section discusses the available techniques and tools for measuring joint kinematics, as well as the mathematical approaches used to represent them. The second section focuses on the lumbar spine, detailing its anatomy, range of motion, and the significance of its kinematic assessment. The third section explores ultrasound imaging, highlighting its applications, advantages, and potential for kinematic measurement. Finally, the hypotheses and objectives of this thesis are presented in detail.

1.1 Joint kinematic determination

Kinematics, as a branch of mechanics, is the study of the motion of an object without considering the factor of force or physical properties. From the mathematical point of view, analyzing the motion of an object requires associating it with a reference frame (Vladimir, 1988). In joint motion assessment, one of the main approaches is to establish such reference frames based on anatomical landmarks on the joint components (Severijns et al., 2021). To this end, anatomical landmarks must be determined on the components, and once the reference frame is established, the motion is expressed using various mathematical methods (Wu & Cavanagh, 1995). However, identifying anatomical markers of a joint components is a challenging step in kinematic assessment due to the lack of direct physical or visual access. In this regard, there are advanced techniques to identify anatomical landmarks and establish reference frames for precise kinematic analysis. These measurement methods can be categorized into two groups based on how the anatomical landmarks are defined, a process known as palpation. Physical palpation involves direct manual identification and placement of physical markers on the region of interest, while virtual palpation uses digital tools, to place virtual markers on the images. Accordingly, kinematic measurement methods are divided into two approaches: motion capture systems that rely on physical markers and medical imaging techniques that often use virtual markers for precise analysis.

1.1.1 Measurement methods

Motion capture

Motion capture systems are a widely used method in biomechanical studies to precisely track the motion of a moving object and represent it in three-dimensional space. In the application of motion capturing (Errabity et al., 2023), passive reflective markers or actively emitting LEDs are strategically attached to specific anatomical landmarks on the subject's body, often the skin overlying critical joints or bones. These markers are then tracked by a series of cameras (or signal receivers in non-optical methods) positioned around the area of study. These cameras capture the spatial position and movement of the markers in three dimensions, and specialized software processes this data to construct a dynamic model of the subject's movement. This setup allows for precise tracking and analysis of complex motions. These systems offer versatile applications across various types of biomechanical studies, from broad analyses to more specific investigations.

More recently, markerless motion capture techniques have been developed as an alternative approach. Instead of relying on physical markers, these systems use advanced computer vision algorithms and machine learning to track body segments directly from video images (Wren et al., 2023). By extracting kinematic data from standard or depth cameras, markerless systems reduce setup time and would eliminate issues such as marker displacement, skin artifacts, or subject discomfort. This method has shown promising results for full gait kinematics applications (Steffensen et al., 2023). However, their performance remains inconsistent, as studies have reported modest-to-poor validity and reliability for joint kinematics, limiting their applicability in clinical settings (Ma et al., 2019).

Medical imaging

Medical imaging serves as an invaluable tool in biomechanics, offering a method to visualize and analyze the structures and movements of the human body. This technology is particularly significant for kinematic determination, providing insights that cannot be achieved through direct observation or external measurement techniques. As quantitative benchmarks, dual-fluoroscopic/DBR systems validated with 2D–3D shape-matching

report mean accuracy < 0.35 mm in translation and repeatability < 0.43 mm and < 0.65° in vivo; quantitative fluoroscopy (QF) shows translation accuracy around 0.1–2.2 mm with moderate-to-substantial reliability (e.g., ICCs ~0.62–0.99 depending on parameter), and inter-/intra-subject repeatability has been demonstrated across L2–S1 (Kai & Qun, 2011).

Based on the context of this research, medical imaging modalities can be classified into two main groups: 2D and 3D modalities. This classification is crucial because the number of anatomical landmarks that can be selected depends on the dimensionality of the images (Effatparvar & Sobczak, 2022). In other words, modalities that provide only 2D images do not supply sufficient morphological data for building reference frames, which are essential for the 3D determination of joint movement (Xu et al., 2024). In the application of medical imaging for kinematics, once visual access to the morphological data is established, anatomical landmarks can be virtually palpated, facilitated by image processing techniques (Dugailly et al., 2011). Understanding the distinctions between these modalities, along with their specific applications and limitations, is beneficial for a comprehensive grasp of their roles in kinematic studies.

Radiography, a fundamental method utilizing X-ray technology, is effective in revealing the detailed geometries of bones, making it particularly useful for examining the spine. The radiographic process involves directing X-ray beams through the body in one direction, which provides a flat representation of the subject being imaged, showing only height and width dimensions (2D) (Raastad et al., 2015). Using this technique, discrete intervertebral displacements can be defined by capturing X-ray images of the region of interest and identifying two anatomical landmarks for recording angular or distance changes. Studies report substantial reliability for intervertebral rotation and finite centre of rotation (FCR) , with ICCs often in the moderate-to-substantial range and typical FCR precision of ~0.3–0.4 mm (fixed-centre conditions) (Breen & Breen, 2016).

Fluoroscopy, another 2D medical imaging technique, employs X-rays to create real-time, continuous imaging, allowing for the observation of joint movements and functions. When used as DBR (two views with 2D–3D registration), vertebra-level accuracy on the lumbar spine reaches sub-millimetre translations and < 1° rotations,

providing a practical ground truth for validation despite radiation/logistical constraints (Kai & Qun, 2011).

Both radiography and fluoroscopy are limited to 2D applications and pose significant concerns regarding exposure to ionizing radiation. Although the dose per second is generally lower for fluoroscopy compared to radiography, fluoroscopy can involve longer exposure times, especially during extended procedures (Mahesh, 2001). This cumulative exposure can increase the risk of radiation-induced effects for both patients and healthcare personnel (Stahl et al., 2016). Additionally, both radiography and fluoroscopy face challenges such as image distortion caused by the divergence of the radiographic beam (West et al., 2003). This distortion can impact measurement precision and requires careful correction during the data processing stage to ensure accuracy.

Recent advancements in image processing techniques have led to the development of methods for creating 3D reconstructions from 2D imaging modalities (Maken & Gupta, 2023), such as stereophotogrammetry (Valstar et al., 2001) and biplanar EOS imaging (Melhem et al., 2016). In both techniques, the third dimension is generated by superimposing images taken from different angles within the same coordinate system in space (Hosseinian & Arefi, 2015). Stereophotogrammetry involves capturing images from multiple perspectives, often requiring markers placed on anatomical landmarks. This method is mostly used in in-vitro studies due to the more precision in marker placement, allowing for accurate 3D reconstructions of skeletal structures (Leardini et al., 2005). Biplanar EOS imaging utilizes low-dose X-rays captured simultaneously in two orthogonal planes (sagittal and coronal) (Rousseau et al., 2011). By combining these two sets of images, a 3D model of the anatomy can be created. However, these developed methods are still based on the application of x-ray which is ionizing and pose safety risks for both the operator and the subject. EOS reports very good reproducibility for spinal parameters (e.g., differences ≤ 0.54 mm for lengths and $\leq 0.33°$ for angles in phantom/validation work), supporting its use for low-dose 3D shape with acknowledged radiation exposure (Melhem et al., 2016).

Computed Tomography (CT), as a high-tech modality creates 3D reconstructed images of the skeletal system by taking series of X-ray images from different angles around

the body and then processing them by a computer to create cross-sectional images (Balasubramanya & Selvarajan, 2020). The ability of creating the cross-sectional images enable it to produce images in all three planes (axial, coronal, and sagittal). Despite its advanced imaging capabilities, CT does have limitations, particularly in spinal kinematic studies (Kim et al., 2020). For instance, scans are typically performed with the subject in a supine (lying down) position, which can be a limitation for studies requiring dynamic movements. Therefore, the application of the CT-scan in kinematics determination are limited to the discrete kinematics analysis by obtaining the images in different lying position, in-vivo studies (Song et al., 2021) or obtaining the images of the marker equipped specimen, in-vitro studies for visualization techniques (Dugailly et al., 2010). In addition, utilization of ionizing radiation is still a significant concern.

Magnetic Resonance Imaging (MRI) is another highly advanced imaging technology, unlike X-ray based methods, uses strong magnetic fields and radio waves to produce detailed and 3D images. However, similar to CT scan, MRI is also limited to static imaging and does not typically capture movement or provide real-time kinematic data (Tavana et al., 2023). Although recent advancements have led to the development of dynamic MRI techniques which could provide significant kinematics data (Michelini et al., 2018), MRI scanners are highly expensive and require specialized facilities, making them less accessible compared to other imaging modalities (Schultz et al., 2019).

Ultrasound imaging is a non-ionizing, portable modality that enables real-time visualization of superficial bony contours as well as musculotendinous structures. In the context of spinal assessment, it has mainly been used in 2D to track vertebral landmarks or segmental motion, with promising but still methodologically limited results. Because ultrasound is the central modality of this thesis, its physical principles, acquisition protocols, and current applications to spinal kinematics are presented in greater detail in Section 1.3.

1.1.2 Marker identification and reference frames

In 3D kinematic analysis techniques, images acquired using any of the aforementioned or other imaging methods must be reconstructed into 3D volumes to enable anatomical landmark selection. To support this process, the International Society of

Biomechanics (ISB) has provided standardized recommendations for anatomical landmark identification and reference frame definition for the entire body (Wu & Cavanagh, 1995; Wu et al., 2002). For instance, in a joint such as the shoulder, anatomical landmarks (ALs) for the scapula and humerus are typically identified through palpation or segmentation of prominent bony features, including the acromial angle, inferior angle, scapular spine, humeral head center, and the medial and lateral epicondyles of the humerus. Anatomical reference frames (ARFs) are then constructed following ISB guidelines. For the humerus, the Y-axis can be defined along the line connecting the medial and lateral epicondyles, the X-axis as perpendicular to the plane formed by the epicondyles and the humeral head center, and the Z-axis as the cross product of the X- and Y-axes. These anatomically based ARFs allow for a standardized description of joint kinematics in terms of relative rotations and translations.

Beyond purely anatomical frames, several other families of axes have been proposed in biomechanics. Geometric or inertial frames can be constructed from fitted primitives (e.g. cylinders or spheres) or from the principal axes of inertia of a bone or segment, providing mathematically well-conditioned axes that are less dependent on individual landmark selection (Conconi et al., 2021). Functional frames define joint axes directly from measured motion, for example through finite or instantaneous helical axis analysis or functional joint-centre identification, and are widely used for various joints (Camomilla et al., 2017). Finally, automatic and semi-automatic approaches have been developed to detect anatomical landmarks and construct reference frames directly from 3D medical images or statistical shape models, reducing manual palpation while preserving anatomical consistency (Brehler et al., 2019). In the present thesis, we rely primarily on anatomically defined ARFs, as they provide a direct link to clinical concepts and to existing ISB recommendations, while acknowledging that geometric, inertial, functional and automatic approaches constitute complementary frameworks with their own advantages and limitations.

1.1.3 Mathematical methods for motion representation

Theoretically, kinematics describes the geometry of motion through mathematical modeling of displacement, which defines the change in position of a point from its initial

to its final location, taking into account the direction of motion (Waldron & Schmiedeler, 2016). In this context, the Cartesian coordinate system serves as a mathematical framework that provides a straightforward and intuitive way to describe, analyze, and visualize motion.

Using this system, a point can be assigned specific coordinates within the global reference framework. The simplest form of displacement, translation in two dimensions, can be calculated by determining the differences between the coordinates of the final and initial positions (Wittenburg, 2016). To assess an object's motion, a specific point, such as the center of mass, should be used as a reference for calculating its translation within the Cartesian system (Alencastre-Miranda et al., 2006). However, an object's motion may be more complex than simple translation if it also involves rotation. In such cases, linear translation alone does not adequately capture the characteristics of the object's motion. Therefore, it becomes necessary to establish a new reference frame on the object to accurately interpret its rotational movements (Siciliano et al., 2009). From a mathematical perspective, determining the orientation of an object in space requires two reference frames to establish a common point of reference. The global reference frame is fixed in space, while the local reference frame is fixed to the object and moves with it (Waldron & Schmiedeler, 2016).

In biomechanics, when analyzing motion within a joint and between its components, the same principles should be followed to describe the motion numerically (Kecskemethy, 2011). In this process, anatomical reference frames (local reference frames) are established based on the mentioned methods, and mathematical techniques are then used to determine the orientation of these frames, thereby representing the movement of the joint components (Robertson et al., 2013).

Fundamentally, all mathematically and mechanically established methods for describing orientation can be applied to analyze the motion of anatomical reference frames (Flash et al., 2013) However, due to the complexity and specificity of motion within human joints, certain methods have been more widely adopted in this context which are as follows (Chèze, 2014):

- *Transformation Matrix*

The establishment of a matrix to describe the motion of a reference frame is based on the relative motion of a local frame with respect to a global frame. This method allows the definition of both linear translation and rotation in a unified manner (Weisstein, 2003). To define this matrix, it is first described in a 2D reference frame. When a local frame rotates within the global frame by an angle θ, if the initial coordinates of the x and y axes were: $x = \begin{bmatrix}1\\0\end{bmatrix}$, and $y = \begin{bmatrix}0\\1\end{bmatrix}$, after rotation, the new coordination will be: $x = \begin{bmatrix}cos\theta\\sin\theta\end{bmatrix}$, and $y = \begin{bmatrix}-sin\theta\\cos\theta\end{bmatrix}$. The combination of these two matrices yields the 2D rotation matrix: $[R] = \begin{bmatrix}cos\theta & -sin\theta\\sin\theta & cos\theta\end{bmatrix}$. This rotation matrix can be extended to describe any other types of rotations (Evans, 2001).

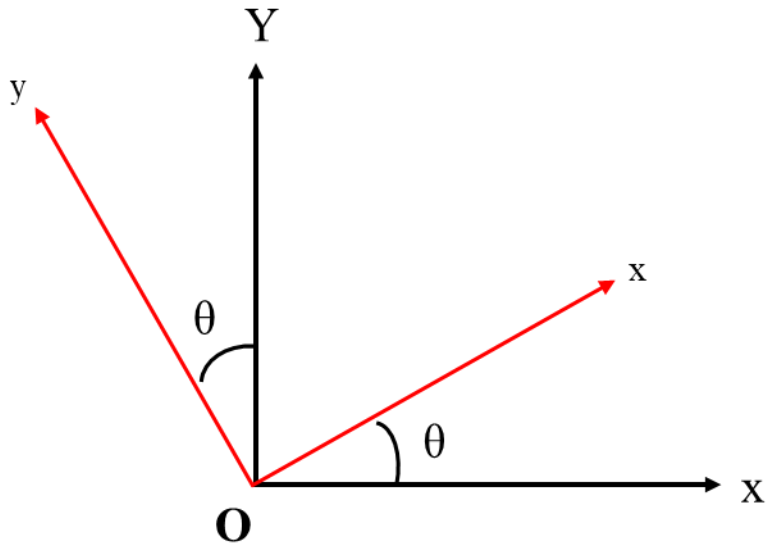

Figure 1. A 2D rotation of a local frame (red) around the global frame

If this frame also undergoes linear displacement by amounts u and v relative to its initial position, the resulting translation will be: $\begin{bmatrix}X\\Y\end{bmatrix} + \begin{bmatrix}u\\v\end{bmatrix}$ (Weisstein, 2003).

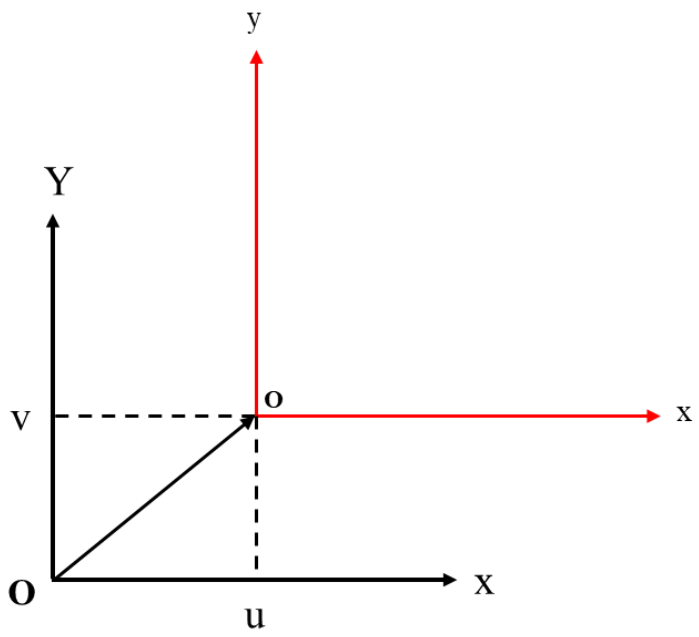

Figure 2. A 2D translation of a local frame (red) from the global frame

By combining these two types of motion into a single matrix, a transformation matrix can be established as: T= $\begin{bmatrix} cos\theta & -sin\theta & u \\ sin\theta & cos\theta & v \\ 0 & 0 & 1 \end{bmatrix} \begin{bmatrix} x \\ y \\ 1 \end{bmatrix}$. The third row in this matrix is added to maintain a square format for easier computations. However, since anatomical segments move in 3D, a third dimension must be incorporated into the matrix (Zagrevskiy & Zagrevskiy, 2016). This addition does not alter the fundamental concept of the system. In this method, if in Figure 8, O-XYZ represents the global coordinate system and o-xyz represents the local coordinate system, the local frame can move freely relative to the global frame. As previously explained, the motion of the local frame is described by both rotation and translation relative to the global frame (Gruber, 2000).

Regarding rotation, if the local frame rotates relative to the global frame without any translation, the axes of the local frame will form angles with the axes of the global frame (Evans, 2001). By considering a vector along each axis of the local frame, the cosine of these angles can be found by dividing the projection of the local axes on the global axes by the length of the vector (the axis of the local frame). For example, in Figure 1, the cosine of the angle between the Y-axis and the x-vector (x-axis) will be:

$$Cos\ Yx = Y/x \qquad (1)$$

And the coordinates of the x-vector on the Y-axis of the global frame will be:

$$Y = xCosYx \qquad (2)$$

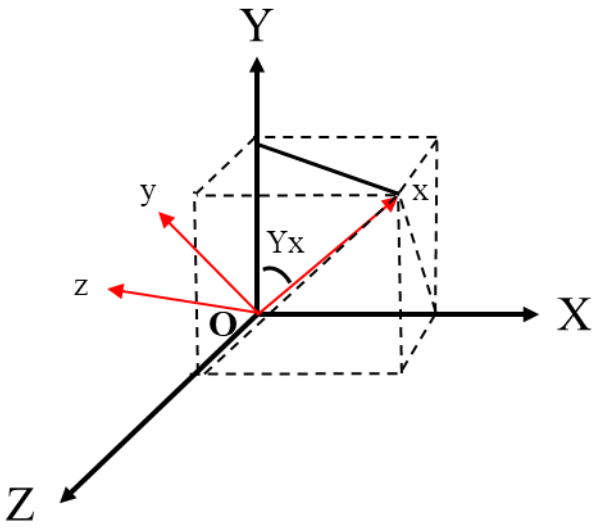

Figure 3. A 3D rotation of the local frame around the global frame

Additionally, since the angles between the axes of the local and global frames change with the amount of rotation of the local frame, equations (1) and (2) can be defined for all axes. By organizing these equations, they can be arranged into a matrix of (Evans, 2001):

$$\begin{bmatrix} X \\ Y \\ Z \end{bmatrix} = \begin{bmatrix} cosXx & cosXy & cosXz \\ cosYx & cosYy & cosYz \\ cosZx & cosZy & CosZz \end{bmatrix} \begin{bmatrix} x \\ y \\ z \end{bmatrix} \qquad (3)$$

In this equation, the matrix of cosines is referred to as the direction cosine matrix or the rotation matrix. Using this equation, the rotation of any local frame can be determined.

On the other hand, regarding translation, if the local frame translates relative to the global frame without any rotation, the vector L_G indicates the amount of translation and provides the coordinates of the local system within the global system as L_X, L_Y, and L_Z (Zatsiorsky, 2002).

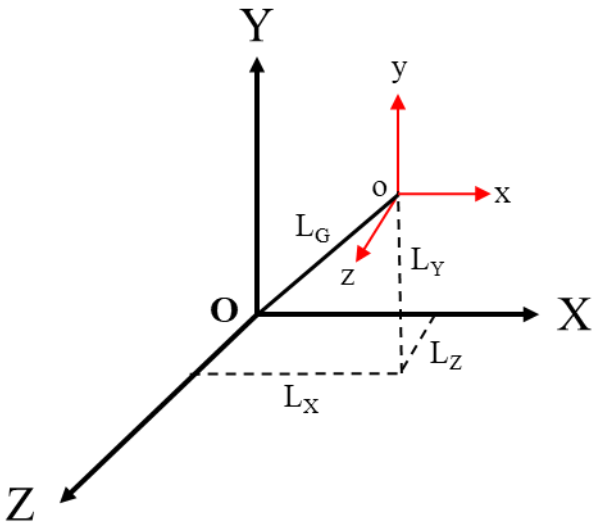

Figure 4. The location of a local frame in the global reference system after the translation

As mentioned previously, expressing the displacement of a local frame requires a combination of rotation and translation. In this context, the translation elements can be integrated into the rotation matrix to form a new 3×4 matrix. However, for mathematical convenience and to maintain a square matrix, a row (1,0,0,0) can be added to create a new translation-rotation matrix as shown in equation (4). This matrix is referred to as the position matrix or transformation matrix (Chèze, 2014).

$$[T] = \begin{bmatrix} 1 & 0 & 0 & 0 \\ Lx & cosXx & cosXy & cosXz \\ Ly & cosYx & cosYy & cosYz \\ Lz & cosZx & cosZy & cosZz \end{bmatrix} \quad (4)$$

Therefore, by rewriting equation (3) to include the translation, the spatial displacement of a local frame can be defined by equation (5):

$$\begin{bmatrix} 1 \\ X \\ Y \\ Z \end{bmatrix} = \begin{bmatrix} 1 & 0 & 0 & 0 \\ Lx & cosXx & cosXy & cosXz \\ Ly & cosYx & cosYy & cosYz \\ Lz & cosZx & cosZy & cosZz \end{bmatrix} \begin{bmatrix} 1 \\ x \\ y \\ z \end{bmatrix} \quad (5)$$

The application of the matrix method in joint motion, known as the orientation vector position, measures the displacement of an object from position 1 to position 2. For

example, in analyzing the shoulder joint, the simple displacement of the arm from the first position to the second can be quantified using the orientation position vector, which is essential for measuring the range of motion. In this context, if the global reference system is defined in the trunk and a local reference system is defined in the arm, with the initial position of the arm represented by a 4×4 matrix T1 and the final position by T2, the displacement between these two local frames is:

$$[T2] = [D12]\,[T1]$$

$$[D12] = [T1]\,[T2]^{-1}$$

- The Euler angles

Another way to describe the change in orientation of a local reference frame in space is by using a set of three angles, known as Euler angles, which represent its rotation around the global reference frame (Weisstein, 2009). In this method, the rotation of a local frame within the global system is determined by the magnitude and sequence of rotations around each axis of the global frame. The sequence of rotation alters the arrangement of the axes in the reference system, such as XYZ or XZY, resulting in different representations of the rotation matrix (Teu et al., 2005). The significance of the rotation sequence lies in its ability to indicate the arrangement of movement in an object or joint.

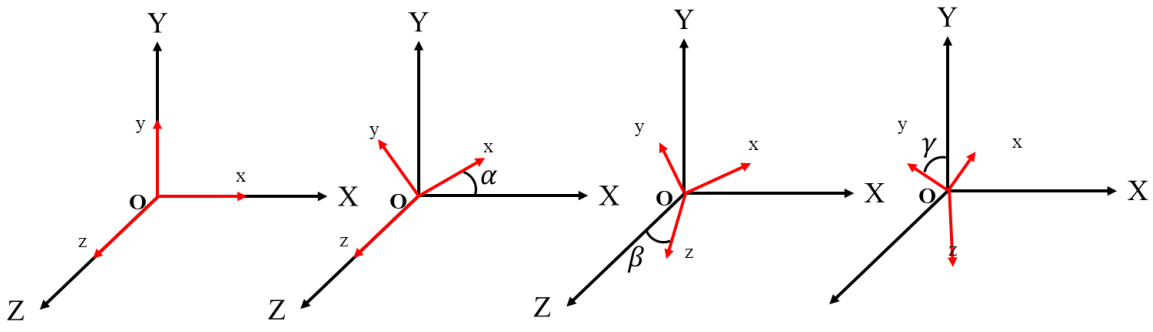

Figure 5. The rotation of a local frame relative to the global frame

Using the Euler method, only one attitude is defined, and it does not combine the translation and rotation, so they should be obtained separately. In this regard, still, using a

3×3 rotation matrix, the Euler angles could be arrayed and defined as a combination of rotations around each axis, as equation (6) (Slabaugh, 1999):

$$[R]=[R_Z][R_Y][R_X]$$

Therefore, the equation (6) could be rewritten as:

$$R = Rz(\gamma)Ry(\beta)Rx(\alpha)$$

$$= \begin{bmatrix} cos\,\gamma & -sin\,\gamma & 0 \\ sin\,\gamma & cos\,\gamma & 0 \\ 0 & 0 & 1 \end{bmatrix} \begin{bmatrix} cos\,\beta & 0 & sin\,\beta \\ 0 & 1 & 0 \\ -sin\,\beta & 0 & cos\,\beta \end{bmatrix} \begin{bmatrix} 1 & 0 & 0 \\ 0 & \cos\alpha & -sin\,\alpha \\ 0 & sin\,\alpha & \cos\alpha \end{bmatrix}$$

$$= \begin{bmatrix} cos\,\beta\,cos\,\gamma & sin\,\alpha\,sin\,\beta\,cos\,\gamma - cos\,\alpha\,sin\,\gamma & cos\,\alpha\,sin\,\beta\,cos\,\gamma + sin\,\alpha\,sin\,\gamma \\ cos\,\beta\,sin\,\gamma & sin\,\alpha\,sin\,\beta\,sin\,\gamma + cos\,\alpha\,cos\,\gamma & cos\,\alpha\,sin\,\beta\,sin\,\gamma - sin\,\alpha\,cos\,\gamma \\ -sin\,\beta & sin\,\alpha\,cos\,\beta & \cos\alpha\,cos\,\beta \end{bmatrix}$$

This equation simply could be replaced in the transformation matrix and be used for the spatial displacement of a local reference frame (Chèze, 2014).

- *The screw (Helical) method*

The screw method is another alternative to describe the spatial orientation of a joint by measuring the amount of rotation around and translation along the joint instantaneous axis of rotation (helical axis) (Chèze, 2014). In this method of displacement measurement, if an object moves from the position i to i+1 because of rotation (φ) and translation (L, magnitude of the translation along the helical axis), the displacement could be determined as (Ancillao, 2022):

$$d = L + d_R.$$

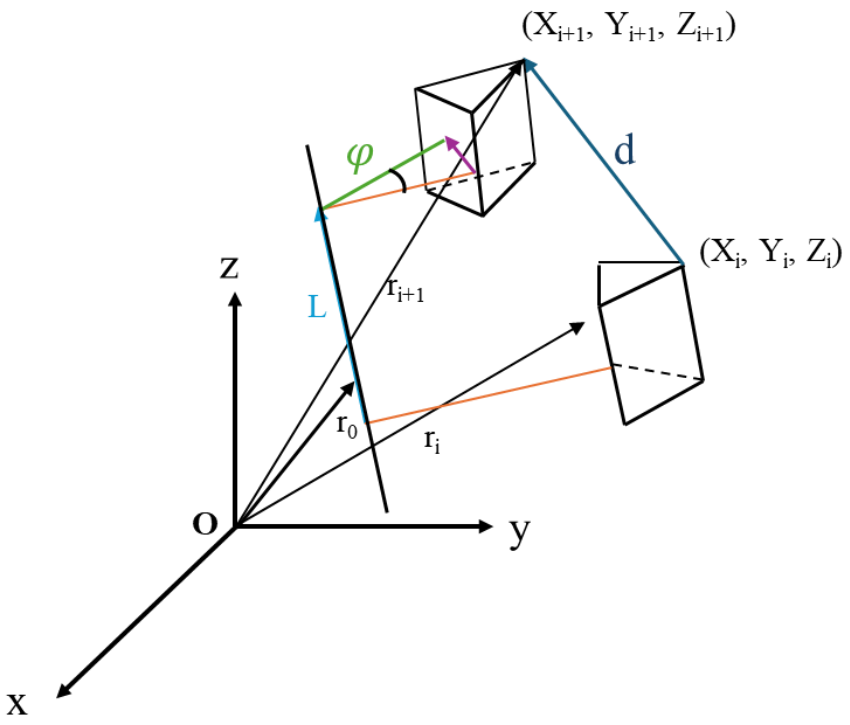

Figure 6. A schematic of screw method to describe rotation and translation

In this method, if the coordination of the helical axis is n_x, n_y, and n_z, the rotation matrix of the helical axis and the amount of φ is (Ancillao, 2022):

$$R_{helical} = \begin{bmatrix} e_0^2 + e_1^2 - e_2^2 - e_3^2 & 2(e_1e_2 + e_0e_3) & 2(e_1e_3 - e_0e_2) \\ 2(e_1e_2 - e_0e_3) & e_0^2 - e_1^2 + e_2^2 - e_3^2 & 2(e_2e_3 + e_0e_1) \\ 2(e_1e_3 + e_0e_2) & 2(e_2e_3 - e_0e_1) & e_0^2 - e_1^2 - e_2^2 + e_3^2 \end{bmatrix}$$

Where:

$$e_0 = \cos\left(\frac{\varphi}{2}\right), e_1 = n_x \sin\left(\frac{\varphi}{2}\right), e_2 = n_y \sin\left(\frac{\varphi}{2}\right), e_3 = n_z \sin\left(\frac{\varphi}{2}\right)$$

And if:

$$R_{helical} = \begin{bmatrix} r_{11} & r_{12} & r_{13} \\ r_{21} & r_{22} & r_{23} \\ r_{31} & r_{32} & r_{33} \end{bmatrix}$$

$$\varphi = sin^{-1}(\sqrt{(r_{32} - r_{23})^2} + (r_{13} - r_{31})^2 + (r_{21} - r_{12})^2/2)$$

- Grood and Suntay *(Joint coordinate system)*

The Joint Coordinate System (JCS) is a method for representing joint motion introduced by Grood and Suntay in 1983 (Grood & Suntay, 1983). This method is widely regarded in joint analysis, and a standard for its use has been recommended by the International Society of Biomechanics (Wu et al., 2002). In the JCS approach, in addition to the Cartesian coordinate system typically used for general motion analysis, a unique joint coordinate system must also be defined for each joint. When two objects form a joint, the JCS is represented by three vectors of e1 (a fixed vector aligned with the axis of rotation of the first object), e3 (a fixed vector aligned with the axis of rotation of the second object), and e2 (a floating vector in space, perpendicular to both e1 and e3) (Grood & Suntay, 1983).

For a joint like the knee, once the local coordinate systems are defined for each bone, the origins of these coordinate systems can be used to form the translation vector. Additionally, two of the axes from these local coordinate systems can serve as the joint coordinate system vectors (Grood & Suntay, 1983).

1.2 Lumbar spine

The lumbar spine encompasses the lower segment of the spinal column (lower back), extending from the last thoracic vertebra (T12) to the initial sacral vertebra (S1), and serves essential functions within the human body including (Bogduk, 2016; Ebraheim et al., 2004; Sassack & Carrier, 2023):

- supporting upper body by absorbing axial forces originating from the head, neck, upper limbs and trunk, aided by the larger lumbar vertebrae.
- protecting the spinal cord and nerves as safeguarding passageway promoting the transmission of information between the central nervous system and the lower extremities.
- facilitating a broad spectrum of trunk motions such as flexion, extension, rotation, and lateral bending.
- distributing upper body mass over the pelvis to support efficient bipedal motion by a concave curvature, known as lumbar lordosis.

This region consists of a combination of five vertebrae (L1-L5), intervertebral discs, ligaments, and muscles, with each of these components playing an important role in both the structure and function of the lumbar spine.

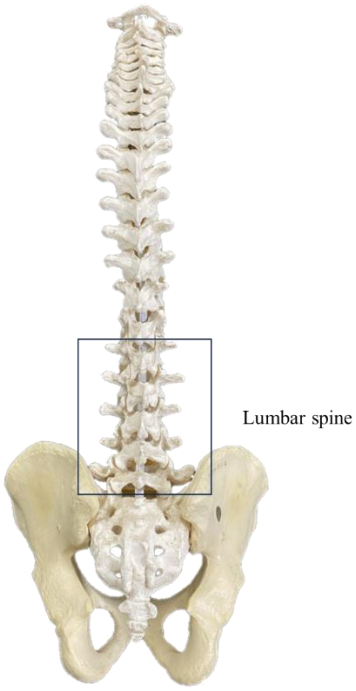

Figure 7. Human lumbar spine from posterior view

1.2.1 Vertebrae and articular surface geometry

Lumbar vertebrae possess the largest vertebral bodies among all spinal segments, increasing in size from L1 to L5. This size gradient reflects the lumbar spine's primary biomechanical role in supporting the upper body's weight and withstanding substantial axial and shear loads during various daily activities (DeSai et al., 2018; Mahadevan, 2018).

A typical lumbar vertebra consists of a large vertebral body, a vertebral arch, bilateral pedicles and laminae, lateral costiform (transverse) processes, and a relatively short, posteriorly projecting spinous process. Each vertebra also contains two superior and two inferior articular processes, which articulate to form the facet (zygapophyseal) joints. These joints serve to maintain vertebral alignment, limit excessive motion, and contribute to load sharing, particularly during flexion-extension and weight-bearing postures (Bogduk, 2016).

The articular surfaces of the lumbar facet joints exhibit specific geometric characteristics that guide intervertebral motion. In the upper lumbar spine (L1–L3), the facet joints are generally oriented in a sagittal plane, whereas in the lower lumbar spine (L4–L5), they adopt a more coronal orientation (Bogduk, 2016; Masharawi et al., 2004). These surfaces are typically trochoid in nature, cylindrical, allowing constrained rotational movement. This morphology facilitates predominantly flexion-extension, while limiting axial rotation and lateral bending (Adams & Dolan, 2005).

The shape and orientation of these joints directly influence the instantaneous axis of rotation, ROM, and overall spinal stability. Understanding these structural features is fundamental to biomechanical modeling and image-based kinematic analysis of the lumbar spine (Panjabi & White III, 1980).

The spinous processes project posteriorly and slightly downward from the vertebral arch and may overlap with adjacent levels depending on the segment. On each side, the costiform processes extend laterally and serve as attachment sites for various ligaments and muscles involved in spinal stability and movement (Mahadevan, 2018).

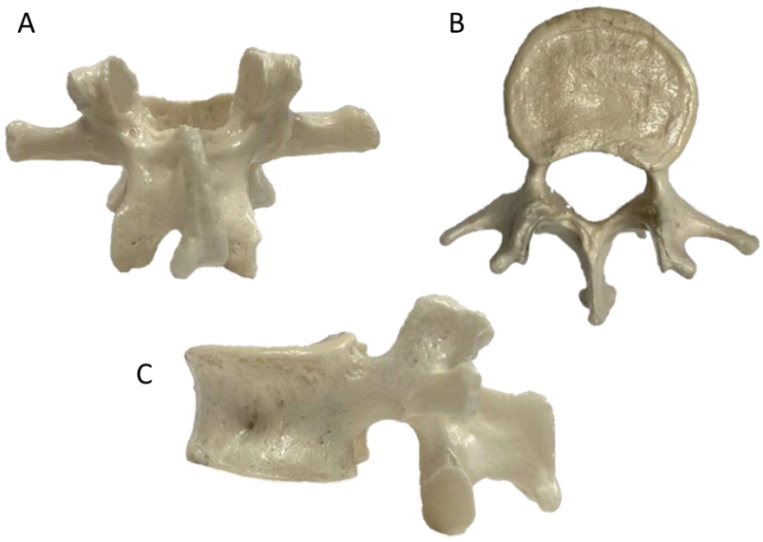

Figure 8. A typical lumbar vertebra
from three different views: posterior (A), superior (B), and lateral view (C)

1.2.2 Anatomical motions within the lumbar region

The lumbar spine is characterized by its capacity for various anatomical motions, including flexion, extension, lateral bending, and axial rotation (McGregor et al., 1995). Flexion involves the forward bending of the spine and rotation within the sagittal plane, reducing the angle between the vertebrae anteriorly (Ebraheim et al., 2004; Pope, 1989). Extension is the opposite motion, increasing that angle and straightening the back, which is essential for standing upright and returning to a neutral position after flexion (Ebraheim et al., 2004; Pope, 1989).

Lateral bending, rotation within the coronal plane, enables the spine to bend to the sides, facilitating movements such as reaching to the sides or twisting the torso to the sides. This motion allows for greater mobility and flexibility of the trunk (Pope, 1989). Axial rotation, within the frontal plane, refers to the twisting motion of the lumbar vertebrae around the vertical axis, which is crucial for activities requiring torso rotation (Ebraheim et al., 2004; Panjabi & White III, 1980; Pope, 1989).

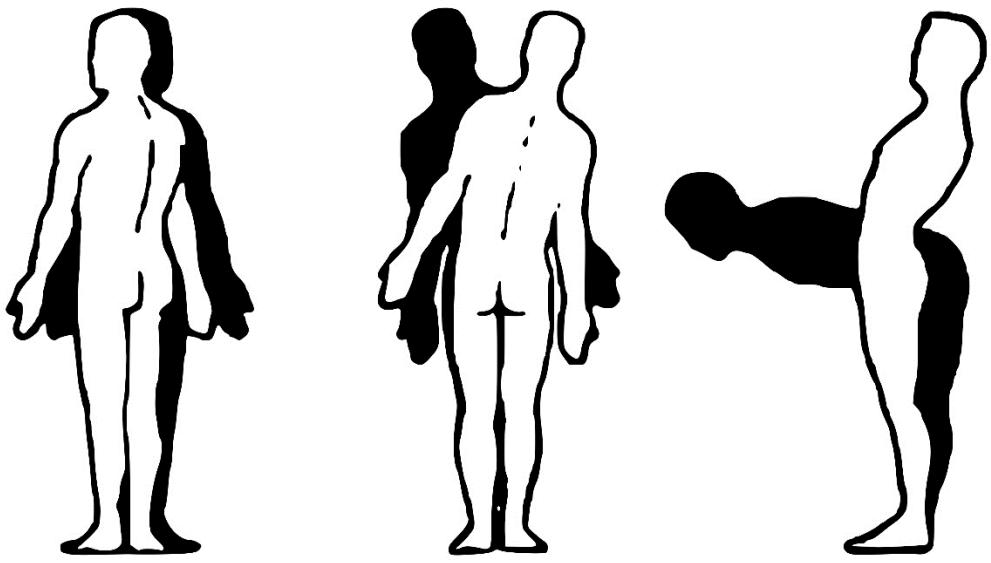

Figure 9. Demonstration of the lumbar rotations
From left to right: axial rotation, side bending and flexion, adopted from (Vincent et al., 2012)

Each of these movements is governed by a complex interplay of anatomical structures, particularly between the vertebrae. Known as intervertebral motion, it occurs in three planes, leading to sagittal, coronal and frontal rotation. However, the translation

between the vertebrae also contributes to the overall motion of the region across all three planes, creating six degrees of freedom for each vertebra in the spine (Panjabi & White III, 1980). When studying the kinematics between the vertebrae, it is essential to consider not only the angular movements but also how the vertebrae slide or translate relative to one another. This combined motion allows for a greater range of movement while maintaining stability and distributing loads evenly across the spinal column.

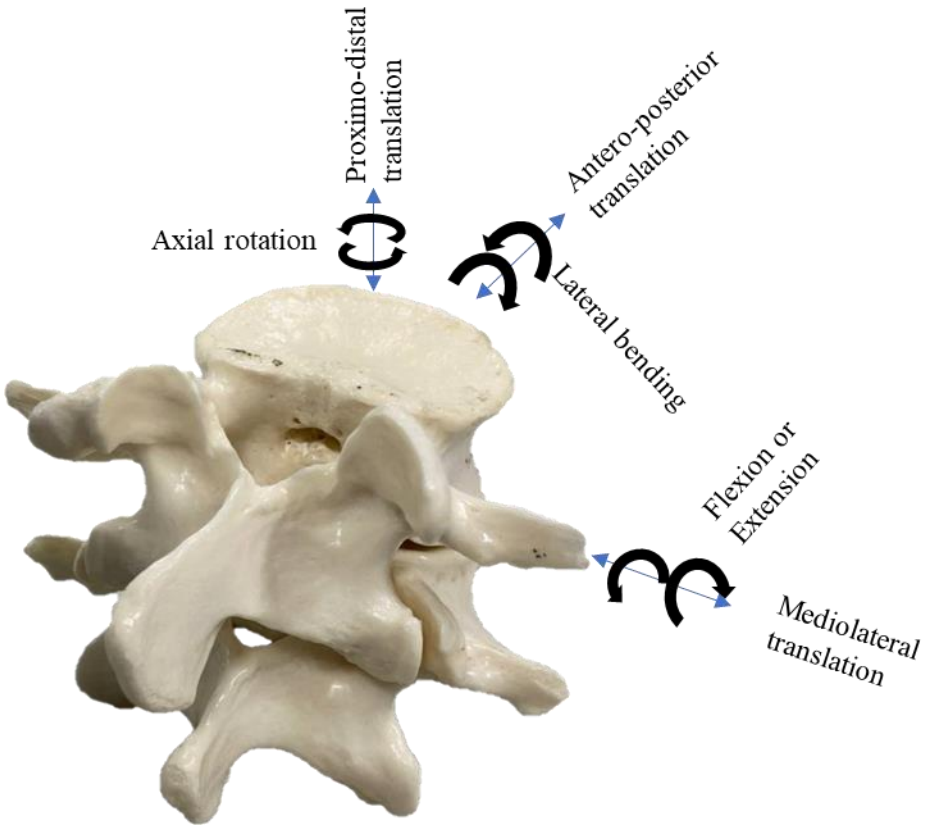

Figure 10. Intervertebral motion kinematics
including three planar rotations and translations

The range of intervertebral motion in the lumbar spine has been measured using various techniques by multiple researchers (Littlewood & May, 2007). These studies have examined different conditions, such as low back pain, spinal degeneration, and other factors that influence spinal kinematics (Errabity et al., 2023). However, the measured range of motion can vary depending on the nature of the primary movement being tested. For example, when flexion-extension is the primary motion, it typically exhibits the

greatest range, with any accompanying lateral bending or axial rotation being secondary and smaller in magnitude. Conversely, when lateral bending is the primary motion, it becomes the dominant component, and flexion-extension is minimized. In this context, several studies have reported intervertebral ranges of motion for healthy individuals as summarized in Table 1.

Table 1. Mean (SD) of segmental range of motion reported from in-vitro and in-vivo studies. Rotational motions are in degree and translational motions are in mm

References	Condition	Flexion-Extension				
		L1-L2	L2-L3	L3-L4	L4-L5	L5-S1
(Panjabi & White III, 1980)	in-vitro	12	14	15	17	20
(Pearcy et al., 1984)	in-vivo	13	13	13	16	14
(Yamamoto et al., 1989)	in-vitro	10.1	10.8	11.2	14.5	17.8
(Wong et al., 2004)	in-vivo	10.65(2.25)	9.9(1.65)	9.4(1.4)	7.25(1.75)	4.3(1.6)
(Kanayama et al., 1996)	in-vivo			9.8(3.5)	15.3(1.6)	12.5(1.9)
(Rozumalski et al., 2008)	in-vivo	14.38(6.09)	16.72(6.29)	17.72(5.12)	16.87(4.74)	14.33(6.64)
				Lateral Bending		
(Panjabi & White III, 1980)	in-vitro	6	6	8	6	3
(Pearcy et al., 1984)	in-vivo	5	5.5	5	3	1.5
(Yamamoto et al., 1989)	in-vitro	4.9	7	5.7	5.7	5.5
(Rozumalski et al., 2008)	in-vivo	10.97(3.85)	14.60(4.86)	14.32(4.63)	10.57(4.57)	7.91(3.47)
				Axial Rotation		
(Panjabi & White III, 1980)	in-vitro	2	2	2	2	5
(Pearcy et al., 1984)	in-vivo	1	1	1.5	1.5	1
(Yamamoto et al., 1989)	in-vitro	2.1	2.6	2.6	2.2	1.3
(Li et al., 2009)	in-vivo		2.5(2.3)	2.4(2.6)	2.9(2.1)	2.6(1.2)
				Proximodistal Translation		
(Pearcy et al., 1984)	in-vivo	1(1)	1(1)	0(1)	0(1)	1(1)
(Aiyangar et al., 2014)	in-vivo		0.76(0.46)	0.72(0.34)	0.25(0.94)	0.94(0.44)
(Byrne et al., 2018)	In-vitro		5.92	6.34	6.59	3.48
				Anteroposterior Translation		
(Pearcy et al., 1984)	in-vivo	4(1)	3(1)	3(1)	3(1)	2(1)
(Aiyangar et al., 2014)	in-vivo		4.94(2.24)	5.44(2.39)	5.78(2.55)	3.93(2.71)
(Byrne et al., 2018)	In-vitro		0.19	0.30	0.44	0.41
				Mediolateral Translation		

(Pearcy et al., 1984)	in-vivo	1(1)	1(1)	2(1)	0(1)	1(1)
(Aiyangar et al., 2014)	in-vivo		0.87(0.44)	0.72(0.32)	0.76(0.24)	0.89(0.32)
(Byrne et al., 2018)	In-vitro		0.68	0.73	1.45	1.63

1.2.3 The importance of kinematic assessment

Measuring the kinematic of the lumbar spine is necessary for understanding normal and abnormal movement patterns (Triantafyllou et al., 2023). This establishes what constitutes normal movement patterns and helps in identifying abnormalities that may indicate underlying issues such as low back pain, instability (hypo-hyper mobility) or degenerative conditions (Widmer et al., 2019).

Low back pain (LBP), as the most important lumbar issues, is a prevalent health issue with estimates suggesting that up to 80% of the population will experience at least one episode during their lives (Rubin, 2007). LBP is primarily associated with non-specific conditions with about 90% of cases (Van Tulder et al., 2006). Importantly, the relationship between LBP and lumbar spine kinematics is crucial for understanding the underlying mechanisms of pain. Research has demonstrated significant differences in lumbar spine kinematics between individuals with and without LBP during various functional activities (Errabity et al., 2023). For instance, a systematic review indicated notable discrepancies in kinematic characteristics during sit-to-stand movements, highlighting how individuals with LBP exhibit altered movement patterns (Sedrez et al., 2019). Furthermore, studies have shown differences in range of motion in the lumbar region related to factors such as age and sex, emphasizing the complexity of LBP and its association with spinal movement (Arshad et al., 2019). These variations in spinal biomechanics may contribute to the onset and persistence of pain, suggesting that a deeper understanding of lumbar spine kinematics is essential for developing effective diagnostic and therapeutic strategies for managing LBP.

Instability of the lumbar spine is a significant factor that can exacerbate LBP, often linked to abnormal intervertebral motion. The concept of instability is often defined as a lack of resistance to forces while the spine is near its neutral position (Panjabi, 1992). Despite the variety of the definitions of spinal instability among specialists, it is generally accepted that abnormal intervertebral motion plays a critical role in the development of instability (Cook et al., 2006; Leone et al., 2007).

In addition to the abnormality diagnosis, lumbar spine kinematics could help in developing and evaluation treatment strategies (Haynes, 2003). Understanding the specific kinematic alterations in an individual can guide the development of personalized rehabilitation strategies. For instance, if a patient has reduced range of motion in a particular direction, targeted exercises can be designed to restore normal kinematics (Bayartai et al., 2023).

In addition, kinematic measurements contribute to the development of advanced diagnostic tools and technologies, such as motion capture systems (Hindle et al., 2021) and wearable devices (García-Jaén et al., 2024), which can continuously monitor spinal motion in real-time. In biomechanical modeling, accurate kinematic data is essential for creating detailed biomechanical models of the spine, which are used in research to simulate different conditions, predict outcomes of surgical interventions (Shapiro, 2020), and understand the effects of various treatments.

1.2.4 Lumbar spine kinematics determination

As previously explained regarding the general principles of joint kinematic analysis, the determination of intervertebral motion in the lumbar spine follows a similar approach. To measure intervertebral kinematics, ARFs are constructed based on the recommendations of the ISB (Wu et al., 2002). These frames are defined using ALs identified on each vertebra. Specifically, two landmarks are placed on the most distal ends of the costiform processes and one on the top of the most posterior end of the spinous process. For the sacral vertebra (S1), ALs are located on the top of the most posterior ends of the median crests and on the most prominent surfaces of the lateral crests.

From these landmarks, the ARFs are constructed as follows: the Z-axis (Blue axis in the figure 11 B) is defined between the left and right costiform process landmarks; the X-axis (Red axis in the figure 11 C) is orthogonal to the Z-axis and passes through the landmark on the spinous process; and the Y-axis (green axis in the figure 11 B and C) is then calculated as the cross product of the X- and Z-axes, ensuring orthogonality (Figure 11).

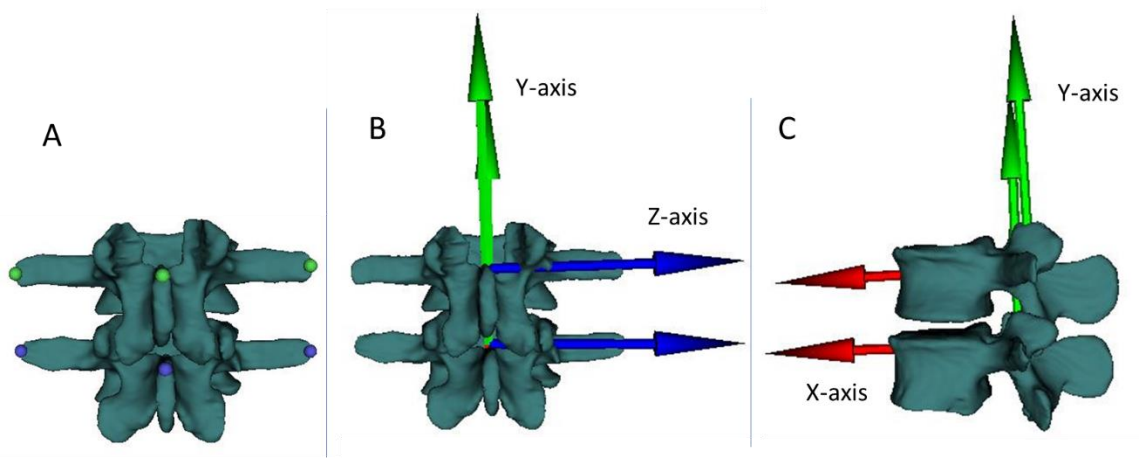

Figure 11. (A) Representation of anatomical landmarks localized on two vertebral levels (B) Anterior (B) and lateral (C) view of the anatomical reference frames established based on the anatomical landmarks. The anatomical references includes Z-axis, which is defined between the left and right costiform process landmarks, the X-axis, which is orthogonal to the Z-axis and passes through the landmark on the spinous process, and the Y-axis, which is then calculated as the cross product of the X- and Z-axes

However, identifying the ALs remains challenging and requires access to detailed morphological data. As a result, traditional clinical methods rely on non-invasive and accessible tools like tape measures (Lemos et al., 2014), goniometers (Pakeloğlu et al., 2023), and inclinometers (Fraeulin et al., 2020) to measure general spinal motion rather than specific intervertebral kinematics. For example, the Schober test uses a tape measure to assess changes in the lumbar spine's range of motion (ROM), while inclinometers and goniometers measure angular motion and alignment during flexion, extension, lateral bending, and rotation. Although these tools are non-invasive and useful in assessing overall lumbar mobility, they offer limited accuracy in detecting detailed intervertebral movement (Fritz et al., 2005; Roach et al., 2013). Tousignant et al. (Tousignant et al., 2005) reported a moderate validity ($r = 0.67$) for the Schober test when compared to X-ray imaging, with

a minimal detectable change (MDC) of 1 cm. This suggests that changes smaller than 1 cm may not be clinically meaningful due to inherent measurement variability. In a separate study, Tojima et al. (Tojima et al., 2013) noted a higher standard error of measurement (SEM) for lumbar spine movements using a goniometer, reporting a SEM of 1.26 ± 0.48°, which was larger compared to results obtained using an optical measurement system, indicating less precision with the goniometer for spinal assessments.

Beyond these clinical approaches, motion capture methods have also been employed for intervertebral motion measurement (Pourahmadi et al., 2018). However, due to the small scale of intervertebral movements, motion capture systems face significant limitations (Benoit et al., 2006). The primary issue arises from attaching markers to the skin, which can move independently of the underlying bony structures. This phenomenon, known as soft tissue artefact, introduces measurement errors, typically ranging from 0.8 to 1.5 mm, thereby reducing the accuracy of the recorded kinematic data (Heneghan & Balanos, 2010). Direct comparisons against medical imaging confirm this limitation: using open/upright MRI, back-marker measures showed posture-dependent STA on the order of ~10 mm and only moderate correspondence with vertebra-based curvature (lumbar $R^2 \approx 0.55$), indicating uncertainty in absolute values (Zemp et al., 2014). Similarly, dual-plane radiography (biplanar/fluoroscopy) studies report level- and plane-dependent discrepancies between skin-marker–derived intervertebral angles and imaging-derived "intrinsic" motion, including overestimation at some lumbar levels during flexion–extension (Xi et al., 2022).

One potential solution to mitigate this problem is to attach markers directly to the bone using intracortical bone pins (Lund et al., 2002). This approach would eliminate the influence of skin movement, resulting in more accurate measurements of intervertebral kinematics (Dickey et al., 2002; Rozumalski et al., 2008). However, it is essential to note that attaching markers to intracortical bone pins is an invasive procedure which is specifically used in cadaveric studies or carries inherent risks, including the potential for infection and tissue damage.

Meanwhile, the use of medical imaging modalities offers a high potential for 3D kinematic analysis. For example, dynamic biplane radiography systems validated against radiostereometric analysis can achieve sub-millimeter and ~1° accuracy at the lumbar spine, though at the cost of radiation exposure and specialized workflows. However, each imaging method capable of 3D vertebral reconstruction presents certain limitations, as previously discussed—for instance, in the case of CT scanning. In contrast, ultrasound imaging presents a promising alternative that can be used for this purpose.

1.3 Ultrasound imaging

Ultrasound imaging, as a medical imaging modality, is distinguished by its versatility, safety, and accessibility. Unlike x-ray-based techniques, which expose patients to ionizing radiation, ultrasound utilizes high-frequency sound waves to create real-time images. This non-invasive method allows for dynamic assessment, making it highly valuable in various clinical applications, including cardiology, obstetrics, and musculoskeletal imaging.

In ultrasound technology, sound waves are transmitted from an ultrasound probe, also known as a transducer, which serves as both the source and receiver of the sound waves used to generate images. The probe contains piezoelectric crystals, which possess the unique property of changing shape when subjected to electrical currents. When an electric current is applied, these crystals vibrate, emitting high-frequency sound waves that penetrate the body.

As the sound waves travel through tissues, they encounter boundaries between different tissue types, such as muscle and bone. At each boundary, a portion of the sound waves is reflected back to the probe, while the remainder continues to travel deeper. The probe detects these returning echoes, which vary in intensity depending on the density and composition of the tissues. These data is then converted into a digital signal, producing the grayscale images seen on the ultrasound display.

Ultrasound probes come in various designs tailored to specific imaging needs, including:

- Linear probes for superficial applications, such as in musculoskeletal imaging.

- Convex probes that provide a wider field of view, making them suitable for abdominal and obstetric imaging.
- Phased array probes, commonly used in cardiac imaging due to their narrow, focused beam for deeper structures.

In recent years, ultrasound applications in musculoskeletal imaging have advanced significantly, with specific attention to bone sonography, such as in fracture detection (Moran & Myers, 2022), fracture reduction (Wu et al., 2021a), and guidance during joint arthroscopic surgeries (Mhaskar et al., 2023). Additionally, ultrasound has been applied in analyzing spine kinematics and been validated with other standard methods, providing insights into the intervertebral motion. For instance, Chleboun et al. (2012) compared ultrasound and MRI measurements of intervertebral linear distances for flexion/extension determination, reporting an error margin of 1.3 mm and similar coefficient variations (ultrasound: 12%, MRI: 9%) (Chleboun et al., 2012). Van den Hoorn et al. (2016) introduced ultrasound-based techniques to measure L5–S1 flexion/extension, achieving explained variances of 93.8–95% compared to fluoroscopy, with absolute errors of 1.7–2.1° (van den Hoorn et al., 2016). Cuesta-Vargas (2015) combined ultrasound with electromagnetic sensors to measure L4–L5 flexion, showing excellent reliability (ICC: 0.995–0.999) and low variation (4.18%) (Cuesta-Vargas, 2015).

For axial rotation, McKinnon et al. (2019) demonstrated a strong correlation ($r > 0.9$) between ultrasound and optical tracking systems for measuring in-vitro cervical vertebrae rotation, with minimal system errors ($< 0.05°$) (McKinnon & Callaghan, 2019). Heneghan et al. (2009), in an in-vivo study, used ultrasound with motion tracking to measure C7 rotation during maximal upper-body movements, achieving high reliability (ICC: 0.72–0.98) (Heneghan et al., 2009). Additionally, McKinnon et al. (2021), in an in-vivo study, assessed lumbar segmental rotation in thoracopelvic movements, reporting gradual increases in rotation angles across the range of motion, with L1–L5 showing the highest contributions (McKinnon & Callaghan, 2021).

However, all the applications of the ultrasound imaging for intervertebral kinematics have been limited to the 2D measurements (Effatparvar & Sobczak, 2022). This limitation stems from the lack of 3D reconstruction and the restriction of virtual palpation

to a maximum of two ALs within a single anatomical plane, such as in measuring lumbar flexion-extension by assessing changes in interspinous distance and angle using two ALs per vertebra (Chleboun et al., 2012; van den Hoorn et al., 2016).

Recent innovations in 3D reconstruction methods for ultrasound imaging have been developed and validated against established 3D reconstruction techniques. These approaches generally fall into two categories of Freehand imaging, tracking the probe's spatial position using external sensors, and Sensorless methods, utilizing computer algorithms to control the probe's speed, direction, and position.

Despite these advancements, no 3D reconstruction methods have been applied to determine lumbar spine intervertebral kinematics, creating a significant gap in the field. This gap has become the focus of our work, and we have outlined several steps to develop and validate a new method against CT scan imaging. Achieving this objective could unlock new possibilities for dynamic and comprehensive assessments of spinal motion, offering improved insights into the biomechanics of the lumbar spine.

1.4 Objectives, Research questions and Hypotheses

Although the principal objective of this thesis was to determine lumbar spine intervertebral kinematics using ultrasound images, it has been divided into five distinct sections, with five phases defined to address the research questions derived from these objectives.

Phase 1) Application of ultrasound in spine kinematic determination: A systematic review. (**Effatparvar, M. R**., & Sobczak, S. (2022). Application of ultrasound in spine kinematic determination: A systemic review. *Journal of Medical Ultrasound*, *30*(1), 6-10.)

Objectives: To systematically review the literature across multiple research databases to evaluate the current use of ultrasound in spine kinematics analysis, assess the implementation of 3D intervertebral measurements using ultrasound images, and determine whether existing methods and findings support clinical applications.

Research questions: Has ultrasound been used for spine kinematics analysis? Have there been any 3D intervertebral measurements using ultrasound images? Have existing studies

and advances been sufficient to make this method practical for in-vivo applications? *Hypothesis:* Ultrasound has been used in certain contexts for spine kinematics analysis; however, the application of 3D intervertebral measurements remains limited. Current advancements in ultrasound technology and methodology may not yet be sufficient for widespread clinical adoption, indicating a significant gap in the field.

Phase 2) Assessment and improvement of a novel ultrasound-based 3D reconstruction method: Registered for lumbar spine. (**Effatparvar, M. R**., Pierre, M. O. S., & Sobczak, S. (2022). Assessment and improvement of a novel ultrasound-based 3D reconstruction method: Registered for lumbar spine. *Journal of Medical and Biological Engineering*, *42*(6), 790-799.)

Objectives: To enhance an existing algorithm for 3D ultrasound image reconstruction with the goal of accurately modeling the full lumbar spine (T12–S1), including soft tissues and a range of fat pad thicknesses, while accounting for body mass indices (BMI) from 15 to 30. To validate the reconstructed models through comparison with CT imaging and assess their reliability across multiple cadaveric specimens.

Research question: Can the algorithm for 3D reconstruction of ultrasound images be improved to accurately reconstruct the entire lumbar spine (T12–S1), including soft tissues and variable fat pad thicknesses? Is this method reliable for lumbar spine reconstruction? *Hypothesis:* The improved 3D reconstruction algorithm enables accurate and reliable modeling of the lumbar spine (T12–S1) in cadavers with BMI values between 15 and 30, with validity comparable to CT-based reconstructions.

Phase 3) Application of Musculoskeletal Ultrasound in Lumbar Spine 3D Kinematics Visualization and Determination: An In-Vitro Study. **(Effatparvar, M. R.**, St-Pierre, M. O., Lavoie, F. A., & Sobczak, S. (2025). Application of Musculoskeletal Ultrasound in Lumbar Spine 3D Kinematics Visualization and Determination: An In-Vitro Study. *Journal of Medical and Biological Engineering*, *45*(2), 230-239.)

Objectives: To evaluate the reliability of MSU-based 3D reconstructions in determining intervertebral range of motion (ROM) during discrete motions, including flexion-

extension, lateral bending, and axial rotation. To assess the validity of these reconstructions by comparing the results with those obtained from CT imaging.

Research question: Is the 3D reconstruction of musculoskeletal ultrasound (MSU) sufficiently accurate and precise to determine lumbar intervertebral kinematics during discrete motions such as flexion-extension, lateral bending, and axial rotation? Are the results valid and reliable? *Hypothesis:* MSU 3D reconstructions are reliable for measuring intervertebral ROM during standard motions and yield valid results that are consistent with CT-based measurements, showing minimal deviations across all motion types.

Phase 4) Lumbar spine 3D kinematics determination using ultrasound imaging: an in-vivo approach to define normative ranges of motion. *(submitted to the journal of Journal of Applied Biomechanics in August 2025)*

Objectives: To determine the reliability of MSU 3D reconstructions in assessing intervertebral ROM during lumbar flexion in live participants, and to quantify the normative flexion range at L4–S1 in individuals aged 20 to 60, comparing the findings with published reference values.

Research question: How reliable is 3D reconstruction of MSU images for measuring lumbar intervertebral flexion range of motion in live participants? What is the normative flexion range for vertebral levels L4–S1 in participants aged 20 to 60 based on ultrasound-based measurements, and how do these values compare with those previously reported in the literature?

Hypothesis: MSU 3D reconstructions can be reliably used to measure lumbar spine range of motion in-vivo, providing accurate and reproducible values. Furthermore, the normative flexion ranges measured at L4–S1 in participants aged 20 to 60 using ultrasound-based methods are consistent with those previously reported in the literature.

Phase 5) Feasibility of Ultrasound Imaging for Determining Shoulder 3D Kinematics: A Pilot Study. (submitted to the Journal of Ultrasound in July 2025)

Objectives: To quantify the reconstruction error of 3D models generated from ultrasound imaging when applied to the entire shoulder complex in an in-vitro setting. To evaluate the

level of agreement between ultrasound-based and CT-based measurements of shoulder kinematics.

Research question: Is the developed 3D kinematic measurement method using ultrasound imaging transferable to other joints of the body? Specifically, how feasible is its application for measuring shoulder joint kinematics?

Hypothesis: Provided that a joint is accessible via ultrasound imaging, the 3D reconstruction method enables accurate determination of joint kinematics. Consequently, the kinematics derived from ultrasound-based models will demonstrate high agreement with those obtained from CT-based models.

Chapter 2 – Application of Ultrasound in Spine Kinematics Determination: A Systematic Review

2.1 Original Contribution of the Student and Co-authors

This second chapter of the thesis presents the first published article entitled *Application of Ultrasound in Spine Kinematics Determination: A Systematic Review*. This article, co-authored by Mohammad Reza Effatparvar and Stéphane Sobczak, was published in 2022 in the *Journal of Medical Ultrasound* (Vol. 30: 6–10).

Effatparvar, M. R., & Sobczak, S. (2022). Application of ultrasound in spine kinematic determination: A systemic review. *Journal of Medical Ultrasound*, *30*(1), 6-10.

Application of ultrasound in spine kinematics determination: A systematic review

Mohammad Reza Effatparvar[1,2*], Stéphane Sobczak[1,2,3]

1- Chaire de recherche en anatomie fonctionnelle, Université du Québec à Trois-Rivières, Trois-Rivières, Québec, Canada.
2- Département d'anatomie, Université du Québec à Trois-Rivières, Trois-Rivières, Québec, Canada.
3- Groupe de Recherche sur les affections neuromusculosquelettiques, Université du Québec à Trois-Rivières, Trois-Rivières, Québec, Canada.

2.2 Abstract

Spine kinematic determination is required to diagnose or rehabilitate back pain due to spinal instability. Ultrasound imaging, as a less harmful and cost-effective method, has been recently applied to kinematic analysis. This study reviews all available published articles to see how much progress has been made in spine kinematic measurement by ultrasound. In this regard, we searched PubMed, Scopus, and Google Scholar among all available studies until 2021, using keywords such as ultrasound, spine, kinematics, rotation, twist, flexion, and bending. Finally, after identifying and scanning 183 articles, only nine articles were included, which analyzed spine kinematics by ultrasound. Among these nine articles, three reported axial displacements, three reported flexion/extension, and three reported axial rotation. Although ultrasound is a suitable alternative to other kinematic measurement methods, very little research and progress have been made in this area. Today, this method is still not used practically for spine kinematic measurement because the bone scans via ultrasound imaging are challenging to understand, and no three-dimensional kinematic measurement technique has been reported. However, recent advances in converting ultrasound images into three-dimensional images can pave the way for further improvements.

Keywords: Back pain, flexion, intervertebral kinematic, rotation, spine kinematics, ultrasound

2.3 Résumé

La détermination de la cinématique de la colonne vertébrale est essentielle pour diagnostiquer ou réhabiliter les lombalgies dues à une instabilité vertébrale. L'imagerie par échographie, en tant que méthode moins nocive et plus rentable, a récemment été appliquée à l'analyse cinématique. Cette étude passe en revue tous les articles publiés disponibles pour évaluer les progrès réalisés dans la mesure de la cinématique de la colonne vertébrale par échographie. À cette fin, nous avons recherché dans PubMed, Scopus et Google Scholar toutes les études disponibles jusqu'en 2021, en utilisant des mots-clés tels qu'échographie, colonne vertébrale, cinématique, rotation, torsion, flexion et inclinaison. Enfin, après avoir identifié et examiné 183 articles, seul neuf ont été inclus, car ils analysaient la cinématique de la colonne vertébrale par échographie. Parmi ces neuf articles, trois rapportaient des déplacements axiaux, trois des mouvements de flexion/extension et trois des rotations axiales. Bien que l'échographie soit une alternative intéressante aux autres méthodes de mesure cinématique, très peu de recherches et de progrès ont été réalisés dans ce domaine. Aujourd'hui, cette méthode n'est toujours pas utilisée de manière pratique pour mesurer la cinématique de la colonne vertébrale, car les analyses osseuses via l'imagerie échographique sont difficiles à interpréter, et aucune technique de mesure cinématique en trois dimensions n'a été rapportée. Cependant, les avancées récentes dans la conversion des images échographiques en images tridimensionnelles peuvent ouvrir la voie à de futures améliorations.

Mots-clés : Lombalgie, flexion, cinématique intervertébrale, rotation, cinématique de la colonne vertébrale, échographie.

2.4 Introduction

Spinal instability is one of the most practical reasons for severe back pain, more prevalent among the elderly. [1-3] An accurate understanding of spine kinematics is beneficial in diagnosing and rehabilitating spinal instability. Today, several methods are employed for kinematic determination, including X-ray imaging, [4,5] magnetic resonance imaging (MRI), [6] and optical tracking systems. [7,8] However, there are apparent obstacles through the introduced methods. For example, X-ray imaging is ionizing and deleterious for the tissue, MRI is expensive and imposes a high cost on the health system, and optical tracking devices based on external markers lead to measurement error due to soft tissue movements. [9] Although internal fixation of markers into the bone minimizes errors, it is not welcomed because of invasiveness. However, ultrasound is a less-harmful method, [10,11] which recently has been applied as a practical musculoskeletal imaging modality. [12,13] In this regard, ultrasound imaging has had several applications in the spine, such as facilitating spinal anesthesia, [14] identifying deformities, [15-18] and spine kinematics determination. This study intends to analyze the results and methods of spine kinematic measurement via ultrasound to see: How much progress has been made? Where does this method stand now? Have the existing studies and advances been enough to make this method practical in medical centers?

2.5 Methods

2.5.1 Protocol of the study

The study was performed according to the Preferred Reporting Items for Systematic Reviews and Meta-Analyses program. [19] Moreover, a recently printed systemic review paper [20] was used as a sample format.

2.5.2 Studies search and selection

The sources in this study are published articles in English and were selected from PubMed, Scopus, Google Scholar, and references list of the cited articles. The keywords including spine, ultrasound, kinematics, rotation, twist, flexion, and bending were used [the search strategy of keywords combination in each database has been provided in

Supplementary Material] regardless of the type of article and from 2000. The search period for this study was August 2021.

2.5.3 Inclusion and exclusion criteria

Studies were included if they (1) analyzed any in-vivo and/or in-vitro study of spine kinematics and (2) applied a two-dimensional (2D) ultrasound imaging device as the primary method of kinematic measurement. On the other hand, the following studies were excluded: (1) analyzing anatomy of the spine; (2) determination of spine deformity; and (3) applying ultrasound tracking systems instead of imaging.

2.5.4 Quality assessment

Joanna Briggs Institute checklists [21] were used to evaluate the studies' quality. It provides robust checklists for the appraisal and assessment of most types of studies.

2.5.5 Data extraction

One author did the data extraction from studies, and another author verified all exclusion. The articles were thoroughly analyzed, and all the data obtained from them were carefully recorded, including the ultrasound machine, statistical, comparing, and validation methods.

2.6 Results

After all identification, the abstracts of 183 articles [Figure 1] were reviewed. Then, 39 articles were included for scrutiny. However, 30 articles were removed from the final list due to lack of spinal examination, experimental results, and kinematic study. Finally, nine articles were eligible. The diagram of the inclusion is shaped in Figure 1.

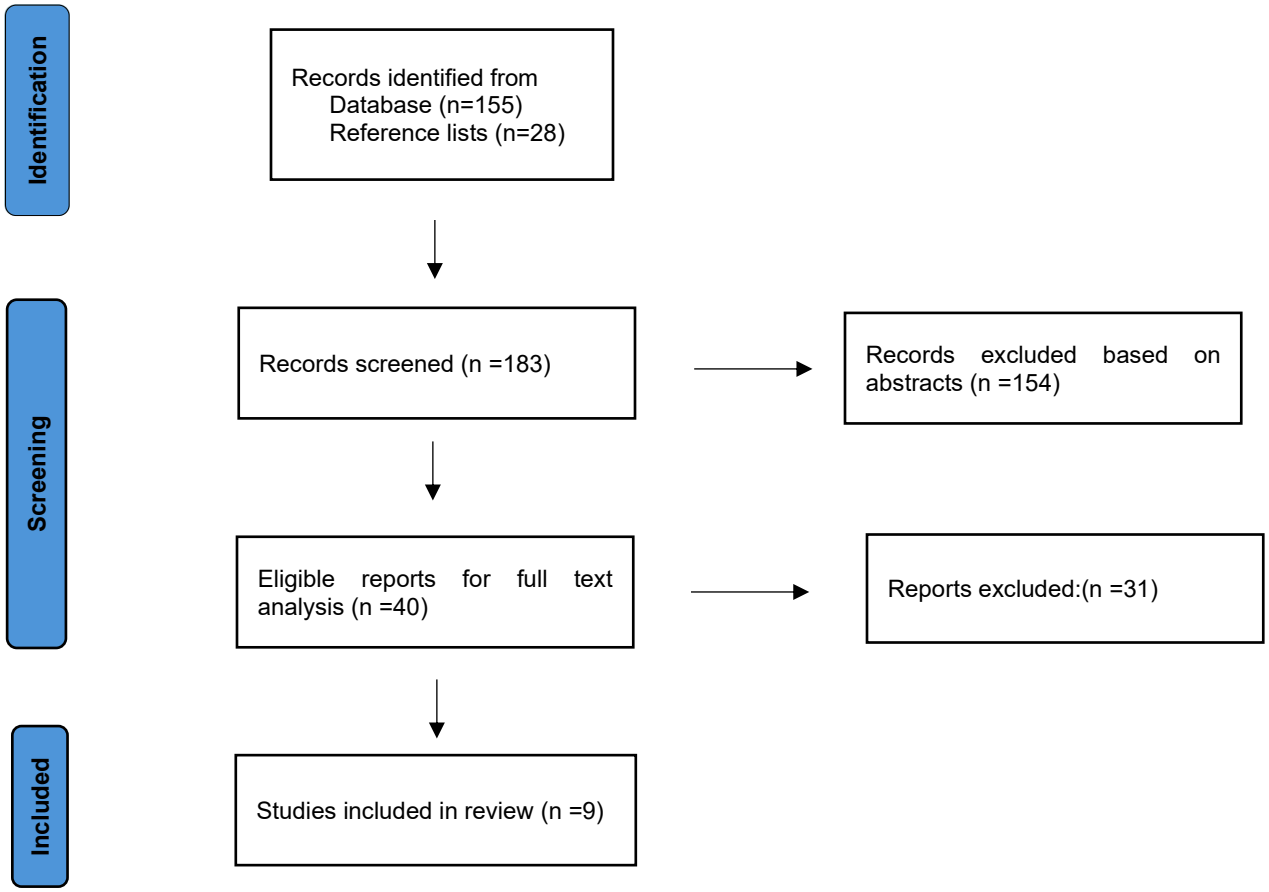

Figure 1: Preferred Reporting Items for Systematic Reviews and Meta-Analyses 2020 flow diagram for new systematic review

Among the final list, three articles [22-24] examined kinematic in vertical displacements such as standing position (in-vivo) or axial traction and compression (in-vitro), three articles studied flexion/extension movements, [25-27] and three articles investigated axial rotation. [28-30] Information about the type of studies is summarized in Table 1. In addition, detailed data about the type of ultrasound machine, transducer, frequency, and the number of samples are provided in Table 2.

Table 1: The method of studies in included records

Study name	Conditions for kinematic test	Type of study	Sample size
Zheng et al. [22]	Vertical displacement	*In vitro* (human)	5
Zheng et al. [23]	Vertical displacement	*In vitro* (human)	4
		In vivo (human)	5
Zheng et al. [24]	Vertical displacement	*In vivo* (human)	9
Van Den Hoorn et al. [25]	Flexion/extension	*In vitro* (human)	1
		In vivo (pig)	1
Cuesta-Vargas [26]	Flexion/extension	*In vivo* (human)	5
Chleboun et al. [27]	Flexion/extension	*In vivo* (human)	6
Mckinnon et al. [29]	Axial rotation	*In vitro* (pig)	12
Heneghan et al. [28]	Axial rotation	*In vivo* (human)	24
Mckinnon et al. [30]	Axial rotation	*In vivo* (human)	16

Table 2: The types of the employed ultrasound machine

Study name	Ultrasound machine	Transducer	Frequency range (MHz)
Zheng et al. [22]	Treason T3000	-	-
Zheng et al. [24]	Treason T3200	Linear array	-
Zheng et al. [24]	Treason T3200	Linear array	4-15 MHz
Van Den Hoorn et al. [25]	Logiq 9	Linear array	7-10 MHz
	Acuson SC2000		
Cuesta-Vargas [26]	M-turbo	Linear array	6-13 MHz
Chleboun et al. [27]	My lab 25	Curvilinear array	6 MHz
Mckinnon et al. [29]	M-turbo	Linear array	6-13 MHz
Heneghan et al. [28]	Sono 5500	Linear array	3-11 MHz
Mckinnon et al. [30]	M-turbo	Linear array	6-13 MHz

2.6.1 Data report

The final reports are divided into three categories according to the types of experiments.

Vertical displacement

To date, only three intervertebral vertical displacement measurements have been reported by Zheng et al. [22-24] In the in-vitro studies, they applied 1 mm frequency motions of 1–8 Hz in the C4–C5 and first compared the one-transducer ultrasound results with optical tracking methods and showed an accuracy of ±0.148 mm at frequencies <6 HZ, then compared the dual-transducer ultrasound results with linear voltage differential transformers, and showed 90% accuracy in frequencies <6 HZ. Moreover, in the in-vivo studies, they designed a jumping test for participants and measured intervertebral compression using one transducer and dual transducer. Not enough numerical results have been reported in their studies, and only the high accuracy of ultrasound has been declared.

Flexion/extension

Chleboun et al. [27] measured the axial distance between the spinous processes of L1–L5 in the neutral supine, lumbar flexion, and lumbar extension postures via ultrasound and MRI. In the 1–6 mm range of spinous processes distances, the average MRI results were 1.3 mm higher than the ultrasound. Besides, the coefficient variation of MRI was 9%, and the coefficient variation of ultrasound was 12%. Next, van den Hoorn et al. [25] first in an in-vitro study introduced two measurement techniques (direct angle measuring, indirect angle measuring) for flexion/extension of L5–S1 via ultrasound and then compared the results with a digital camcorder. The mean errors between ultrasound and digital camera were about 0.715° in 20%–100% of range of motion (RoM, 2.8°–14.1°). Furthermore, the explained variances between the ultrasound and digital camera results were 97% and 77% in two different measurement techniques. Then, in an in-vivo study, they replaced the digital camera with a fluoroscope. The explained variance between the ultrasound and fluoroscopy in the first technique was 93.8% and for the second technique was 95%. Plus, for the first technique, the corresponding linear regression was 0.995, with an absolute prediction error of 2.1°. Concerning the second technique, the corresponding linear

regression was 0.997, with an absolute prediction error of 1.7°. In the third article, Cuesta-Vargas [26] combined ultrasound and electromagnetic sensors to measure the mean composite range of L4–L5 during the full flexion, which was 15.5° ± 2.04°, the standard error of the mean was 0.54°, and the coefficient of variation was 4.18% in a single trial. Moreover, reliability was excellent for both within days (0.995–0.999) and between days (0.996–0.999).

Axial rotation

In an in-vitro study,[29] the rotations of several C3–C4 and C5–C6 were measured via ultrasound and optical tracking system in three positions of neutral, flexion (5.58° ± 1.18°), and extension (2.37° ± 1.72°). The maximum rotation was 3.5° in flexion and about 3.2° for neural and extension. Therefore, the correlation between the two systems was higher than 0.903, and the absolute system error across all flexion/extension was 0.01° ± 0.05°. Moreover, Heneghan et al. [28] combined ultrasound and motion tracking sensors to measure the C7 rotation in maximal upper body rotations of participants. The mean range of axial rotation was 85.15°. The intraclass coefficient correlation was "excellent" for within days (0.89–0.98) and "good/excellent" for between days (0.72–0.94). Finally, McKinnon et al. [30] investigated the effect of maximum external thoracopelvic angle (41.1° ± 6.8°) on the lumbar segmental axial rotation angle. The results in 25% of RoM were L1 = 3° ± 2.4°, L2 = 2.6° ± 2.6°, L3 = 1.4° ± 1.9°, L4 = 1.2° ± 2.0°, L5 = 1.1° ± 1.4°, S1 = −0.2° ± 1.1°; in 50% of RoM were L1 = 7.4° ± 2.3°, L2 = 6.9° ± 2.9°, L3 = 4.7° ± 2.8°, L4 = 4° ± 3.2°, L5 = 3.8° ± 2.3°, S1 = 1.8° ± 2.8°; and in 75% of RoM were L1 = 12.4° ± 4°, L2 = 11.7° ± 3.3°, L3 = 8.4° ± 2.5°, L4 = 7.9° ± 2.7°, L5 = 6.9° ± 3.4°, S1 = 6.9° ± 3.4°.

A summary of the strengths and weaknesses of different methodologies is summarized in Table 3.

Table 3: Assessment of applied methodology

	Strengths	Weaknesses
Heneghan et al. [28]	First spine kinematics measurement in a RoM study Designing the novel method of combination of ultrasound with motion tracking sensors	No image processing No coordinate transform system No compare with other methods
Chleboun et al. [27]	First intervertebral study Comparing the results with MRI	The method was only for supine position Small sample size applied for only discrete kinematic
Zheng et al. [22]	Kinematic measurement in a dynamic movement Comparing ultrasound results with optical tracking motion Both in-vivo and in-vitro tests	Only vertical intervertebral motion analysis. No ability to be developed for other kinematic measurements Probability of probe movement in dynamic studies. Small sample size
Zheng et al. [23]	Kinematic measurement in a dynamic movement Applying a novel dual-ultrasound technique as a more accurate method Comparing results with linear voltage differential transformers	Only vertical intervertebral motion analysis Employing a similar test procedure to the last study
Zheng et al. [24]	Kinematic measurement in a dynamic movement Applying the dual-ultrasound method for an in-vivo study	Only vertical intervertebral motion analysis Employing a similar test procedure to the last studies No comparing with other methods Probability of probes instability while dynamic movement Small sample size
Cuesta-Vargas [26]	Develop the method of combining ultrasound and motion tracking sensors Employing coordinate transform system Employing a novel image processing method	Small sample size No compare with other methods Applied for Only limited postures
Van Den Hoorn et al. [25]	Introduced a novel method of indirect angle measurement	Obscurity of landmarks Complexity of movement Not applicable for shorter RoM

Mckinnon et al. [29]	Evaluating the transducer measurement angle Comparing with a motion capture system Employing coordinate transform system	
Mckinnon et al. [30]	Develop the previous methods for RoM measurement	Limitation in the experimental setup Applying only passive motions

2.7 Discussion

Diagnosing spinal instability and the related rehabilitation requires accurate kinematic determination. Accordingly, it needs extensive research to facilitate the measurement process. Today, several methods have been applied, while they are associated with various drawbacks. At the same time, ultrasound as a convenient system may help compensate for the shortcoming. Still, the image quality of bone scans via ultrasound has led to less attention being paid to spinal kinematics. However, nine articles have analyzed spine kinematics and are included in this study. Regarding the years of publication, Heneghan et al. [28] are the first group that analyzed spine kinematics using ultrasound in 2009. They combined ultrasound and electromagnetic sensors to measure C7-T1 axial rotation (85.15°), which their results were very similar to earlier declared reports (85°). [31] Three years later, in 2012, Chleboun et al. [27] recorded lumbar spine intervertebral flexion/ extension based on the axial distance between spinous processes and reported significantly similar results compared to MRI. Next, in 2013 and 2014, Zheng et al. [22-24] applied intervertebral vertical frequent motions to compare the measurement accuracy of oneultrasound with optical tracking systems and dual ultrasound with linear voltage differential transformers. They showed about 90% accuracy in low-frequency motion.

After that, in 2015, Cuesta-Vargas [26] developed the previously introduced technique of combined ultrasound and electromagnetic sensors to measure the mean composite range of L4–L5 (15.5° ± 2.04°) during the full flexion and reported the similar results of earlier published direct pin-based records (16.87° ± 4.74°). [32]

Then, in 2016, Zheng et al. [21] used the dual-ultrasound method again in an in-vivo jump test and showed high accuracy in intervertebral vertical displacement. No more

numerical results have been provided in their studies. Moreover, in the same year, van den Hoorn et al. [25] used two different ultrasound imaging techniques to measure intervertebral flexion/extension and showed high accuracy and reliability compared to digital cameras and fluoroscopes.

Finally, in the most recent studies, in 2019 and 2021, Mckinnon et al. [29,30] first showed a high correlation between ultrasound results and optical tracking systems measuring cervical axial rotation. As well, the reported error (0.1° in 3° RoM) was lower in comparison to the results obtained in the older record (2.1° in 14° RoM). Second, they measured lumbar segmental vertebrae axial rotations and showed significant similarity to earlier publications. [32]

A review of existing articles shows that very few studies have applied ultrasound in spine kinematic determination; therefore, much progress has not been made yet. Although available examinations have reported high accuracy and reliability of ultrasound results, all have been limited to 2D measurements, and no practical technique for 3D measurement has been introduced. As a result, this method is currently not clinically used by therapists. If enough advancement is made in this field, the advantages of ultrasound will place it as an ideal alternative. It seems that recently developed spine 3D modeling via ultrasound images [33] can help future studies record spine kinematics in 3D models. This method converts 2D ultrasound images to 3D ones, thanks to the image processing techniques. As a result, the location of the bony landmarks gets more visible. Then, the displacement of these landmarks in any direction on three anatomical plates could be accurately recorded. By improving this technique, the real-time intervertebral 3D kinematics is measurable.

2.8 Conclusion

Studies showed that spine kinematic measurement via ultrasound is still a toddler who needs much upbringing. High-accuracy 2D spine kinematic determination via ultrasound has been reported to date, while they are not enough because spine kinematics need to be analyzed 3D. The recently developed 3D spine modeling helps further progress of ultrasound to compete with other imaging methods such as CT scans and MRI. By

producing accurate 3D data, other benefits of ultrasound, such as portability and being real-time, which is functional for in-vivo studies, make it superior to different systems.

2.9 Financial support and sponsorship

The authors thank Natural Sciences and Engineering Research Council of Canada (NSERC) for the financing this research project (RGPIN-2016-05717).

2.10 Conflicts of interest

There are no conflicts of interest.

2.11 References

1. Vos T, Abajobir AA, Abate KH, Abbafati C, Abbas KM, Abd-Allah F, et al. Global, regional, and national incidence, prevalence, and years lived with disability for 328 diseases and injuries for 195 countries, 1990–2016: A systematic analysis for the Global Burden of Disease Study 2016. Lancet 2017; 390:1211-59.

2. Mokdad AH, Ballestros K, Echko M, Glenn S, Olsen HE, Mullany E, et al. The state of US health, 1990-2016: burden of diseases, injuries, and risk factors among US states. Jama. 2018; 319:1444-72.

3. Nunn ML, Hayden JA, Magee K. Current management practices for patients presenting with low back pain to a large emergency department in Canada. BMC Musculoskelet Disord 2017; 18:92.

4. Dugailly PM, Sobczak S, Moiseev F, Sholukha V, Salvia P, Feipel V, et al. Musculoskeletal modeling of the suboccipital spine: Kinematics analysis, muscle lengths, and muscle moment arms during axial rotation and flexion extension. Spine (Phila Pa 1976) 2011; 36: E413-22.

5. Dugailly PM, Sobczak S, Sholukha V, Van Sint Jan S, Salvia P, Feipel V, et al. In vitro 3D-kinematics of the upper cervical spine: Helical axis and simulation for axial rotation and flexion extension. Surg Radiol Anat 2010; 32:141-51.

6. Paholpak P, Shah I, Acevedo-Moreno LA, Tamai K, Buser Z, Wang JC. Thoracic spine disc degeneration, translation, and angular motion: An analysis using thoracic spine kinematic MRI (kMRI). J Clin Neurosci 2019; 66:113-20.

7. Mitchell K, Porter M, Anderson L, Phillips C, Arceo G, Montz B, et al. Differences in lumbar spine and lower extremity kinematics in people with and without low back pain during a step-up task: A cross-sectional study. BMC Musculoskelet Disord 2017; 18:369.

8. Beyer B, Sobczak S, Salem W, Feipel V, Dugailly PM. 3D motion reliability of occipital condylar glide testing: From concept to kinematics evidence. Man Ther 2016; 21:159-64.

9. Heneghan NR, Balanos GM. Soft tissue artefact in the thoracic spine during axial rotation and arm elevation using ultrasound imaging: A descriptive study. Man Ther 2010; 15:599-602.

10. Naredo E. Ultrasound in rheumatology: Two decades of rapid development and evolving implementation. Med Ultrason 2015; 17:3-4.

11. Marshburn TH, Hadfield CA, Sargsyan AE, Garcia K, Ebert D, Dulchavsky SA. New heights in ultrasound: First report of spinal ultrasound from the international space station. J Emerg Med 2014; 46:61-70.

12. Romero-Morales C, Bravo-Aguilar M, Ruiz-Ruiz B, Almazán-Polo J, López-López D, Blanco-Morales M, et al. Current advances and research in ultrasound imaging to the assessment and management of musculoskeletal disorders. Dis Mon 2021 ; 67 :101050.

13. Passmore E, Lai A, Sangeux M, Schache AG, Pandy MG. Application of ultrasound imaging to subject-specific modelling of the human musculoskeletal system. Meccanica. 2017; 52:665-76.

14. Chin KJ, Perlas A, Chan V, Brown-Shreves D, Koshkin A, Vaishnav V. Ultrasound imaging facilitates spinal anesthesia in adults with difficult surface anatomic landmarks. Anesthesiology 2011; 115:94-101.

15. Vo QN, Le LH, Lou E. A semi-automatic 3D ultrasound reconstruction method to assess the true severity of adolescent idiopathic scoliosis. Med Biol Eng Comput 2019; 57:2115-28.

16. Vo QN, Lou EH, Le LH. Measurement of axial vertebral rotation using three-dimensional ultrasound images. Scoliosis 2015;10:S7.

17. Vo QN, Lou EH, Le LH. 3D ultrasound imaging method to assess the true spinal deformity. Annu Int Conf IEEE Eng Med Biol Soc 2015;2015:1540-3.

18. Wang Q, Li M, Lou EH, Chu WC, Lam TP, Cheng JC, et al. Validity study of vertebral rotation measurement using 3-D ultrasound in adolescent idiopathic scoliosis. Ultrasound Med Biol 2016;42:1473-81.

19. Page MJ, McKenzie JE, Bossuyt PM, Boutron I, Hoffmann TC, Mulrow CD, et al. The PRISMA 2020 statement: An updated guideline for reporting systematic reviews. BMJ 2021;372:n71.

20. Chen KC, Lee TM, Wu WT, Wang TG, Han DS, Chang KV. Assessment of tongue strength in sarcopenia and sarcopenic dysphagia: A systematic review and meta-analysis. Front Nutr 2021;8:684840.

21. Moola SZ, Munn Z, Tufanaru C, Aromataris E, Sears K, Sfetcu R, et al. Systematic reviews of etiology and risk. In: Joanna Briggs Institute Reviewer's Manual. Ch. 7. Adelaide: The Joanna Briggs Institute; 2017. p. 5.

22. Zheng M, Shiuan K, Masoudi A, Buckland D, Szabo T, Snyder B. Dynamic ultrasound imaging of cervical spine intervertebral discs. IEEE International Ultrasonics Symposium (IUS); 2013. p. 836-9.

23. Zheng M, Masoudi A, Buckland D, Stemper B, Yoganandan N, Szabo T, et al. Dynamic Ultrasound Imaging of Cervical Spine Intervertebral Discs. IEEE International Ultrasonics Symposium (IUS); 2014. p. 448-51.

24. Zheng M, Mohamodi A, Szabo T, Snyder B. In-vivo cervical spine FSU dynamic motion measured by dual ultrasound: The effect of muscle activation. IEEE International Ultrasonics Symposium 2016. p. 1-4.

25. van den Hoorn W, Coppieters MW, van Dieën JH, Hodges PW. Development and validation of a method to measure lumbosacral motion using ultrasound imaging. Ultrasound Med Biol 2016;42:1221-9.

26. Cuesta-Vargas AI. Development of a new ultrasound-based system for tracking motion of the human lumbar spine: Reliability, stability and repeatability during forward bending movement trials. Ultrasound Med Biol 2015;41:2049-56.

27. Chleboun GS, Amway MJ, Hill JG, Root KJ, Murray HC, Sergeev AV. Measurement of segmental lumbar spine flexion and extension using ultrasound imaging. J Orthop Sports Phys Ther 2012;42:880-5.

28. Heneghan NR, Hall A, Hollands M, Balanos GM. Stability and intra-tester reliability of an in vivo measurement of thoracic axial rotation using an innovative methodology. Man Ther 2009;14:452-5.

29. McKinnon CD, Callaghan JP. Validation of an ultrasound protocol to measure intervertebral axial twist during functional twisting movements in isolated functional spinal units. Ultrasound Med Biol 2019;45:642-9.

30. McKinnon CD, Callaghan JP. The relationship between external thoracopelvic angle and lumbar segmental axial twist angle using an ultrasound imaging technique. Hum Mov Sci 2021;78:102824.

31. Muscolino JE. Kinesiology E Book: The Skeletal System and Muscle Function. Maryland Heights, Missouri: Elsevier Health Sciences; 2014.

32. Rozumalski A, Schwartz MH, Wervey R, Swanson A, Dykes DC, Novacheck T. The in vivo three-dimensional motion of the human lumbar spine during gait. Gait Posture 2008;28:378-84.

33. Forbes A, Cantin V, Develle Y, Dubé Y, Bertrand-Grenier A, Ménard-Lebel C, et al. Musculoskeletal ultrasound for 3D bone modeling: A preliminary study applied to lumbar vertebra. J Back Musculoskelet Rehabil 2021;34:937-50.

Chapter 3 – Assessment and Improvement of a Novel Ultrasound-Based 3D Reconstruction Method: Registered for Lumbar Spine

3.1 Original Contribution of the Student and Co-authors

This third chapter of the thesis presents the second published article entitled *Assessment and Improvement of a Novel Ultrasound-Based 3D Reconstruction Method: Registered for Lumbar Spine*. This article, co-authored by Mohammad Reza Effatparvar, Marc-Olivier St-Pierre, and Stéphane Sobczak, was published in 2022 in the *Journal of Medical and Biological Engineering* (Vol. 42: 790–799).

Effatparvar, M. R., Pierre, M. O. S., & Sobczak, S. (2022). Assessment and improvement of a novel ultrasound-based 3D reconstruction method: Registered for lumbar spine. *Journal of Medical and Biological Engineering*, *42*(6), 790-799.

Assessment and Improvement of a Novel ultrasound-based 3D Reconstruction Method: Registered for Lumbar Spine

Mohammad Reza Effatparvar[1,2,3*], Marc-Olivier St-Pierre[1,2,3], Stéphane Sobczak[1,2,3]

1- Chaire de recherche en anatomie fonctionnelle, Université du Québec à Trois-Rivières, Trois-Rivières, Québec, Canada.
2- Département d'anatomie, Université du Québec à Trois-Rivières, Trois-Rivières, Québec, Canada.
3- Groupe de Recherche sur les affections neuromusculosquelettiques, Université du Québec à Trois-Rivières, Trois-Rivières, Québec, Canada.

3.2 Abstract

Purpose Bone three-dimensional (3D) modelling using imaging techniques is applied for 3D kinematic measurement. Ultrasound has been recently introduced for 3D bone modelling. This study intends to assess and improve an ultrasound-based 3D modelling algorithm to a soft tissue-compatible version.

Methods Six lumbar spines with attached soft tissues were dissected from human cadavers with different body mass indexes (BMIs). Ultrasound and computed tomography (CT) scan imaging were performed, and the images were reconstructed three dimensionally using image processing techniques. Regarding reliability, an operator repeated the reconstruction processes of two specimens three times. Regarding validity, 3D models were directly compared; then, volumes were calculated, and limits of agreement were obtained. Finally, the fat pad thickness of all spinous processes was measured to calculate the effect of different BMIs on reconstruction errors.

Results The reliability analysis using intraclass correlation coefficients [95% CI] showed high intra-operator reliability in the CT-scan- (0.966 ± 0.014) and ultrasound-based (0.930 ± 0.012) models. The low mean mean reconstruction errors (mm) (0.18 ± 0.04, 0.24 ± 0.11, 0.06 ± 0.15, 0.04 ± 0.36, 0.44 ± 0.24, and 0.42 ± 0.27, respectively from specimen 1 to 6), And also the inclusion of all differences within the limit of agreement verified the validity of ultrasound-based models compared to CT-scan-based models. Moreover, the linear regression showed a weak correlation ($R = 0.33$) between the reconstruction error and fat pad thickness.

Conclusion This study showed that the 3D reconstruction of the lumbar spine obtained from ultrasound images is highly similar to those obtained from CT scan images and is not significantly affected by the posterior fat pad, which makes it appropriate for kinematic studies.

Keywords Lumbar spine · Ultrasound · CT scan · Kinematic · 3D spine modelling

3.3 Résumé

Objectif : La modélisation tridimensionnelle (3D) des os à l'aide de techniques d'imagerie est utilisée pour la mesure cinématique en 3D. L'échographie a été récemment introduite pour la modélisation osseuse en 3D. Cette étude vise à évaluer et améliorer un algorithme de modélisation 3D basé sur l'échographie afin de le rendre compatible avec les tissus mous.

Méthodes : Six colonnes lombaires avec tissus mous attachés ont été prélevées sur des cadavres humains ayant des indices de masse corporelle (IMC) variés. Des échographies et des tomodensitométries (CT scan) ont été réalisées, et les images ont été reconstruites en 3D à l'aide de techniques de traitement d'images. Concernant la fiabilité, un opérateur a répété les processus de reconstruction de deux spécimens à trois reprises. Concernant la validité, les modèles 3D ont été directement comparés, les volumes ont été calculés, et les limites d'accord ont été déterminées. Enfin, l'épaisseur de la couche graisseuse de tous les processus épineux a été mesurée pour évaluer l'effet des différents IMC sur les erreurs de reconstruction.

Résultats : L'analyse de la fiabilité, basée sur les coefficients de corrélation intra-classes [IC à 95 %], a montré une grande fiabilité intra-opérateur pour les modèles basés sur le CT scan (0,966 ± 0,014) et sur l'échographie (0,930 ± 0,012). Les faibles erreurs moyennes de reconstruction (mm) (0,18 ± 0,04, 0,24 ± 0,11, 0,06 ± 0,15, 0,04 ± 0,36, 0,44 ± 0,24, et 0,42 ± 0,27, respectivement pour les spécimens 1 à 6) ainsi que l'inclusion de toutes les différences dans les limites d'accord ont confirmé la validité des modèles basés sur l'échographie par rapport à ceux basés sur le CT scan. Par ailleurs, la régression linéaire a montré une faible corrélation (R = 0,33) entre l'erreur de reconstruction et l'épaisseur de la couche graisseuse.

Conclusion : Cette étude a démontré que la reconstruction 3D de la colonne lombaire obtenue à partir d'images échographiques est très similaire à celle obtenue à partir de CT scan et n'est pas significativement affectée par la couche graisseuse postérieure, ce qui la rend appropriée pour des études cinématiques.

Mots-clés : Colonne lombaire · Échographie · CT scan · Cinématique · Modélisation 3D de la colonne

3.4 Introduction

Three-dimensional (3D) bone reconstruction using medical imaging as one of the most effective modelling methods is used for different purposes such as mechanical tests, surgical preplanning, and kinematic study. Magnetic resonance imaging (MRI) [1] and computed tomography (CT) scan [2] are the leading imaging systems for creating 3D models. However, the introduced approaches have many disadvantages; X-ray imaging is ionizing and deleterious for the body tissue. MRI is very expensive and imposes a high cost on the health system. Hence, employing an alternative imaging method with lesser drawbacks is crucial.

Meanwhile, ultrasound imaging as an affordable, portable, and non-ionizing modality can fill the available gap. Although in the opinion of many researchers, this imaging method still faces many limitations, validation results of the ultrasound images compared to other methods like comparison with CT scan in aortic aneurysm diameter measurements with a measurement error of 0.11 ± 4.26 mm [3], comparison with MRI-CT images of a beating heart phantom with a measurement error of 1.7 ± 0.4 mm [4], comparison with a caliper in spine height measurement with a measurement error of $5.5 \pm 1.5\%$ [5], and recent innovative developments have made it replaceable with other imaging systems in certain situations. As an example, several intra-operative applications like fracture reduction [6], arthroscopic surgeries [7], screw insertion, anatomical bone landmark determination, tumour border delineation [8], and point-of-care applications like bone fractures identification [9–11], spinal cord injuries diagnosis [12] could be mentioned.

In addition, ultrasound images have been recently used for bone 3D reconstruction to make the less intelligible images highly acceptable. Newly, many applications of ultrasound-based bone 3D modelling have been reported, such as the modelling of the knee joint for robotic knee arthroplasty [13], co-applying of the ultrasound imaging system and the electromagnetic tracker for the knee 3D reconstruction [14], and co-registering the ultrasound with CT scan images to model cow femur [15]. Moreover, various methods of

spine 3D modelling have been applied in order to measure spinal rotation, scoliosis, and other deformities using a 3D ultrasound machine [16–19].

Nevertheless, among the ultrasound applications, less attention has been paid to the issue of spine kinematics measurement, and the existing studies have been limited to two-dimensional measurements [20]. While spine kinematics, as an essential criterion in movement limitation examination, should be analysed three-dimensionally. On the other hand, since the spine 3D models could be used to localize bone landmarks to determine spine kinematics, we decided to study the possibility of 3D reconstruction of the lumbar spine through ultrasound images. In this regard, we aimed to assess and develop an available algorithm of one dry lumbar spine 3D reconstruction [21] to a more substantial version by reconstructing complete lumbar spines (T12-S1) with soft tissues and different fat pad thicknesses, so linked to the body mass indexes (BMIs). Thanks to valid 3D bone models from ultrasound, we will be able to determine in-vivo lumbar spine kinematics in the near future.

3.5 Materials and Methods

3.5.1 Specimen

After attaining approval from the Université du Québec à Trois-Rivières Institutional Review Board (SCELERA 21 − 13), Six human cadavers with different BMIs ranged from 18 to 26 (Mean: 21.8, SD: ± 3.3) and ages from 62 to 89 years (Mean: 76.3 SD: ± 10) were dissected to extract the lumbar spines from T12 to S2. During the dissections process, First, palpating the spinous processes, two longitudinal incisions were made 15 to 20 cm laterally away from the spinous processes to leave an adequate amount of soft tissue covering the lumbar spine posteriorly. Then, dissections were continued obliquely up to the anterior side of the vertebral body to keep all the attached lateral soft tissues intact. Next, the edges of the skins were sutured to get a cylindrical form, and two orthopaedic Schanz screws were inserted through all vertebral bodies to avoid inter vertebral displacement (Fig. 1a). Then, the Schanz screws were fixed on a threaded rod using external fixation clamps. Following, each specimen was installed in the centre of a

home-made cylinder plastic frame (D = 165 mm), and the frame was filled up with porcine gelatine (Gelatine, Type A, Pork Skin, mi. Bloom 225) (Fig. 1b).

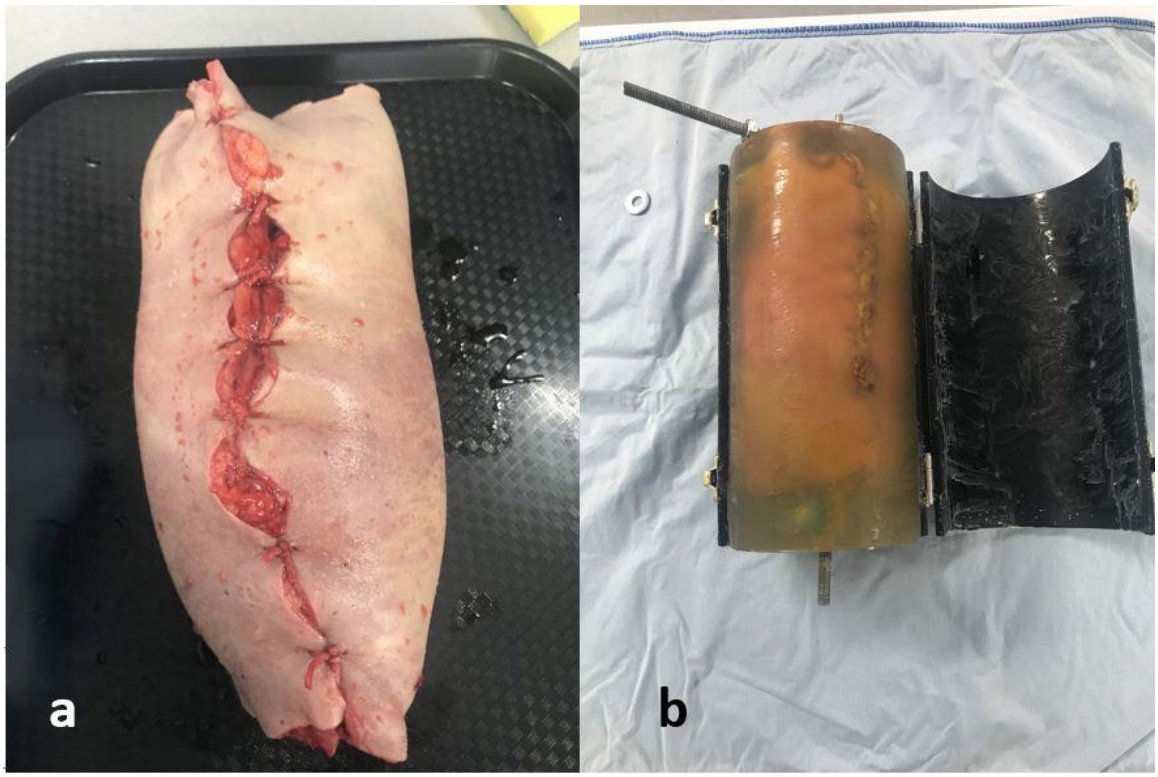

Fig. 1 (a) a dissected lumbar spine after suture. (b) a specimen fixed in the gelatine after hardening

3.5.2 CT scan

After gelatine hardening, a CT scan device (GE Healthcare, Revolution EVO) was used to collect the images of the specimens. In this regard, after setting up the CT scan machine (convolution Kernel = standard, filter type = body filter, window centre = 50, window width = 500, focal spot = 1.2 mm) the DICOM format images (reconstruction slice thickness = 0.5 mm, inter-slice spacing = 0.625 mm, each image size = 514 KB) were obtained.

3.5.3 Ultrasound

After CT scan imaging, the specimens were stabilized into a computer-assisted mechanical frame (CAM) [21], facilitating whole-length ultrasonography. The CAM (Fig. 2) provides a graduated circular mobile plate that moves upward and downward at the desired speed, controlled by a step motor. Moreover, this mobile plate contains a holder

for the ultrasound transducer, which could be set to the desired degree. Through these facilities, ultrasound collects the images from down to up at each upward movement of the mobile plate. Then, the transducer holder is moved in the circular path to the next position, and the imaging is repeated; this process is continued until finishing imaging all around the spine. For this study, the imaging processes were performed using a linear transducer of an ultrasound machine (NextGen LOGIQ e Ultrasound, GE Healthcare, USA - Mode = Musculoskeletal, Frequency = 8.0 MHz, Distance = 8 cm, Gain = 76). Furthermore, the CAM setup was at 0.5 mm/s of linear velocity (upward downward) and every 30 to 40 degrees (circular path). These degrees were calculated using the Eq. (1) and depending on the circumferences of the specimens; to be fully covered in the images with the fewest overlap, preventing shadows.

$$\theta \approx \frac{360T}{2\pi r}$$

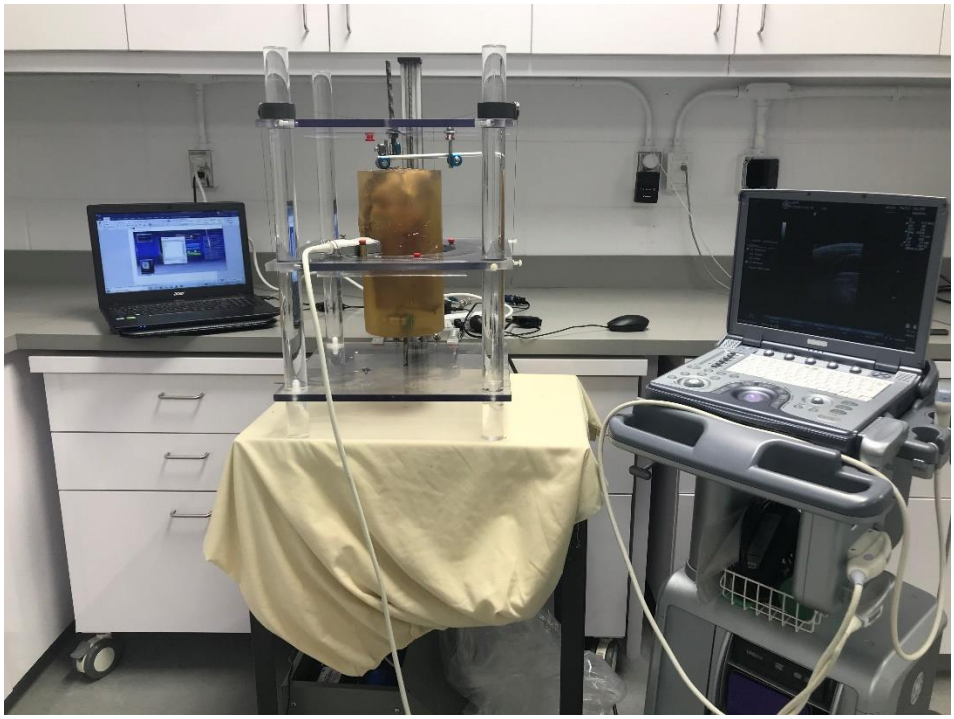

Fig. 2 The procedure of ultrasound imaging using CAM.

In this equation, “θ” is the degree setup of the mobile plate, “T” is the transducer width and “2πr” is the circumference of the specimen.

3.5.4 Image Processing and 3D Reconstruction

After finishing the ultrasound imaging process, 9 to 12 (360/θ) sets of ultrasound files, including 400 DICOM format images (each image size = 22.2 KB), were obtained. Then, using a homemade MATLAB software (MathWorks, R2021 a) script, the sets of images were merged to produce one series of 360-degree DICOM format images (image amount = 400). Next, to simplify the reconstruction process, the quality of images was enhanced using intensity transform, Laplacian spatial filter, high pass filter, and colour thresholds (Fig. 3).

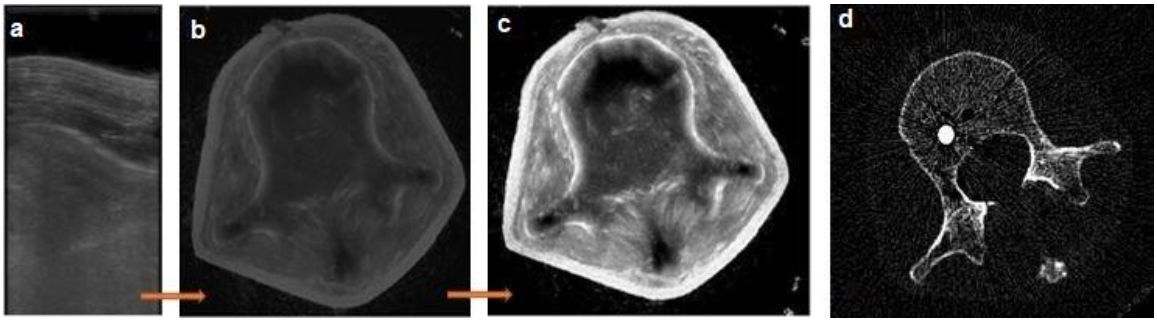

Fig. 3 (a) one of the obtained images from ultrasound. (b) a 360-degree image after the merging process. (c) a quality enhanced image after image processing. (d) intensity boundaries changed CT scan image of the same level

In the following step, using the segmentation tool of Amira software (5.2.2®, Germany), the images obtained from the ultrasound and the CT scan (gold standard) were separately segmented to create 3D models (Fig. 4).

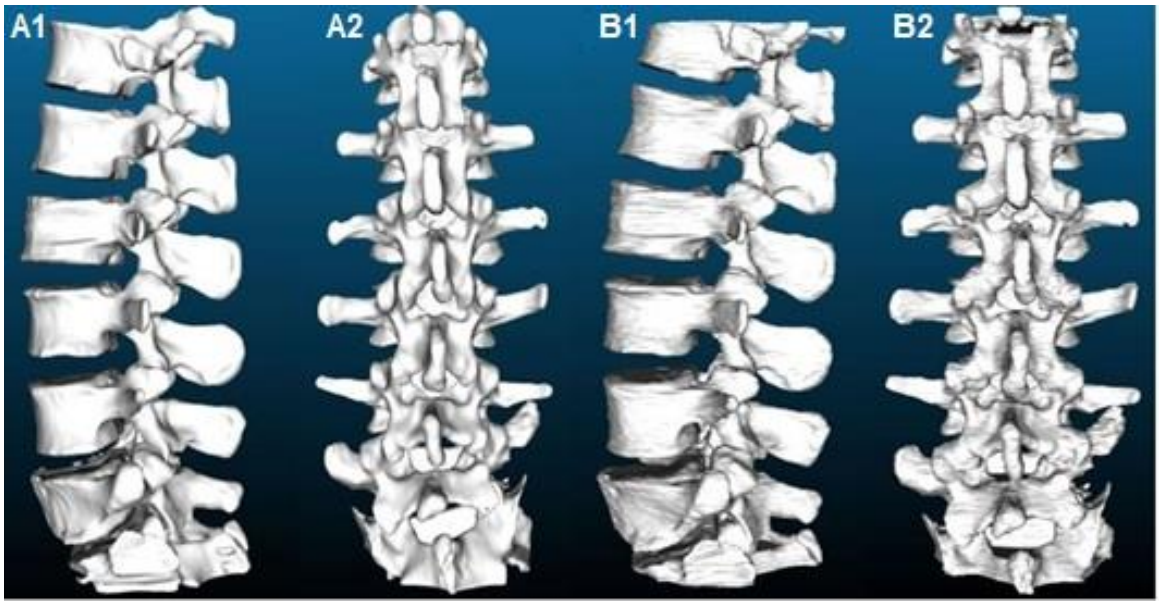

Fig. 4 The lateral view (a1) and the posterior view (a2) of a CT-scan-based 3D model. the lateral view (b1) and the posterior view (b2) of an ultrasound-based 3D model from one specimen

3.5.5 Comparison and Measurement

Reliability Procedure

The segmentation processes of the ultrasound images and CT scan images belonging to the first and second specimens were each repeated three times by the same operator. Then, using CloudCompare software (v2.12 Beta, France) all vertebrae were separated, the volumes were determined and compared to measure the intra-operator reliability of 3D reconstruction. To separate the vertebrae, since the articular processes were not easily separable between two vertebrae in ultrasound-based 3D models because of the limitations, first, CT-scan-based and ultrasound-based 3D models were aligned by picking equivalent point pairs. Then, the vertebrae in the ultrasound-based models were separated using the pattern created through the CT-scan-based models. After separating the vertebrae, the volume of each were determined.

Validation Process

After reconstructions, two validation steps were applied. Concerning the first step, using CloudCompare [22], ultrasound-based models were directly compared to the CT-scan-based models as the gold standard; in this step, all vertebrae were separated and

compared one by one. In this comparison, the distances are computed based on the nearest neighbour distance technique. It means that the software selects a point on the reference model (CT scan), then searches for the nearest point on the compared model (ultrasound), measures the direct distance (mm), and finally reports the mean of all point-to-point (mesh-to-mesh) distances as the reconstruction error. In addition, colour maps were provided in the comparison images to highlight the differences between the two models graphically.

Then, in the second step, using the same software, the volume of each vertebra was computed, the mean volumes of vertebrae were compared and the agreement between the two modelling techniques were analysed.

Correlation Measurement

Since posterior elements are the most important part of 3D reconstructions to be used in kinematic studies, the thickness of the fad pad between the skin and spinous process was considered a criterion and was measured using CT scan images. For this measurement, the image slides in which spinous processes were in the maximum length were used. Then, the correlation of the fat pad with reconstruction errors was calculated to see the effect of the fat pad on ultrasound-based 3D reconstructions.

3.5.6 Statistical Analysis

In order to assess the intra-operator reliability, intraclass correlations coefficient (ICC – 2.1 Two-Way random) on volumes measured on CT-scan- and ultrasound-based 3D bone reconstructions with 95% CI were calculated. Regarding the second step of validation, since the specimens are considered as whole samples, the limits of agreement between CT-scan- and ultrasound-based models were calculated and Bland-Altman plots were reported. Finally, the linear regression was graphed to calculate the correlation between reconstruction error and fat pad thickness. All statistical analysis was performed using SPSS software (SPSS Statistics 236 for Windows, version 28.0; IBM Corp., Armonk, NY, 237 USA).

3.6 Results

Concerning the intra-operator reliability, the intraclass correlations coefficients [95% CI] between different times of reconstructions were calculated (Table 1), and the mean intra-operator reliabilities for the CT-scan-based and the ultrasound-based models were 0.966 ± 0.014 and 0.930 ± 0.012, respectively.

Table 1 Intra-operator intraclass correlation coefficient [95% CI]

	Intra-operator	
	CT-scan-based model	Ultrasound-based model
Specimen 1	0.977 [0.898-0.997]	0.939 [0.408-0.994]
Specimen 2	0.956 [0.803-0.995]	0.922 [0.584-0.991]
Mean	0.966	0.930
SD	0.014	0.012

Concerning the verification of the validity of the ultrasound- based 3D models, first, they were directly compared with the CT-scan-based 3D models as a gold standard. In this comparison, the mean mean reconstruction errors (mm) by specimen were: 0.18 ± 0.04 for specimen 1, 0.24 ± 0.11 for specimen 2, 0.06 ± 0.15 for specimen 3, 0.04 ± 0.36 for specimen 4, 0.44 ± 0.24 for specimen 5 and 0.42 ± 0.27 for specimen 6. Moreover, the mean mean reconstruction errors (mm) by vertebra were: 0.23 ± 0.12 for L1, 0.15 ± 0.39 for L2, 0.3 ± 0.31 for L3, 0.31 ± 0.29 for L4 and 0.15 ± 0.05 for L5. The reconstruction errors of each specimen and vertebra are reported in Table 2.

Table 2 Reconstruction errors (mm) between the ultrasound-based and the CT-scan-based models. In this table, SP stands for specimen and L stands for Lumbar vertebra. The negative errors mean the compared models (ultrasound) have lower values.

	SP1 Mean error (BMI≈18)	SP2 Mean error (BMI≈19)	SP3 Mean error (BMI≈20)	SP4 Mean error (BMI≈23)	SP5Mean error (BMI≈25)	SP6 Mean Error (BMI≈26)	Mean mean error
L1	0.1±0.6	0.4±1.2	0.1±0.7	0.2±1.1	0.3±0.4	0.3±0.8	0.23±0.12
L2	0.2±0.5	0.2±0.7	0.2±0.5	-0.6±0.4	0.6±0.6	0.3±0.7	0.15±0.39
L3	0.2±0.6	0.1±0.9	-0.1±0.4	0.3±0.2	0.5±0.6	0.8±0.4	0.3±0.31
L4	0.2±0.5	0.3±0.8	-0.1±0.5	0.2±0.3	0.7±0.5	0.6±0.3	0.31±0.29
L5	0.2±0.5	0.2±0.9	0.2±0.6	0.1±0.3	0.1±0.8	0.1±0.6	0.15±0.05
Mean mean error	0.18±0.04	0.24±0.11	0.06±0.15	0.04±0.36	0.44±0.24	0.42±0.27	

Also, the graphical models indicating colormaps in the range of − 1 to 1 mm were extracted to demonstrate the comparisons (Fig. 5). one specimen's figures are presented here due to space limitations.

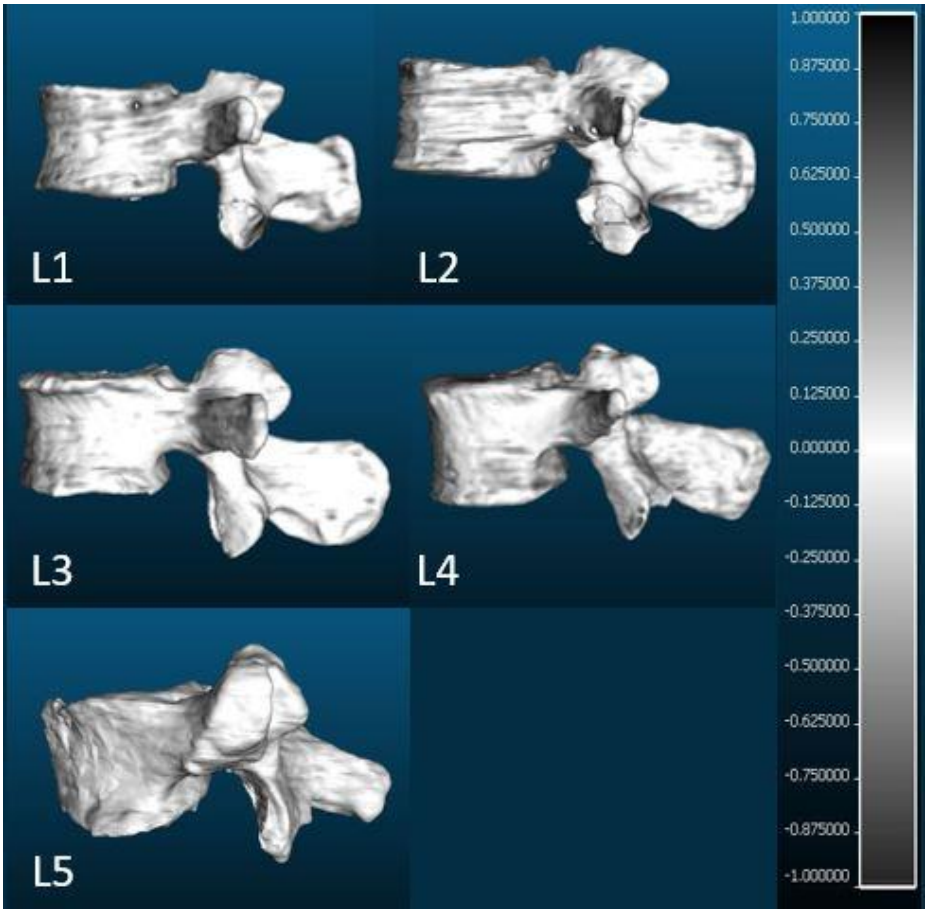

Fig. 5. Lateral views of 3D reconstructions comparative images from one specimen

In addition, as the second validation step, the volume of each vertebra was calculated in two methods separately; the mean mean volume of all vertebrae for the CT-scan-based 3D models was 55788.8 ± 1942.32 mm3 with a coefficient of variation of 3.48% and standard error of 868.63 mm3 and for the ultrasound-based 3D models was 56790.5 ± 2100.71 mm3 with a coefficient of variation of 3.69% and standard error of 939.46 mm3. The mean values are presented in Table 3. Then, considering specimens as whole samples, limits of agreement (95% ± 1.96 Sd) (Table 4) and the Bland-Altman plot (Fig. 6) between the two reconstruction techniques were obtained. The mean mean difference was 1001.7 ± 683.16 mm3.

Table 3 Mean volume, standard deviation (SD), coefficient of variation (%), and standard error (SE) of the mean of all lumbar vertebrae (L) among all specimens. All values are in mm3.

	Mean volumes from the CT-scan-based models	Mean volumes from the ultrasound-based models
L1	53040.05	54043.43
L2	55048.93	55880.85
L3	57810.2	58827.56
L4	57477.68	58981.78
L5	55567.13	56218.86
Mean	55788.8	56790.5
SD	1942.32	2100.71
CV (%)	3.48%	3.69%
SE	868.63	939.46

Table 4 Mean differences (MD), upper and lower limits of agreements (95%±1.96 Sd) for all specimens with overall vertebrae. All values are in $mm^{3.}$

	MD	Limits of agreement	
		Upper	Lower
Specimen 1	966.23	2421.74	489.22
Specimen 2	1058.84	1682.58	435.09
Specimen 3	326.62	2220.91	-1567.68
Specimen 4	145.6	2682.73	-489.22
Specimen 5	1780.34	3844.19	-283.51
Specimen 6	1732.54	3860.61	-215.53
Mean	1001.7		
SD	683.16		

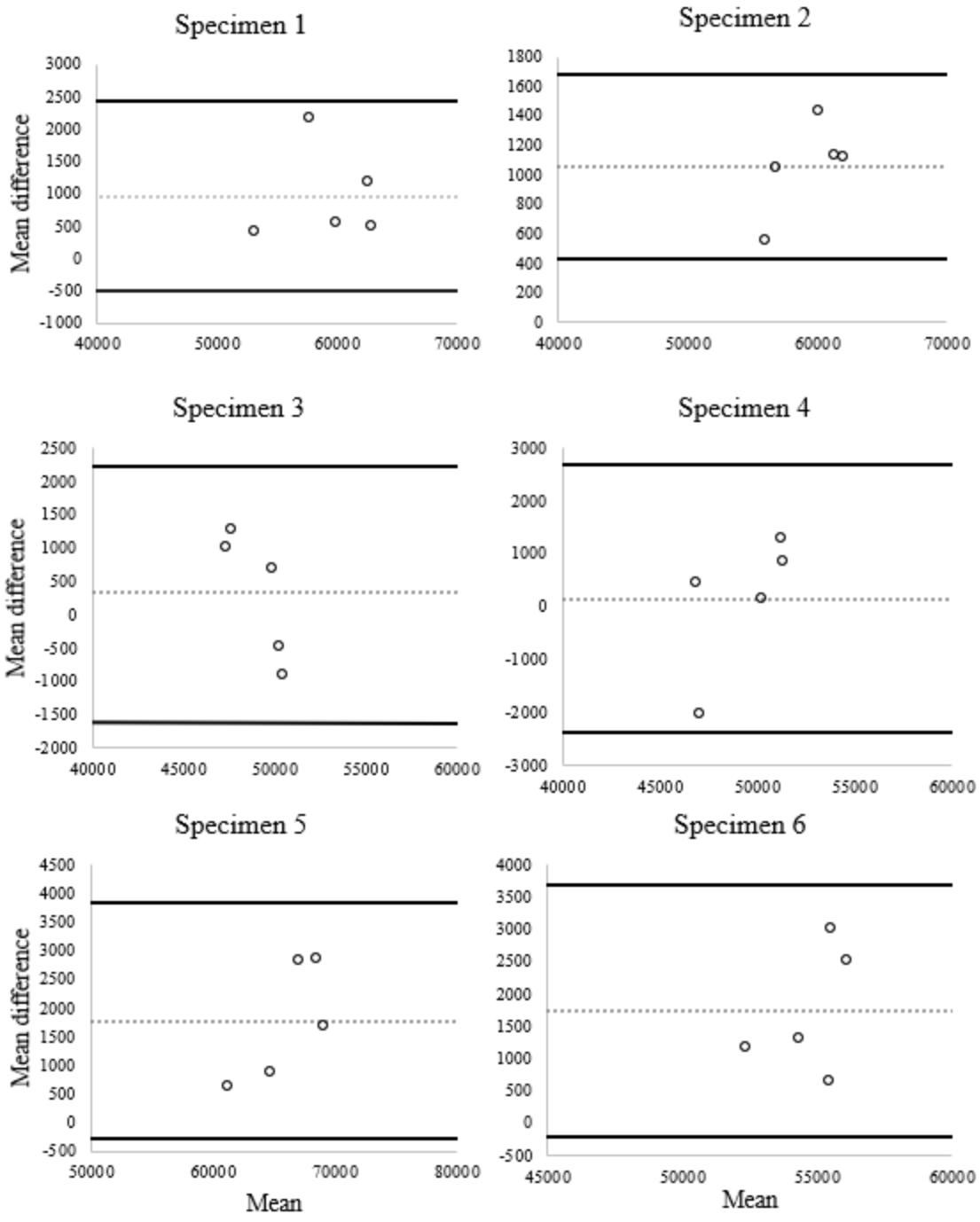

Fig. 6. Bland and Altman plots: comparisons between ultrasound-based 3D models and CT-scan-based 3D models. Dotted lines represent the mean differences and continuous lines represent the upper and lower limits of agreement. Values are reported in Table 3.

Concerning the correlation between the reconstruction error and the fat pad thickness (Table 5), the linear regression (Fig. 7) showed a correlation of R = 0.33.

Table 5. Fat pad thickness between spinous process and skin. These values were measured in the image slides in which spinous processes were in the maximum length. The letters L stand for Lumbar vertebrae. All values are in mm.

	specimen 1	specimen 2	specimen 3	specimen 4	specimen 5	specimen 6
L1	0.8	1.8	2.9	6.3	8.5	9.7
L2	0.9	1.7	2.8	6.2	8.6	9.6
L3	0.8	1.8	2.7	6.2	8.4	9.5
L4	0.8	1.9	2.9	6.5	8.4	9.7
L5	0.8	2.4	3.3	7.3	8.9	11.6

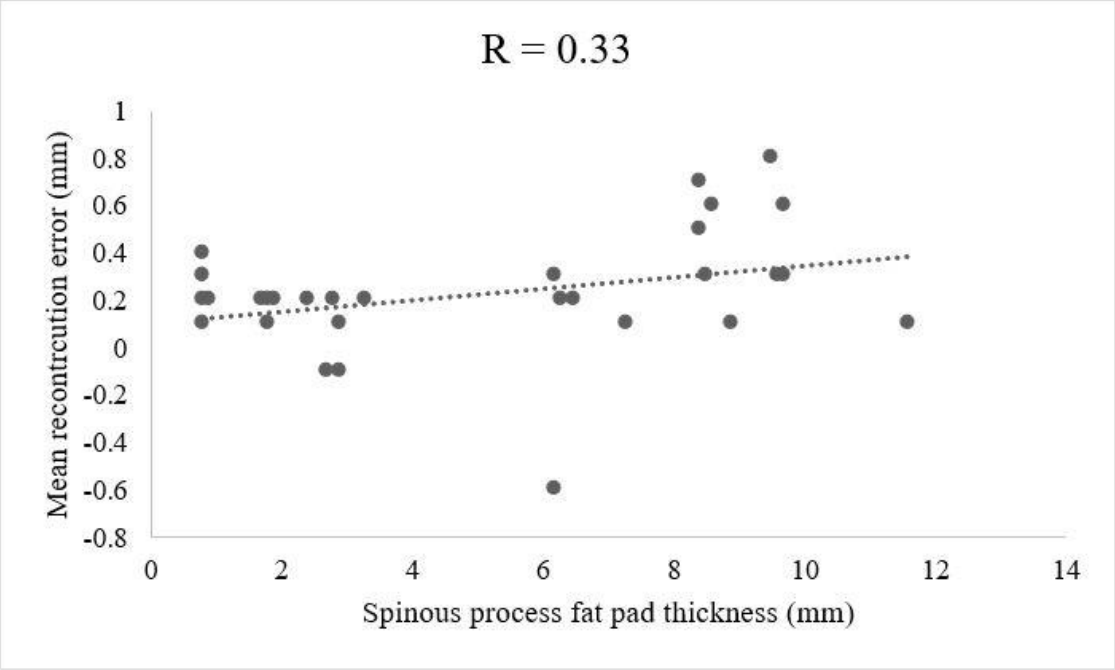

Fig. 7. Linear regression of reconstruction error and spinous process fat pad thickness

3.7 Discussion

Measuring spine kinematics is essential to analyse and diagnose the spine's movement abnormalities, such as hypermobility or hypo-mobility. Today, several methods are used to measure spine kinematics; meanwhile, clinically, it has been limited to a physical examination. Still, for 3D measurement, the method of localizing bone landmarks on the spine 3D model has been developed recently. Concerning obtaining 3D models of

the spine, two imaging modalities are mostly used: CT scan and MRI. Yet, these modalities have disadvantages as previously mentioned.

In the meantime, the ultrasound machine could act as an alternative. Therefore, the primary purpose of this study was to improve an algorithm for imaging the spine using ultrasound and converting the obtained images into 3D models. For this purpose, since an innovative technique for 3D reconstruction of a dry vertebra has been recently introduced with significant accuracy and precision [21], in this study, we tried to assess and improve this technique in the 3D reconstruction of six lumbar spines with different BMIs and fat pad thicknesses. So, in this regard, the imaging operations were experimentally performed in certain degrees, definable by Eq. (1), to cover the entire specimen and reduce the shadow. Then, since the vertebrae were covered with soft tissue, the image processing techniques were applied to enhance the quality of images and facilitate the segmentation process (Fig. 3).

After finishing the 3D reconstruction processes, two steps were introduced to verify the validity of the ultrasound- based 3D models compared to the CT-scan-based 3D models (gold standard). In the first step, using Cloud- Compare, all the vertebrae of each specimen were separated and compared one by one. In this regard, the mean mean reconstruction errors reported in Table 2 show that, globally, there is a slight overestimation for the ultrasound-based 3D models compared to the CT-scan-based 3D models. However, although there are overestimations for the ultrasound-based models, low variations between the reconstructions regarding the vertebrae sizes demonstrate the high validity of the models obtained from ultrasound. Moreover, the overestimated results in this research, in addition to being similar to the previous study [21] which was 0.44 ± 0.63 mm, have also been observed in other ultrasound-Ct scan comparative studies, like in measuring kidney stone size with an average overestimation of 3.8 ± 2.4 mm [23], and measuring aortic aneurysm diameter with an average overestimation of 0.11 ± 4.26 mm [3].

In addition, the graphical models (Fig. 5) with the related colour map in the range of -1 to 1 mm were extracted to show the differences between the two methods of reconstructions. Since in these graphical models, the vertebrae were coloured in white, and

the errors in each area were changed from white at zero to black at − 1 and 1 mm, the slight colour change in the comparative image indicates the high accuracy of ultrasound models.

Concerning the second validation step, the volumes of all vertebrae in the ultrasound- and CT-scan-based 3D models were computed and compared. Since the first validation step showed overestimations in linear distance between ultrasound-and CT-scan-based 3D models, larger volumes for ultrasound-based 3D models are expected. Therefore, based on the reported values in Table 3, the vertebrae of the ultrasound-based 3D models have higher volumes than the CT-scan-based 3D models, although the differences are insignificant considering the amounts of volumes. Also, the CVs of mean volumes coming from the same table showed the low variability of measurement for both ultrasound-based and CT-scan-based methods. In addition, considering all specimens as whole samples, the limits of agreement were calculated and plotted using the Bland-Altman method. As observed in Fig. 6, all differences were included within the limit of agreement, which indicates that the results obtained from ultrasound compared to CT scan are valid.

Concerning the intra-operator reliability, a high degree of reliability was observed between the different reconstruction times of CT-scan (0.966 ± 0.014) and ultrasound images (0.930 ± 0.012). These reliability results are similar to the previous studies [5, 21, 24–26] and showed a high consistency for the current reconstruction algorithm.

On the other hand, one of the main objectives of this study was to investigate the effect of the soft tissue of the lumbar spine on the results of reconstructions. Therefore, the soft tissue in the posterior part of the lumbar spine remained intact. Since fat tissue has the most significant effect on ultrasound, in this study, the amount of fat pad between the spinous processes and the skin was considered a criterion for examining the correlation between the fat pad thickness and reconstruction error. Based on the linear regression diagram results in Fig. 6, there is a weak correlation ($r = 0.33$) between reconstruction error and the fat pad thickness. Although there have been slightly higher errors for some of the vertebrae, the weak correlation shows that the posterior soft tissues would not significantly affect the reconstructions. Since the posterior elements are the most functional anatomical parts for the kinematic study to locate the landmarks, only posterior soft tissues were kept

intact. Otherwise, if the abdominal fat tissue in the anterior part was kept, it could make difficulties in imaging.

Regardless of all numerical data, the delicate appearance of the spinous and costiform processes in the ultrasound-based 3D models would indicate an acceptable ability of this method to be used for kinematic studies and locate bones landmarks.

As limitations of this study, as previously mentioned, the CT-scan-based 3D models were used as a pattern to separate the facet joints of vertebrae in ultrasound-based models. Although this method covers the reconstruction errors in the ultrasound-based models, the limitations are negligible since the articular processes are not considered to be used for kinematic study. The second limitation of this study was the 3D reconstruction of all around the vertebrae, which is not applicable for in-vivo kinematic study because of the abdominal fat pad and viscera. Still, since the precise localization of three landmarks is required to introduce a coordinate system and accurately measure the kinematic, the complete lumbar spines were used for this in-vitro study.

Regarding the feasibility of this method in clinical measurements, as mentioned in the limitation, although it is not practicable in the current format, the improvement of ultrasound imaging methods and 3D reconstruction of the posterior elements of the lumbar spine will make this method easily achievable for clinical measurement.

In conclusion, this study's results showed that the 3D reconstruction of the lumbar spine obtained from ultrasound images is highly similar to those obtained from CT scan images and is not significantly affected by the posterior fat pad, which makes it appropriate for kinematic studies.

Acknowledgements We thank Collège Laflèche's (Trois-Rivières, Quebec, Canada) radiology department for providing the CT scan system. We would like to give special thanks to all the people who have donated their bodies to science, as well as their families. We are also very grateful to the technicians of the anatomy laboratory where this research was conducted.

Author Contributions All authors contributed to the study conception and design. The first draft of the manuscript was written by Mohammad Reza Effatparvar, and all

authors commented on previous versions of the manuscript. All authors read and approved the final manuscript.

Funding Author Mohammad Reza Effatparvar has received research support from Fonds de recherche du Québec – Nature et Technologie (FRQNT) under grant [319993]. Author Stephane Sobczak has received research support from Natural Sciences and Engineering Research Council of Canada (NSERC) under grant [RGPIN-2016-05717].

3.8 Declarations

Conflict of interest The authors have no relevant financial or non-financial interests to disclose.

Ethical Approval This study was performed in line with the principles of the Declaration of Helsinki. Approval was granted by 'The Ethics Subcommittee of the Anatomy Laboratory for Teaching and Research' of Université du Québec à Trois-Rivières (Date: 2021/10/12- No: SCELERA 21 − 13).

3.9 References

1. Li, G., Wang, S., Passias, P., Xia, Q., Li, G., & Wood, K. (2009). Segmental in vivo vertebral motion during functional human lumbar spine activities. European Spine Journal, 18(7), 1013–1021.

2. Vania, M., Mureja, D., & Lee, D. (2019). Automatic spine segmentation from CT images using convolutional neural network via redundant generation of class labels. Journal of Computational Design and Engineering, 6(2), 224–232.

3. Han, S. M., Patel, K., Rowe, V. L., Perese, S., Bond, A., & Weaver, F. A. (2010). Ultrasound-determined diameter measurements are more accurate than axial computed tomography after endovascular aortic aneurysm repair. Journal of Vascular Surgery, 51(6), 1381–1389.

4. Huang, X., Moore, J., Guiraudon, G., Jones, D. L., Bainbridge, D., Ren, J., & Peters, T. M. (2009). Dynamic 2D ultrasound and 3D CT image registration of the beating heart. IEEE Transactions on Medical Imaging, 28(8), 1179–1189.

5. Sobczak, S., Dugailly, P. M., Gilbert, K. K., Hooper, T. L., Sizer Jr, P. S., James, C. R., & Brismée, J. M. (2016). Reliability and validation of in vitro lumbar spine height measurements using musculoskeletal ultrasound: a preliminary investigation. Journal of Back and Musculoskeletal Rehabilitation, 29(1), 171–182.

6. Wu, Y., Lu, R., Liao, S., Ding, X., Su, W., & Wei, Q. (2021). Application of ultrasound in the closed reduction and percutaneous pinning in supracondylar humeral fractures. Journal of Orthopaedic Surgery and Research, 16(1), 1–8.

7. Mhaskar, V. A., Agrahari, H., & Maheshwari, J. (2022). Ultrasound guided arthroscopic meniscus surgery. Journal of Ultrasound. https:// doi. org/ 10. 1007/ s40477- 022- 00680-5

8. Patel, M. R., Jacob, K. C., Parsons, A. W., Chavez, F. A., Ribot, M. A., Munim, M. A., Vanjani, N. N., Pawlowski, H., Prabhu, M. C., & Singh, K. (2022). Systematic Review: Applications of Intraoperative Ultrasound in Spinal Surgery. World Neurosurgery. https:// doi. org/ 10. 1016/j. wneu. 2022. 02. 130

9. Moran, M., & Myers, M. (2022). Use of ultrasonography for identification of long bone fractures. Visual Journal of Emergency Medicine, 28, 101381.

10. Champagne, N., Eadie, L., Regan, L., & Wilson, P. (2019). The effectiveness of ultrasound in the detection of fractures in adults with suspected upper or lower limb injury: A systematic review and subgroup meta-analysis. BMC Emergency Medicine, 19(1), 1–15.

11. Qadi, H., Davidson, J., Trauer, M., & Beese, R. (2020). Ultrasound of bone fractures. Ultrasound, 28(2), 118–123.

12. Vk, V., Bhoi, S., Aggarwal, P., Murmu, L. R., Agrawal, D., Kumar, A., Sinha, T. P., & Galwankar, S. (2021). Diagnostic utility of point of care ultrasound in identifying cervical spine injury in emergency settings. Australasian Journal of Ultrasound in Medicine, 24(4), 208–216.

13. Kerr, W., Rowe, P., & Pierce, S. G. (2017). Accurate 3D reconstruction of bony surfaces using ultrasonic synthetic aperture techniques for robotic knee arthroplasty. Computerized Medical Imaging and Graphics, 58, 23–32.

14. Mahfouz, M. R., Fatah, A., Johnson, E. E., J. M., & Komistek, R. D. (2021). A novel approach to 3D bone creation in minutes: 3D ultrasound. The Bone & Joint Journal, 103(6 Supple A), 81–86.

15. Gonçalves, P. J., & Torres, P. M. (2010). Registration of Bone Ultrasound Images to CT based 3D Bone Models. In 6th International Conference on Technology and Medical Sciences, Porto, Portugal (pp. 21–23).

16. Vo, Q. N., Le, L. H., & Lou, E. (2019). A semi-automatic 3D ultrasound reconstruction method to assess the true severity of adolescent idiopathic scoliosis. Medical & Biological Engineering & Computing, 57(10), 2115–2128.

17. Vo, Q. N., Lou, E. H., & Le, L. H. (2015). Measurement of axial vertebral rotation using three-dimensional ultrasound images. Scoliosis, 10(2), 1–4.

18. Vo, Q. N., Lou, E. H., & Le, L. H. (2015). 3D ultrasound imaging method to assess the true spinal deformity. In 2015 37th Annual International Conference of the IEEE Engineering in Medicine and Biology Society (EMBC) (pp. 1540–1543). IEEE.

19. Nguyen, D. V., Vo, Q. N., Le, L. H., & Lou, E. H. (2015). Validation of 3D surface reconstruction of vertebrae and spinal column using 3D ultrasound data–A pilot study. Medical Engineering & Physics, 37(2), 239–244.

20. Effatparvar, M. R., & Sobczak, S. (2022). Application of ultrasound in spine kinematic determination: A systemic review. Journal of Medical Ultrasound, 30(1), 6.

21. Forbes, A., Cantin, V., Develle, Y., Dubé, Y., Bertrand-Grenier, A., Ménard-Lebel, C., & Sobczak, S. (2021). Musculoskeletal ultrasound for 3D bone modeling: A preliminary study applied to lumbar vertebra. Journal of Back and Musculoskeletal Rehabilitation, 34(6), 937–950.

22. Fournier, G., Savall, F., Galibourg, A., Gély, L., Telmon, N., & Maret, D. (2020). Three-dimensional analysis of bitemarks: A validation study using an intraoral scanner. Forensic Science International, 309, 110198.

23. Dai, J. C., Dunmire, B., Sternberg, K. M., Liu, Z., Larson, T., Thiel, J., Chang, H. C., Harper, J. D., Bailey, M. R., & Sorensen, M. D. (2018). Retrospective comparison of measured stone size and posterior acoustic shadow width in clinical ultrasound images. World Journal of Urology, 36(5), 727–732.

24. Zheng, Y. P., Lee, T. T. Y., Lai, K. K. L., Yip, B. H. K., Zhou, G. Q., Jiang, W. W., Cheung, J. C., Wong, M. S., Ng, B. K., Cheng, J. C., & Lam, T. P. (2016). A reliability and validity study for Scolioscan: A radiation-free scoliosis assessment system using 3D ultrasound imaging. Scoliosis and Spinal Disorders, 11(1), 1–15.

25. Sayed, T., Khodaei, M., Hill, D., & Lou, E. (2022). Intra-and inter-rater reliabilities and differences of kyphotic angle measurements on ultrasound images versus radiographs for children with adolescent idiopathic scoliosis: a preliminary study. Spine Deformity, 10(3), 501–507.

26. Daniel, E. S., Lee, R. Y., & Williams, J. M. (2022). The reliability of video fluoroscopy, ultrasound imaging, magnetic resonance imaging and radiography for measurements of lumbar spine segmental range of motion in-vivo: A review. Journal of Back and Musculoskeletal Rehabilitation. https:// doi. org/ 10. 3233/ BMR- 210285

Chapter 4 – Application of Musculoskeletal Ultrasound in Lumbar Spine 3D Kinematics Visualization and Determination: An In-Vitro Study

4.1 Original Contribution of the Student and Co-authors

This fourth chapter of the thesis presents the third published article entitled *Application of Musculoskeletal Ultrasound in Lumbar Spine 3D Kinematics Visualization and Determination: An In-Vitro Study*. This article, co-authored by Mohammad Reza Effatparvar, Marc-Olivier St-Pierre, Felix-Antoine Lavoie, and Stéphane Sobczak, was published in 2025 in the *Journal of Medical and Biological Engineering* (Vol. 45: 230–239).

Effatparvar, M. R., St-Pierre, M. O., Lavoie, F. A., & Sobczak, S. (2025). Application of Musculoskeletal Ultrasound in Lumbar Spine 3D Kinematics Visualization and Determination: An In-Vitro Study. *Journal of Medical and Biological Engineering*, *45*(2), 230-239.

Application of Musculoskeletal Ultrasound in Lumbar Spine 3D Kinematics Visualization and Determination: An In-Vitro Study

Mohammad Reza Effatparvar[1,2,4*], Marc-Olivier St-Pierre[1,3,4], Felix-Antoine Lavoie[1,3,4] , Stéphane Sobczak[1,2,3,4]

1- Chaire de Recherche en Anatomie Fonctionnelle, Université du Québec à Trois-Rivières, 3351, Boulevard Des Forges, Trois-Rivieres, Québec G8Z 4M3, Canada
2- Institut National d'Anatomie (INA), Université du Québec à Trois-Rivières, Trois-Rivieres, Québec, Canada
3- Département d'anatomie, Université du Québec à Trois-Rivières, Trois-Rivières, Québec, Canada.
4- Groupe de Recherche sur les affections neuromusculosquelettiques, Université du Québec à Trois-Rivières, Trois-Rivières, Québec, Canada.

4.2 Abstract

Purpose: Determining lumbar spine 3D kinematics requires the reconstruction of medical images. Current imaging modalities, such as Computed Tomography (CT) scans and Magnetic Resonance Imaging (MRI), have limitations, including ionizing radiation and high costs. Musculoskeletal ultrasound (MSU) presents a promising alternative; however, its application in 3D kinematic analysis has not yet been reported. The aim of this study is to assess the reliability and validity of MSU-based 3D reconstruction for determining intervertebral kinematics.

Methods: Seven lumbar spines were dissected, and technical markers (TMs) were attached to the vertebrae. MSU and CT images were captured, and 3D reconstructed. Discrete motions were applied to the specimens, and the TMs were digitized. The motions were visualized on the 3D reconstructions using a visualization technique. Anatomical landmarks were identified, and reference frames were established. Intervertebral range of motion (ROM) was measured using Euler angles. Reliability was assessed through repeated measurements, and validity was evaluated by comparing the ROM results between the MSU and CT scans.

Results: The intra-operator reliability showed good (ICC = 0.89 ± 0.01) and excellent (ICC = 0.91 ± 0.01) reliability for the MSU and CT scan, respectively, with slight differences in mean detectable changes (3.23% ± 1.52% for MSU, 2.65% ± 0.75% for CT). Regarding validity, no significant mean difference was observed (− 0.23° ± 0.20°, p = 0.57) between the mean ROMs, and good agreement was found, with a mean difference of 0.22° ± 0.07° and most data points falling within limits of agreement.

Conclusion: This study confirms the accuracy and precision of 3D MSU in measuring lumbar spine range of motion, validating its use for 3D kinematic analysis and paves the way for in-vivo analysis.

Keywords: Ultrasound · Kinematics · Lumbar spine · Range of motion · CT-scan

4.3 Résumé

Objectif : La détermination de la cinématique 3D de la colonne lombaire nécessite la reconstruction d'images médicales. Les modalités d'imagerie actuelles, telles que la tomodensitométrie (CT) et l'imagerie par résonance magnétique (IRM), présentent des limites, notamment une exposition aux radiations ionisantes et des coûts élevés. L'échographie musculosquelettique (MSU) constitue une alternative prometteuse ; cependant, son application dans l'analyse cinématique 3D n'a pas encore été rapportée. Cette étude vise à évaluer la fiabilité et la validité de la reconstruction 3D basée sur la MSU pour la détermination de la cinématique intervertébrale.

Méthodes : Sept colonnes lombaires ont été disséquées et des marqueurs techniques (MTs) ont été fixés aux vertèbres. Des images MSU et CT ont été acquises et reconstruites en 3D. Des mouvements discrets ont été appliqués aux spécimens et les MTs ont été numérisés. La visualisation des mouvements sur les reconstructions 3D a été réalisée à l'aide d'une technique spécifique. Les repères anatomiques ont été identifiés et des référentiels anatomiques établis. L'amplitude de mouvement intervertébrale (ROM) a été mesurée à l'aide des angles d'Euler. La fiabilité a été évaluée par des mesures répétées et la validité par la comparaison des résultats de ROM entre MSU et CT.

Résultats : La fiabilité intra-opérateur était bonne (ICC = 0,89 ± 0,01) pour la MSU et excellente (ICC = 0,91 ± 0,01) pour le CT, avec de légères différences dans les changements détectables moyens (3,23 % ± 1,52 % pour la MSU et 2,65 % ± 0,75 % pour le CT). Concernant la validité, aucune différence significative n'a été observée entre les ROMs moyens (−0,23° ± 0,20°, p = 0,57), avec une bonne concordance (différence moyenne de 0,22° ± 0,07°) et la plupart des points de données situés dans les limites d'accord.

Conclusion : Cette étude confirme la précision et l'exactitude de la MSU 3D pour la mesure de l'amplitude de mouvement de la colonne lombaire, validant son utilisation pour l'analyse cinématique 3D et ouvrant la voie à une application in-vivo.

Mots-clés : Échographie · Cinématique · Colonne lombaire · Amplitude de mouvement · Tomodensitométrie

4.4 Introduction

Determining lumbar spine intervertebral three-dimensional (3D) kinematics requires associating 3D anatomical reference frames (ARF), local reference frames, with the vertebrae. These frames are fixed to the vertebrae and move accordingly [1]. Mathematical methods [2] are then used to measure the displacement of the anatomical reference frames (ARF), representing the motion of each vertebra [3]. Establishing these ARFs can be challenging, because it requires identifying at least three anatomical landmarks (ALs) [4, 5]. Accuracy in this process is crucial as errors in landmark localization can lead to the misorientation of ARFs, resulting in altered joint displacement and increase in angular (rotation) and linear (translation) displacements [6–8].

Medical imaging is the primary method for identifying ALs because it provides sufficient morphological data. Landmark selection in this method is achieved through image processing techniques, known as virtual palpation (mouse click). However, 3D image reconstruction is necessary to identify at least three ALs. Consequently, 2D modalities like radiography and fluoroscopy, despite their ability to capture discrete or continuous motions in various positions, are limited to 2D kinematic determinations [9, 10]. Recent advancements like roentgen stereophotogrammetry [11] and biplanar radiography (EOS) [12] address these issues but involve the use of X-rays, leading to radiation exposure. Computed Tomography (CT) scan [13] and Magnetic resonance imaging (MRI) [14], as the leading 3D imaging modalities, offer high quality 3D reconstructions. Nonetheless, CT scan also involves radiation exposure, MRI is expensive, and both are generally limited to static imaging in the supine position [4].

Musculoskeletal ultrasound (MSU) stands out among imaging modalities as an important alternative due to its affordability, accessibility, and minimal harmful effects [15]. Recently, many innovative applications of MSU have been introduced, such as fracture determination [16], fracture reduction [17], arthroscopic surgeries [18] and tumor border delineation [19]. MSU has also been used in lumbar spine kinematics determination, but this application has so far been limited to 2D measurements [20]. This limitation arises from the lack of 3D reconstruction and the restriction of virtual palpation to a maximum of two ALs within a single anatomical plane, such as in measuring lumbar flexion– extension

by assessing changes in interspinous distance and angle using two ALs per vertebra [21, 22]. Although novel 3D ultrasound reconstruction methods, employing either manual or AI-based segmentation, have recently been introduced [23–25], their validity for accurately identifying ALs in kinematic assessments has not yet been verified, highlighting a gap in the field.

To address this gap, a newly introduced in-vitro MSU 3D reconstruction technique [26], developed and validated against CT scan 3D reconstruction with an overestimation error of 0.44 ± 0.24 mm for ultrasound [27], was applied in this study. The two main objectives are: (1) to verify the reliability of the MSU 3D reconstructions in determining the intervertebral range of motion (ROM), and (2) to assess the validity of the MSU 3D reconstructions in determining intervertebral ROM compared to those from CT scan.

4.5 Materials and Methods

4.5.1 Specimen Preparation

Seven lumbar spines (T12-S2) were isolated from thawed human cadavers, aged between 64 to 83 years (Mean = 75.28, SD = 6.62). Following the initial specimen preparation as previously described [27], small incisions were made on the skin, and semi-spherical holes were created in the spinous processes and distal end of the costiform processes of L1 to L5, as well as in the spinous process and adjacent to the protruding surface of the lateral crests of S1. The bony surfaces were cleaned with acetone and three spherical technical polypropylene markers (TMs), each with a diameter of 4.5 mm, were glued using cyanoacrylate glue. These TMs were necessary for creating a link between imaging and motion, a technique known as motion visualization, which allows for the visualization of recorded passive motions on the 3D reconstructions coming from medical images [28].

4.5.2 Pre-Imaging Specimen Preparation

Two orthopedic Schanz screws were inserted through all vertebral bodies in the specimens' anatomical position to prevent intervertebral displacement. The specimens were placed inside a plastic cylinder frame (diameter = 165 mm), and the frame was filled with porcine gelatin (Gelatine, Type A, Pork Skin, min. Bloom 225). The setup was stored

in a refrigerator to allow the gelatin to harden. After the gelatin set, the specimens were securely fixed within a Computer Assisted Mechanical (CAM) frame [26], specifically designed to facilitate ultrasound imaging and kinematic analysis.

4.5.3 MSU Imaging

MSU imaging was performed with a linear probe (General Electric, 12L-RS) of an ultrasound machine (Next- Gen LOGIQ e Ultrasound, General Electric Healthcare, USA—Mode = Musculoskeletal, Frequency = 8.0 MHz, Distance = 8 cm, Gain = 76). The probe was mounted on the mobile plate inside CAM, which moved up and down along the specimen at a velocity of 0.5 mm/s. This plate was driven by a stepper motor and was manually rotated at intervals of 30–40 degrees [27].

4.5.4 CT Scan Imaging

CT scan images were acquired (GE Healthcare, Revolution EVO; reconstruction parameters: Slice thickness = 0.5 mm, inter-slice spacing = 0.625 mm; image format: DICOM), with the specimens kept within the CAM and positioned identically to the MSU imaging.

4.5.5 Image Processing and Segmentation

The collected MSU and CT scan images of the specimens in their anatomical positions were reconstructed in 3D. For the MSU images, the previously mentioned algorithm was applied, and the images were fused into a 360-degree series using MATLAB [27]. Then, the MSU and CT scan images were separately segmented using Amira software (5.2.2®, Germany) (Fig. 1). For the MSU images, despite the possibility of full segmentation [27], only the posterior key elements of the lumbar spine, crucial for virtual palpation and defining ARFs, were manually segmented. This approach improves efficiency and reduces time consumption.

During the segmentations, along with the bone surfaces, the TMs were also segmented separately. After completing the 3D reconstructions, Blender Software (Version 3.3, Netherlands) was used to determine the coordinates of the TMs. centroids in the 3D reconstructions for both the MSU and CT scan.

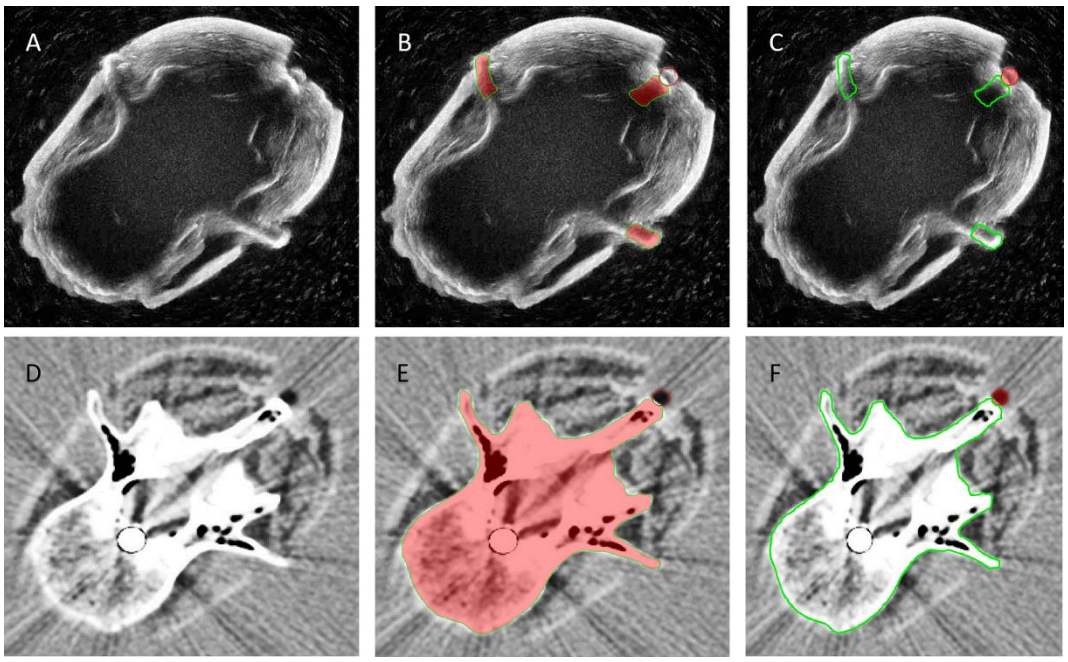

Fig. 1 Segmentation process for MSU and CT scan images of the same cross-section. **A, B, C** show an MSU image before segmentation, with bone and TM segmentation highlighted, respectively. **D, E, F** show a CT scan image before segmentation, with bone and TM segmentation highlighted, respectively

4.5.6 Applying Discrete Motions

After imaging, the gelatin and primary Schanz screws were removed. Then, a vertical threaded rod connected to T12 within the CAM was used to apply a series of motions, including maximum and mid-range flexion/extension, maximum and mid-range right and left side bending, and maximum right and left axial rotations.

To standardize these motions across all cadavers, the maximum ROM for the first cadaver was manually reached and marked in flexion/extension, side bending, and axial rotation. A sandbag loading system was subsequently employed to determine the weights needed to replicate these maximum positions: 800 g for full flexion, 680 g for full extension, 750 g for side bending, and 350 g for axial rotation. Half of these weights were used to achieve mid-maximum ROMs, and the same weights were consistently applied to all cadavers.

Once each specimen was positioned as intended, it was locked in place, and the centroids of the TMs were digitized using a 3D digitizer (Hexagon Absolute Arm, with a measurement error of 0.008 mm) (Fig. 2).

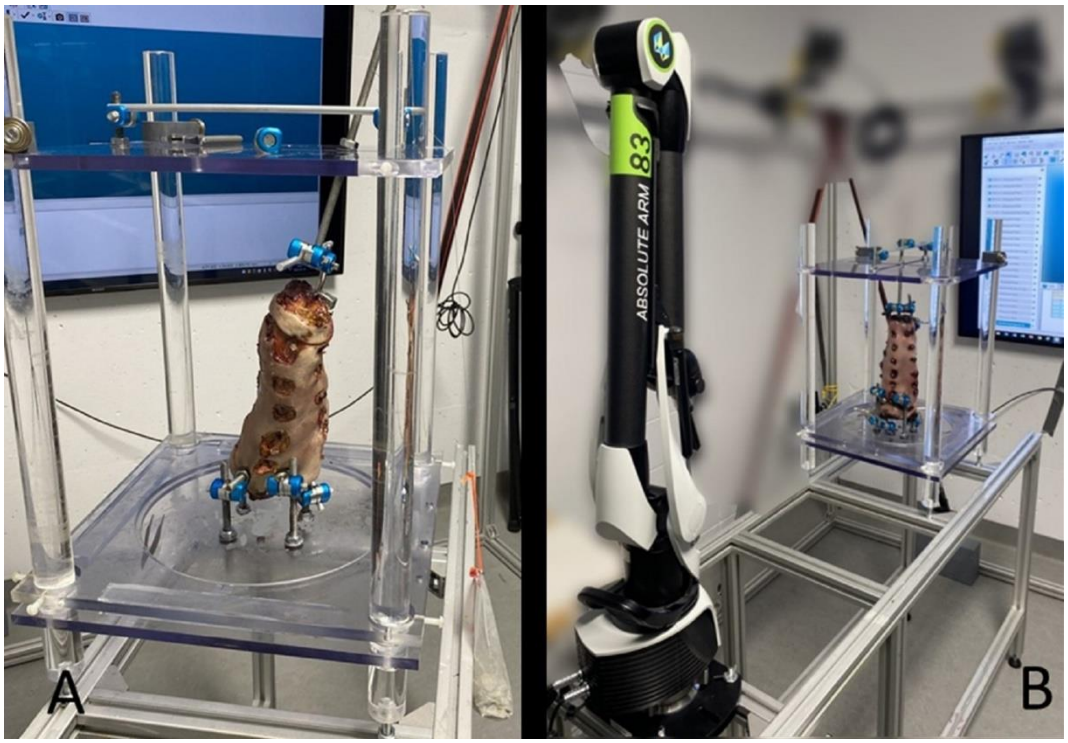

Fig. 2 A A specimen positioned in the CAM frame during discrete motion application. **B** The 3D digitizer mounted on a table in front of the specimen for centroid digitization

4.5.7 Motion Visualization by Registration Procedure

The digitization of the TMs provided their centroid coordinates within the digitizer coordinate system, which was used to establish local reference frames for each vertebra. These local frames are referred to here as technical reference frames (TRFs). Transformation matrices of the TRFs were calculated to represent the applied motions on the specimens.

Additionally, segmentation of the TMs provided their centroid coordinates within the MSU and CT scan coordinate systems, enabling TRFs to be established on the 3D reconstructions as well.

By applying the calculated transformation matrices to the TRFs of the 3D reconstructions, the actual motions were visualized on the 3D reconstructions. This

approach, known as motion visualization by registration of transformation matrices, was implemented in LhpFusionBox software [29] (ULB, Belgium), a tool specifically developed for kinematic studies.

4.5.8 Definition of Anatomical Reference Frames

After visualizing the motions on the 3D reconstructions, ALs were selected by clicking on the target surface using the landmark detection feature in LhpFusionBox (Fig. 3). For vertebrae L1 to L5, ALs were defined at the most distal ends of the costiform processes and the superior, posterior ends of the spinous processes. For S1, ALs were placed at the posterior ends of the median crests and the most protruding points of the lateral crests. The ARFs were then established in accordance with the guidelines of the International Society of Biomechanics (ISB) [30]. The Z-axis was oriented between the ALs on the right and left costiform processes, while the X-axis was set as an orthogonal axis to the Z-axis, intersecting the AL on the spinous process. The Y-axis was defined as the third axis, perpendicular to both the X- and Z-axes (Fig. 3).

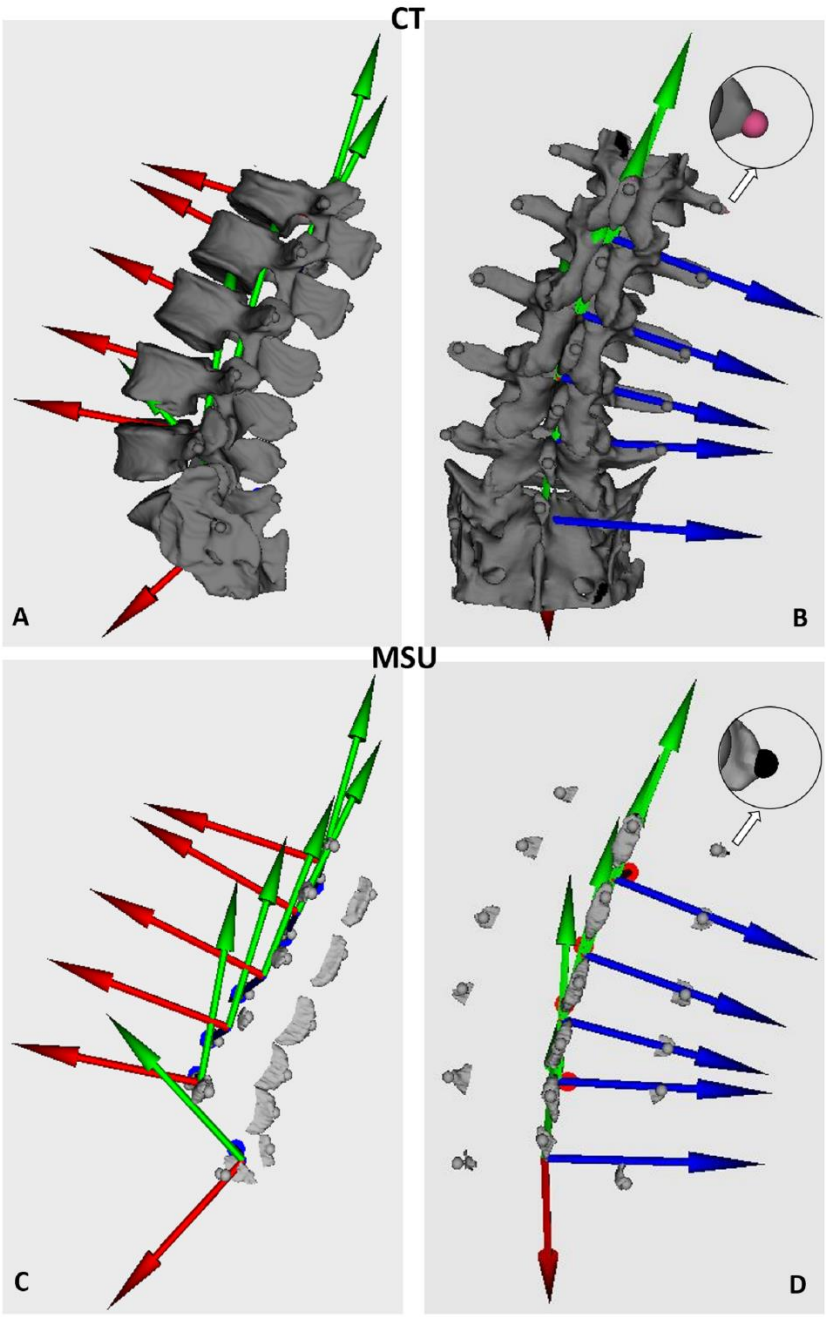

Fig. 3 ARFs established on vertebrae in CT scan (**A, B**) and MSU (**C, D**) models. (**A, C**) show the specimen in full extension; (**B, D**) show it in full right bending. The reference frame for L1 is hidden in (**B, D**) to magnify an AL on the costiform process

4.5.9 ROM Measurement

The intervertebral ROMs were measured by extracting the Euler angles between the ARFs, using the Euler sequences recommended by ISB. The anatomical motion

components, including the flexion–extension, side bending and axial rotation, were defined around the Z, X and Y-axes, respectively.

4.5.10 Reliability and Validity

For intra-operator reliability, all procedures, from applying the discrete motions to measuring the ROMs, were repeated three times for two specimens. A reliability test was then performed on the intervertebral ROM results obtained from both the MSU and CT scan. Additionally, using reliability data, the minimal detectable changes (MDCs) were calculated.

To assess the validity of the ROMs from MSU, their mean values, limits of agreement, and motion patterns were compared with the ones from CT scan (gold standard).

4.5.11 Orientation Error

The determination of intervertebral kinematics is highly sensitive to the initial orientation of the ARFs. To calculate the orientation error in the MSU, the initial orientation differences between the ARFs of the MSU and CT scan were computed and compared. To evaluate the impact of these orientation errors on ROM measurements, a correlation analysis was conducted between the mean orientation errors and the mean ROM differences. Because negative values represent directional differences within the coordinate system rather than error magnitude, absolute values were used (mean of |x|, |y|, and |z|) to prevent underestimation of the mean error.

4.5.12 Statistical Analysis

The intra-operator reliability was tested using the Intraclass Correlation Coefficient (ICC–2,1). For the validity assessment, after confirming normality with the Kolmogorov–Smirnov test, the t-test (for equality of variance using Levene's test) and Bland–Altman plots were employed to compare the means and the limits of agreement between MSU and CT scan, with each vertebral level considered as a distinct sample (Fig. 4). Polynomial trendlines were used to graph the motion patterns based on the mean ROMs (Fig. 5). The Pearson correlation test was applied to evaluate the correlation between orientation errors

and mean ROM differences. All statistical analyses were conducted using SPSS software (SPSS Statistics 236 for Windows, version 28.0; IBM Corp., Armonk, NY, USA).

4.6 Results

Concerning the reliability, the mean intra-operator reliability (95% CI) of specimen 1 (0.90 [0.78–0.99]) and specimen 2 (0.88 [0.81–0.96]) was 0.89 ± 0.01 for MSU, and the mean intra-operator reliability of specimen 1 (0.92 [0.84–0.96]) and specimen 2 (0.90 [0.86–0.97]) was 0.91 ± 0.01 for CT scan. Based on the results from the reliability test, the mean MDC % of specimen 1 (2.16% ± 1.63%) and specimen 2 (4.31% ± 3.79%) was 3.23% ± 1.52% for MSU, and the mean MDC of specimen 1 (2.12% ± 1.39%) and specimen 2 (3.19% ± 3.03%) was 2.65% ± 0.75% for CT-scan.

Concerning the validity, the mean ROM (Table 1) across all motions for all specimens was 4.14° ± 0.72° for MSU and 3.91° ± 0.70° for CT scan, resulting in a mean difference of − 0.23° ± 0.20° (p = 0.57) (Table 2). According to the Bland–Altman plots, most of the ROM values fell within the limits of agreement (95% CI, ± 1.96 SD), with an overall mean difference of − 0.22° ± 0.07° between the two methods (Fig. 4). Additionally, the polynomial graph showed similar trendlines for motion patterns between the MSU and CT scan methods (Fig. 5).

Table 1 ROMs of each vertebral level. SP stands for specimen

		L1-L2		L2-L3		L3-L4		L4-L5		L5-S1		Mean ± SD	
		CT	MSU	CT	MSU	CT	MSU	CT	MSU	CT	MSU	CT	MSU
SP1	Flex-Ext	1.07	0.97	2.77	2.6	4.48	5.03	7.57	8.41	7.38	8.15	4.65±2.84	5.03±3.30
	Side bend	2.04	2.26	4.83	5.33	7.74	8.52	8.08	8.84	4.5	5.08	5.44±2.50	6.01±2.72
	Axial rot	0.9	0.79	2.49	2.82	3.1	3.77	3.76	3.98	1.89	2.13	2.43±1.10	2.70±1.30
SP2	Flex-Ext	2.22	2.86	0.87	0.97	3.46	3.74	3.14	3.76	3.6	3.96	2.66±1.13	3.06±1.24
	Side bend	1.47	1.94	0.61	0.7	4.65	4.93	7.01	7.91	6.17	6.55	3.98±2.83	4.41±3.04
	Axial rot	2.1	2.54	0.58	0.77	3.21	3.78	4.44	4.34	3.44	3.84	2.75±1.47	3.05±1.44
SP3	Flex-Ext	5.42	5.19	4.58	4.45	5	5.17	9.92	9.03	1.63	1.88	5.31±2.98	5.14±2.56
	Side bend	3.94	3.58	5.82	5.94	8.14	8.25	7.84	7.19	3.99	3.67	5.95±2.02	5.73±2.09
	Axial rot	1.59	1.49	0.48	0.48	2.66	2.49	4.49	4.25	0.39	0.42	1.92±1.71	1.83±1.60
SP4	Flex-Ext	3.02	3.99	3.46	3.88	3.24	3.96	7.12	7.9	7.76	7.08	4.92±2.32	5.36±1.96
	Side bend	4.67	4.5	5.47	5.56	6.91	6.14	6.43	6.33	3.12	2.9	5.32±1.50	5.09±1.41
	Axial rot	3.87	4.11	3.65	3.87	4.15	4.86	4.03	4.69	1.43	1.54	3.43±1.13	3.81±1.33
SP5	Flex-Ext	7.66	7.39	5.01	5.13	8.73	8.31	6.55	6.68	0.51	0.24	5.69±3.21	5.55±3.19
	Side bend	1.48	2.66	4.76	5	7.25	7.86	7.11	7.91	0.47	0.53	4.21±3.14	4.79±3.24
	Axial rot	0.32	0.55	0.98	1.56	1.39	1.96	1.23	1.94	0.61	0.87	0.91±0.44	1.38±0.64
SP6	Flex-Ext	2.43	1.78	4.83	4.59	5.95	5.41	5.77	5.85	5.55	5.45	4.91±1.45	4.62±1.65
	Side bend	2.33	2.76	3.2	3.57	1.03	1.55	4.56	4.82	5.38	5.73	3.30±1.73	3.69±1.65
	Axial rot	0.41	0.66	0.65	0.72	0.49	0.53	0.45	0.83	0.8	1.16	0.56±0.16	0.78±0.24
SP7	Flex-Ext	6.18	6.62	4.55	4.93	5.3	5.83	6.41	6.76	7.11	7.74	5.91±1.00	6.38±1.06
	Side bend	3.78	3.93	6.17	6.74	5.52	5.38	4.06	4.62	4.38	4.76	4.78±1.02	5.09±1.06
	Axial rot	3.65	3.94	2.65	2.61	3.13	3.82	2.96	3.91	4.75	4.56	3.43±0.82	3.77±0.71
Mean ± SD	Flex-Ext	4.00±2.43	4.11±2.42	3.72±1.50	3.79±1.50	5.17±1.85	5.35±1.51	6.64±2.04	6.91±1.77	4.79±2.92	4.93±3.04		
	Side bend	2.82±1.30	3.09±0.93	4.41±1.93	4.69±2.01	5.89±2.47	6.09±2.46	6.44±1.56	6.80±1.62	4.00±1.84	4.17±2.02		
	Axial rot	1.83±1.46	2.01±1.53	1.64±1.27	1.83±1.29	2.59±1.24	3.03±1.46	3.05±1.61	3.42±1.45	1.90±1.63	2.07±1.56		

Table 2 The Mean difference between MSU and CT scan results. The negative mean difference indicates a higher value for the MSU. SP stands for specimen. All values are in degree.

	CT		MSU		*t-Test*	
	Mean	SD	Mean	SD		*Mean difference*
SP1	4.17	2.48	4.57	2.78	*0.67*	-0.40
SP2	3.13	1.91	3.50	2.02	*0.60*	-0.37
SP3	4.39	2.80	4.23	2.64	*0.87*	0.16
SP4	4.55	1.80	4.75	1.63	*0.75*	-0.20
SP5	3.60	3.17	3.90	3.08	*0.79*	-0.30
SP6	2.92	2.21	3.02	2.10	*0.89*	-0.10
SP7	4.70	1.37	5.07	1.41	*0.47*	-0.37
Mean	3.91	0.70	4.14	0.72		*
*Mean mean difference = -0.23 ± 0.20 (p = 0.57)						

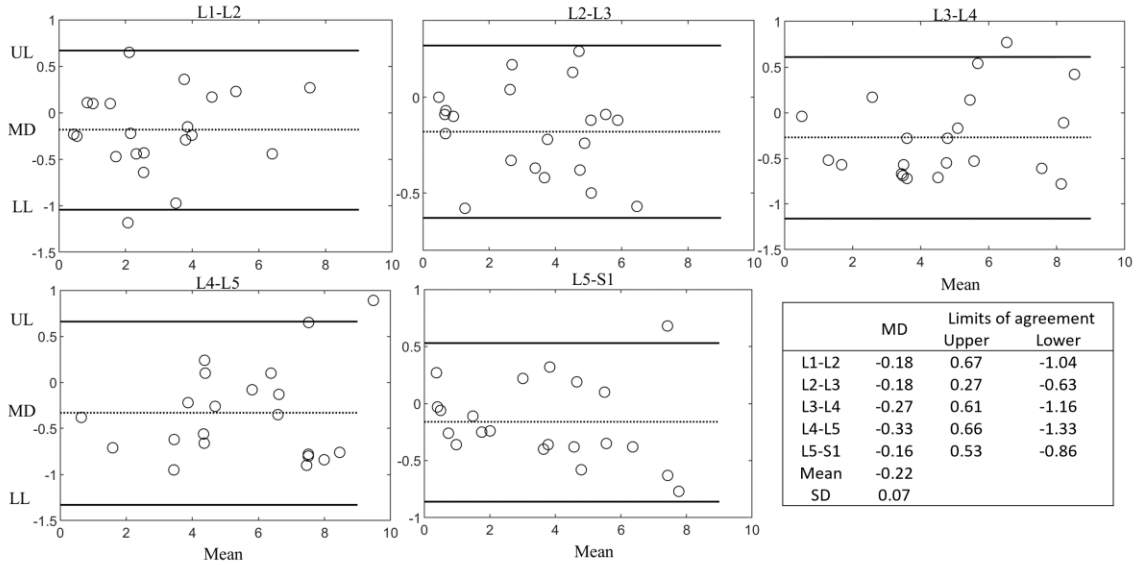

Fig4 Bland-Altman plots showing the limits of agreement between the MSU and CT scan. Mean differences are represented by dotted lines, and upper and lower limits of agreement by solid lines. A table in the bottom right corner presents the mean differences (MD), upper and lower limits of agreement (95% CI, ±1.96 SD) for the ROMs at all vertebral levels across all specimens. All values are in degrees.

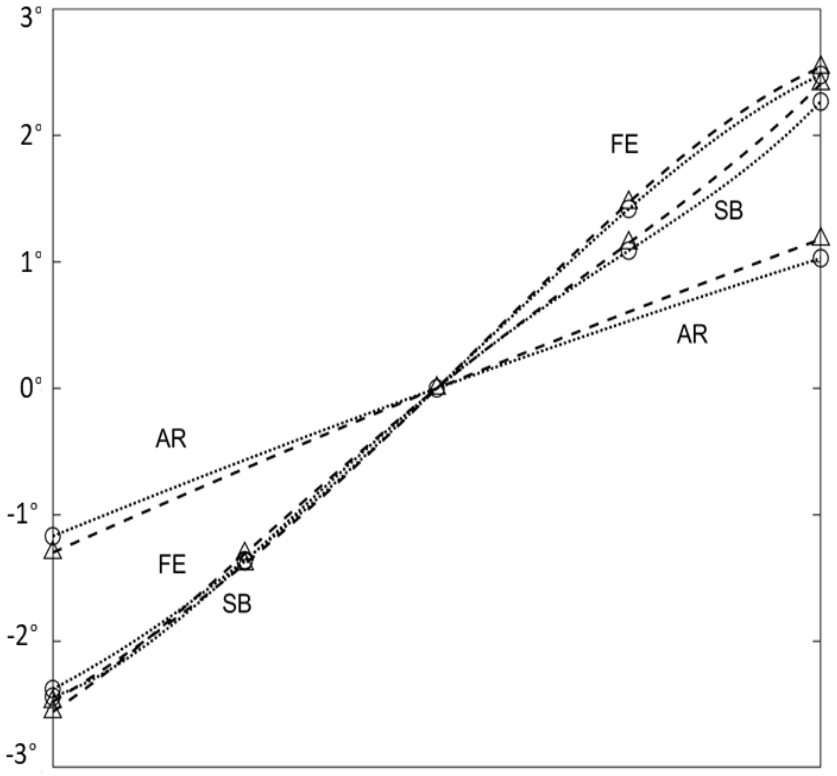

Fig5 Motion patterns based on the mean ROM of all specimens, featuring a fourth-order polynomial trendline for flexion-extension (FE) and side bending (SB), and a second-order polynomial trendline for axial rotation (AR). For flexion-extension and side bending, markers indicate the neutral, maximum, and mid positions; for axial rotation, markers indicate only the neutral and maximum positions. Dotted lines with circular markers represent the results from CT scans model, while dashed lines with triangular markers represent the results from MSU model. All values are in degrees.

Concerning the orientation error, the mean difference of the initial orientation of the ARFs between the MSU and CT scan was − 0.49 ± 0.26°, 0.92 ± 0.23°, and − 0.92 ± 0.17°, for the X, Y, and Z respectively (Table 3). Additionally, the Pearson correlation test showed a correlation of r = − 0.85 between the mean orientation errors and the mean ROM differences.

Table 3 Orientation errors for the ARFs. The negative mean differences indicate a higher value for the MSU. SP stands for specimens. All values are in degree.

	Mean difference		
	X	Y	Z
SP1	-0.65	0.99	-1.15
SP2	-0.69	1.19	-1.00
SP3	-0.17	0.69	-0.74
SP4	-0.35	0.80	-0.85
SP5	-0.42	0.91	-0.86
SP6	-0.25	0.64	-0.74
SP7	-0.87	1.22	-1.11
Mean	-0.49	0.92	-0.92
SD	0.26	0.23	0.17

4.7 Discussion

3D reconstruction of medical images is essential for establishing 3D ARFs in kinematic analysis [31]. Conventional imaging modalities such as radiography, fluoroscopy, CT scans, and MRI have limitations for this purpose, including radiation exposure, high costs, and the requirement for patients to be in supine positions [4]. In contrast, MSU imaging as a viable alternative with fewer drawbacks has recently been applied for 3D reconstruction using various techniques. While the validity of these reconstructions has been verified for different objectives [24, 32], their precision and accuracy in determining lumbar spine kinematics have not yet been confirmed [20]. This study aimed to assess the reliability and validity of 3D reconstructions of MSU images for determining lumbar intervertebral kinematics, providing insights into the clinical potential of MSU for kinematic analysis.

The intra-operator reliability results showed a good and excellent consistency for MSU (0.89 ± 0.01) and CT scan (0.91 ± 0.01), respectively, supporting MSU's reliability as a measurement tool for lumbar spine motion. These values are comparable to previous studies involving the reconstruction of single vertebrae (ICC = 0.97 ± 0.03 [26] and complete lumbar spines (ICC = 0.93 ± 0.01) [27], indicating that MSU offers similar precision for intervertebral ROM measurement. The mean MDC [33] for both MSU and CT scans were also in agreement, which further underscores the high precision of MSU

measurements. The relatively low MDC values demonstrate that MSU can reliably capture intervertebral ROM with minimal measurement error, comparable to CT scans. Despite some variability at specific vertebral levels, such as L2-L3 in specimen two, the low MDC results indicate that MSU is a viable and precise tool for assessing intervertebral ROM. This is particularly important for clinical applications requiring accurate diagnoses and informed treatment planning for patients with lumbar spine issues [34].

Regarding the validity of the ROM results from MSU, the *t*-test indicated no significant difference ($p = 0.57 > 0.05$) compared to CT scan results. However, the ROMs from MSU showed a slight overestimation ($-0.23° \pm 0.20°$), likely due to the previously noted overestimation in 3D MSU reconstructions relative to CT scan [27]. Similarly, the matching motion patterns across vertebral levels (Fig. 5) support the correspondence between the two methods. Additionally, Bland–Altman plots demonstrated good agreement, with mean differences near zero and most data points within narrow limits of agreement.

Additionally, the Pearson correlation ($r = -0.85$) between orientation errors and ROM differences highlights the role of accurate AL identification in the precision of 3D reconstructions. While orientation errors slightly impacted the results, they did not significantly affect the overall kinematic measurements ($p > 0.05$). This finding underscores that, despite minor technical challenges, MSU could provide clinically meaningful data comparable to CT scans for lumbar spine kinematics [35].

The originality of this study and the absence of identical methodologies limit the possibility of direct comparisons of our results with those of previous studies. However, reports on 2D lumbar spine kinematics determination using ultrasound imaging have demonstrated its high validity and accuracy. For instance, ultrasound has shown mean absolute differences ranging from 0.67 to 2.1° when compared with a digital camcorder and fluoroscopy [22]. Additionally, it has exhibited an extremely low absolute error of 0.01° in comparison with optical tracking [36], and a measurement error of only 1.3 mm when compared to MRI [21]. In contrast, traditional methods such as fluoroscopy and radiography are often limited by their 2D nature and the risks associated with ionizing radiation. Fluoroscopy, while enabling real-time imaging, only captures limited

movements within the sagittal and coronal planes and may lead to increased radiation exposure during extended procedures [37]. MRI, although offering superior soft tissue contrast and 3D imaging capabilities, is typically limited to static imaging and requires expensive equipment, making it less accessible for kinematic studies [14]. Ultrasound, on the other hand, offers a non-invasive, radiation-free alternative that not only provides comparable accuracy but also has the advantage of real-time assessment of intervertebral motion. These comparisons underscore the potential of ultrasound as a more accessible and safer tool for evaluating lumbar spine kinematics, with the added benefit of offering high precision without the drawbacks of other imaging methods. Regarding the kinematic results measured in this study, all specimens were from elderly individuals, and no pre-screening limitations were applied to evaluate the cadavers beforehand, as the primary objective was to compare MSU and CT scan methodologies. Nonetheless, the mean results align closely with previously reported kinematics in older populations [38, 39].

The main limitation of this study involves the MSU image collection technique, which requires rotation around the specimens. However, as the primary focus of this study was to verify the capacity of MSU 3D reconstruction in providing precise and accurate ALs for kinematic determinations, the in-vitro imaging method was considered appropriate for the intended purpose. Future studies should aim to refine the image acquisition process for in-vivo applications, enhancing its clinical applicability.

In summary, this study demonstrated the reliability and validity of the kinematic determination using the 3D reconstruction of MSU images. The potential development of MSU 3D reconstructions for in-vivo applications, along with its other advantages, could significantly improve assessment procedures. This positions MSU as an ideal alternative for regular monitoring in the diagnosis and rehabilitation of movement-related lower back pain.

Acknowledgements We extend our special thanks to the individuals who generously donated their bodies to science, enabling us to advance our understanding in the field. We also wish to express our sincere thanks to the technicians in the anatomy laboratory for their invaluable assistance throughout the study.

Author Contributions All authors contributed to the study conception and design. Material preparation, data collection and analysis were performed by Mohammad Reza Effatparvar, Marc-Olivier St-Pierre, Félix-Antoine Lavoie and Stéphane Sobczak. The first draft of the manuscript was written by Mohammad Reza Effatparvar, and all authors commented on previous versions of the manuscript. All authors read and approved the final manuscript.

Funding Author Mohammad Reza Effatparvar received research support from Fonds de recherche du Québec—Nature et Technologie (FRQNT) under the grant [319993]. Author Stephane Sobczak received research support from Natural Sciences and Engineering Research Council of Canada (NSERC) under the grant [RGPIN-2016–05717].

Declarations Competing Interests The authors have no relevant financial or nonfinancial interests to disclose.

Ethical Approval This study was performed in line with the principles of the Declaration of Helsinki. Approval was granted by 'The Ethics Subcommittee of the Anatomy Laboratory for Teaching and Research' of Université du Québec à Trois-Rivières (Date: 2022/12/10 No: SCELERA 21 − 13).

4.8 References

1. Wei, S.-H., McQuade, K. J., & Smidt, G. L. (1993). Three-dimensional joint range of motion measurements from skeletal coordinat data. Journal of Orthopaedic and Sports Physical Therapy, 18(6), 687–691.

2. Grood, E. S., & Suntay, W. J. (1983). A joint coordinate system for the clinical description of three-dimensional motions: Application to the knee. Journal of Biomechanical Engineering. https:// doi.org/ 10. 1115/ 13138 397

3. Yoshimine, F., & Ginbayashi, K. (2002). A mathematical formula to calculate the theoretical range of motion for total hip replacement. Journal of Biomechanics, 35(7), 989–993.

4. Daniel, E. S., Lee, R. Y., & Williams, J. M. (2023). The reliability of video fluoroscopy, ultrasound imaging, magnetic resonance imaging and radiography for measurements of

lumbar spine segmental range of motion in-vivo: A review. Journal of Back and Musculoskeletal Rehabilitation, 36(1), 117–135.

5. Dugailly, P.-M., Beyer, B., Sobczak, S., Salvia, P., & Feipel, V. (2014). Global and regional kinematics of the cervical spine during upper cervical spine manipulation: A reliability analysis of 3D motion data. Manual Therapy, 19(5), 472–477.

6. Morton, N. A., Maletsky, L. P., Pal, S., & Laz, P. J. (2007). Effect of variability in anatomical landmark location on knee kinematic description. Journal of Orthopaedic Research, 25(9), 1221–1230.

7. Langenderfer, J. E., Rullkoetter, P. J., Mell, A. G., & Laz, P. J. (2009). A multi-subject evaluation of uncertainty in anatomical landmark location on shoulder kinematic description. Computer Methods in Biomechanics and Biomedical Engineering, 12(2),

211–216.

8. Adhia, D. B., Bussey, M. D., Ribeiro, D. C., Tumilty, S., & Milosavljevic, S. (2013). Validity and reliability of palpationdigitization for non-invasive kinematic measurement–A systematic review. Manual Therapy, 18(1), 26–34.

9. Pearson, A. M., Spratt, K. F., Genuario, J., McGough, W., Kosman, K., Lurie, J., & Sengupta, D. K. (2011). Precision of lumbar intervertebral measurements: Does a computer-assisted technique improve reliability? Spine, 36(7), 572–580.

10. Breen, A., Hemming, R., Mellor, F., & Breen, A. (2019). Intrasubject repeatability of in vivo intervertebral motion parameters using quantitative fluoroscopy. European Spine Journal, 28, 450–460.

11. Keller, M. C., Hurschler, C., & Schwarze, M. (2021). Experimental evaluation of precision and accuracy of RSA in the lumbar spine. European Spine Journal, 30, 2060–2068.

12. Lawrence, R. L., Zauel, R., & Bey, M. J. (2021). Measuring 3D in-vivo shoulder kinematics using biplanar videoradiography. Journal of Visualized Experiments: JoVE. https:// doi. org/ 10. 3791/62210

13. Dugailly, P.-M., Sobczak, S., Sholukha, V., Van Sint Jan, S., Salvia, P., Feipel, V., & Rooze, M. (2010). In vitro 3D-kinematics of the upper cervical spine: Helical axis and simulation for axial rotation and flexion extension. Surgical and Radiologic Anatomy, 32, 141–151.

14. Tavana, S., Davis, B., Canali, I., Scott, K., Leong, J., Freedman, B., & Newell, N. (2023). A novel tool to quantify in vivo lumbar spine kinematics and 3D intervertebral disc strains using clinical MRI. Journal of the Mechanical Behavior of Biomedical Materials, 140, 105730.

15. Heneghan, N. R., Hall, A., Hollands, M., & Balanos, G. M. (2009). Stability and intra-tester reliability of an in vivo measurement of thoracic axial rotation using an innovative methodology. Manual Therapy, 14(4), 452–455.

16. Moran, M., & Myers, M. (2022). Use of ultrasonography for identification of long bone fractures. Visual Journal of Emergency Medicine, 28, 101381.

17. Wu, Y., Lu, R., Liao, S., Ding, X., Su, W., & Wei, Q. (2021). Application of ultrasound in the closed reduction and percutaneous pinning in supracondylar humeral fractures. Journal of Orthopaedic Surgery and Research, 16, 1–8.

18. Mhaskar, V. A., Agrahari, H., & Maheshwari, J. (2023). Ultrasound guided arthroscopic meniscus surgery. Journal of Ultrasound, 26(2), 577–581.

19. Patel, M. R., Jacob, K. C., Parsons, A. W., Chavez, F. A., Ribot, M. A., Munim, M. A., Vanjani, N. N., Pawlowski, H., Prabhu, M. C., & Singh, K. (2022). Systematic review: Applications of intraoperative ultrasonography in spinal surgery. World Neurosurgery, 164, e45–e58.

20. Effatparvar, M. R., & Sobczak, S. (2022). Application of ultrasound in spine kinematic determination: A systemic review. Journal of Medical Ultrasound, 30(1), 6–10.

21. Chleboun, G. S., Amway, M. J., Hill, J. G., Root, K. J., Murray, H. C., & Sergeev, A. V. (2012). Measurement of segmental lumbar spine flexion and extension using ultrasound imaging. *Journal of Orthopaedic and Sports Physical Therapy, 42*(10), 880–885.

22. van den Hoorn, W., Coppieters, M. W., van Dieën, J. H., & Hodges, P. W. (2016). Development and validation of a method to measure lumbosacral motion using ultrasound imaging. *Ultrasound in Medicine and Biology, 42*(5), 1221–1229.

23. Mahfouz, M. R., Fatah, E. E. A., Johnson, J. M., & Komistek, R. D. (2021). A novel approach to 3D bone creation in minutes: 3D ultrasound. *The Bone and Joint Journal*. https:// doi. org/ 10. 1302/ 0301- 620X. 103B6. BJJ- 2020- 2455. R1

24. Ungi, T., Greer, H., Sunderland, K. R., Wu, V., Baum, Z. M., Schlenger, C., Oetgen, M., Cleary, K., Aylward, S. R., & Fichtinger, G. (2020). Automatic spine ultrasound segmentation for scoliosis visualization and measurement. *IEEE Transactions on Biomedical Engineering, 67*(11), 3234–3241.

25. Jiang, W., Chen, X., & Yu, C. (2022). A real-time freehand 3D ultrasound imaging method for scoliosis assessment. *Journal of Applied Clinical Medical Physics, 23*(8), e13709.

26. Forbes, A., Cantin, V., Develle, Y., Dubé, Y., Bertrand-Grenier, A., Ménard-Lebel, C., & Sobczak, S. (2021). Musculoskeletal ultrasound for 3D bone modeling: A preliminary study applied to lumbar vertebra. *Journal of Back and Musculoskeletal Rehabilitation, 34*(6), 937–950.

27. Effatparvar, M. R., Pierre, M.-O.S., & Sobczak, S. (2022). Assessment and improvement of a novel ultrasound-based 3D reconstruction method: Registered for lumbar spine. *Journal of Medical and Biological Engineering, 42*(6), 790–799.

28. Dugailly, P.-M., Sobczak, S., Moiseev, F., Sholukha, V., Salvia, P., Feipel, V., Rooze, M., & Jan, S. V. S. (2011). Musculoskeletal modeling of the suboccipital spine: Kinematics analysis, muscle lengths, and muscle moment arms during axial rotation and flexion extension. *Spine, 36*(6), E413–E422.

29. Chapman, T., Semal, P., Moiseev, F., Louryan, S., Rooze, M., & Jan, S. V. S. (2013). Application du logiciel de modélisation musculo-squelettique lhpFusionBox à une problématique paléoanthropologique- Spyrou le Néandertalien marche! *Médecine/Sciences*. https:// doi. org/ 10. 1051/ medsci/ 20132 96015

30. Wu, G., Siegler, S., Allard, P., Kirtley, C., Leardini, A., Rosenbaum, D., Whittle, M., D'Lima, D. D., & CristofoliniWitte, L. H. (2002). ISB recommendation on definitions of joint coordinate system of various joints for the reporting of human joint motion— Part I: Ankle, hip, and spine. *Journal of Biomechanics, 35*(4), 543–548.

31. Svedmark, P., Berg, S., Noz, M. E., Maguire, G. Q., Jr., Zeleznik, M. P., Weidenhielm, L., Nemeth, G., & Olivecrona, H. (2015). A new CT method for assessing 3D movements in lumbar facet joints and vertebrae in patients before and after TDR. *BioMed Research International, 2015*(1), 260703.

32. Lyu, Y., Shen, Y., Zhang, M., & Wang, J. (2024). Real-time 3D ultrasound imaging system based on a hybrid reconstruction algorithm. *Chinese Journal of Electronics, 33*(1), 245–255.

33. Wilken, J. M., Rodriguez, K. M., Brawner, M., & Darter, B. J. (2012). Reliability and minimal detectible change values for gait kinematics and kinetics in healthy adults. *Gait and Posture, 35*(2), 301–307.

34. Brihmat, N., Loubinoux, I., Castel-Lacanal, E., Marque, P., & Gasq, D. (2020). Kinematic parameters obtained with the ArmeoSpring for upper-limb assessment after stroke: A reliability and learning effect study for guiding parameter use. *Journal of Neuroengineering and Rehabilitation, 17*, 1–12.

35. Zsoldos, R., Groesel, M., Kotschwar, A., Kotschwar, A., Licka, T., & Peham, C. (2010). A preliminary modelling study on the equine cervical spine with inverse kinematics at walk. *Equine Veterinary Journal, 42*, 516–522.

36. McKinnon, C. D., & Callaghan, J. P. (2019). Validation of an ultrasound protocol to measure intervertebral axial twist during functional twisting movements in isolated functional spinal units. *Ultrasound in Medicine and Biology, 45*(3), 642–649.

37. Zhao, K. D., Ben-Abraham, E. I., Magnuson, D. J., Camp, J. J., Berglund, L. J., An, K.-N., Bronfort, G., & Gay, R. E. (2016). Effect of off-axis fluoroscopy imaging on two-dimensional kinematics in the lumbar spine: A dynamic in vitro validation study. *Journal of Biomechanical Engineering, 138*(5), 054502.

38. Dreischarf, M., Albiol, L., Rohlmann, A., Pries, E., Bashkuev, M., Zander, T., Duda, G., Druschel, C., Strube, P., & Putzier, M. (2014). Age-related loss of lumbar spinal lordosis and mobility– A study of 323 asymptomatic volunteers. *PLoS ONE, 9*(12), e116186.

39. Ma, H. T., Griffith, J. F., Yang, Z., Kwok, A. W. L., Leung, P. C., & Lee, R. Y. (2009). Kinematics of the lumbar spine in elderly subjects with decreased bone mineral density. *Medical and Biological Engineering and Computing, 47*, 783–789.

Chapter 5- Lumbar Spine 3D Kinematics Determination Using Ultrasound Imaging: An In-Vivo Approach to Define Normative Range of Motion

5.1 Original Contribution of the Student and Co-authors

This fifth chapter of the thesis presents an article entitled *Lumbar spine 3D kinematics determination using ultrasound imaging: an in-vivo approach to define normative ranges of motion.* This article, co-authored by Mohammad Reza Effatparvar, Hugo Lacombe, and Stéphane Sobczak, was submitted to the *Journal of Applied Biomechanics* in August 2025.

Lumbar spine 3D kinematics determination using ultrasound imaging: an in-vivo approach to define normative ranges of motion

Mohammad Reza Effatparvar[1,2,3*], Hugo Lacombe[4], Stéphane Sobczak[1,2,3]

[1]Département d'anatomie, Université du Québec à Trois-Rivières, Trois-Rivières, Québec, Canada.

[2]Institut National d'Anatomie (INA), Université du Québec à Trois-Rivières, Trois-Rivières, Québec, Canada

[3]Groupe de Recherche sur les Affections Neuromusculosquelettiques (GRAN), Université du Québec à Trois-Rivières, Trois-Rivières, Québec, Canada

Conflict of Interest Disclosure: None.

Correspondence Address:

Mohammad Reza Effatparvar

Département d'anatomie, Université du Québec à Trois-Rivières

3351, boulevard des Forges

Trois-Rivières, Québec, Canda, G8Z 4M3

Phone: +1 819 376-5011 Email: Mohammad.reza.effatparvar@uqtr.ca

5.2 Abstract

The determination of 3D lumbar spine kinematics is essential for diagnosing and rehabilitating movement restrictions. 3D reconstruction from CT and MRI images is commonly used for this purpose, but these techniques have certain limitations. Ultrasound offers a validated, non-ionizing alternative. This study aimed to apply an ultrasound technique, validate it in-vitro, and then use it to determine the ROM at the L4–L5 and L5–S1 levels in standing and full-flexion positions. Two cadaveric lumbar specimens were imaged using CT and ultrasound. 3D models were generated, and intervertebral ROM was determined and compared. Subsequently, 56 healthy participants aged 20 to 60 years with no history of low back problems were recruited. ROM was calculated from 3D ultrasound reconstructions. Reliability was tested in two participants. The mean ROM difference between ultrasound and CT was 0.61° ± 0.17°, with ultrasound overestimating by 13.6%. Bland–Altman plots confirmed agreement between the two methods. Within-day and between-days ICCs were 0.91 ± 0.02 and 0.92 ± 0.01, respectively. Significant age-related differences were observed for flexion, proximodistal and anteroposterior translations, indicating a decrease in kinematics with age. For flexion, significant differences were found between the 20–30 and 40–50 age groups (1.64° ± 2.12°, $p = 0.02$), 20–30 and 50–60 (2.17° ± 2.39°, $p < 0.01$), and 30–40 and 50–60 (1.70° ± 2.71°, $p = 0.02$). For proximodistal translation, significant differences were observed between 20–30 and 40–50 (0.44 ± 0.57 mm, $p = 0.03$), 20–30 and 50–60 (0.58 ± 0.65 mm, $p < 0.01$), and 30–40 and 50–60 (0.43 ± 0.78 mm, $p = 0.04$). Regarding anteroposterior translation, significant differences were found between 20–30 and 50–60 (0.92 ± 0.83 mm, $p < 0.01$), and between 30–40 and 50–60 (0.66 ± 0.95 mm, $p < 0.01$). These last two variables were also correlated with flexion ($\rho = 0.86$ and 0.61, $p < 0.05$). No sex-related differences were observed. The method demonstrated high reliability and strong agreement with CT, supporting its potential for practical and clinical application, particularly with future advances in AI-based segmentation.

Keywords: motion analysis, freehand ultrasound, 3D reconstrcution

5.3 Résumé

La détermination de la cinématique 3D de la colonne lombaire est essentielle pour le diagnostic et la réadaptation des restrictions de mouvements. La reconstruction 3D à partir de CT et d'IRM est courante, mais ces techniques ont des limites. L'échographie représente une alternative et non ionisante. Cette étude visait à appliquer une technique d'échographie, à la valider in-vitro, et ensuite à l'utiliser pour déterminer les amplitudes de mouvements des niveaux L4-L5 et à L5-S1 en position debout et lors de la flexion. Deux spécimens lombaires ont été imagés par CT-Scan et par échographie. Des modèles 3D ont été générés et les ROM intervertébrales ont été déterminées et comparées. Ensuite, 56 participants en santé âgés de 20 à 60 ans sans problème lombaire ont été recrutés. Les ROM ont été calculées à partir de reconstructions échographiques 3D. La fidélité a été testée chez deux participants. L'écart moyen de ROM entre l'échographie et le CT était de 0,61° ± 0,17°, avec une surestimation pour l'échographie de 13.6%. Les diagrammes de Bland–Altman ont confirmé l'accord entre les deux méthodes. Les ICC intra-journaliers et inter-journaliers étaient respectivement de 0,91 ± 0,02 et 0,92 ± 0.01. Des différences significatives liées à l'âge ont été observées pour la flexion, ainsi que pour les translations proximodistale et antéro-postérieure, indiquant une diminution de la cinématique avec l'âge. Pour la flexion, des différences significatives ont été observées entre les groupes d'âge 20–30 et 40–50 ans (1,64 ± 2,12°, $p = 0,026$), 20–30 et 50–60 ans (2,17 ± 2,39°, $p = 0,001$), ainsi qu'entre 30–40 et 50–60 ans (1,70 ± 2,71°, $p = 0,21$). Pour la translation proximodistale, des différences significatives ont été relevées entre les groupes 20–30 et 40–50 ans (0,44 ± 0,57 mm, $p = 0,033$), 20–30 et 50–60 ans (0,58 ± 0,65 mm, $p = 0,001$), et 30–40 et 50–60 ans (0,43 ± 0,78 mm, $p = 0,043$). Concernant la translation antéro-postérieure, des différences significatives ont été observées entre les groupes 20–30 et 50–60 ans (0,92 ± 0,83 mm, $p < 0,001$), ainsi qu'entre 30–40 et 50–60 ans (0,66 ± 0,95 mm, $p = 0,003$). Ces deux dernières variables étaient corrélées à la flexion ($\rho = 0,86$ et 0,61, $p < 0,05$). Aucune différence liée au sexe n'a été observée. La méthode a montré une fidélité et une concordance avec le CT, soutenant son potentiel d'application pratique et clinique, notamment avec les avancées en segmentation basée sur l'intelligence artificielle.

Mots-clés : analyse du mouvement, échographie libre, reconstruction 3D

5.4 Introduction

Assessment of lumbar spine kinematics is essential for both diagnosing mobility restrictions and monitoring rehabilitation progress. Various methods are available for evaluating spinal motion, including manual measurements, motion capture systems, and medical imaging techniques. Manual methods are the most commonly used in clinical practice, but they lack three-dimensional (3D) capabilities and often have low accuracy [1]. Motion capture systems provide high accuracy and 3D analysis. However, when using skin-attached markers, they are unsuitable for assessing intervertebral kinematics due to soft tissue artifacts, which can introduce measurement errors of 0.8–1.5 mm [2]. This limitation can be addressed by using intracortical pins, but such procedures are highly invasive and impractical for routine clinical assessments [3].

Medical imaging is the only approach in determining intervertebral kinematics by providing detailed morphological data. However, conventional radiography [4] and fluoroscopy [5] are limited to two-dimensional (2D) imaging and involve exposure to ionizing radiation. While Computed tomography (CT) scans [6] and magnetic resonance imaging (MRI) [7] provide high-quality 3D images, the former involves ionizing radiation, the latter is expensive, and both are typically limited to static and supine imaging. More recently, the biplanar radiography imaging system [8] has been developed to enable kinematic assessment in the standing position with improved accessibility, though it still relies on ionizing radiation.

Ultrasound imaging is a non-ionizing and affordable alternative with high potential for various musculoskeletal applications [9]. Among these applications, it has also been applied to assess lumbar spine kinematics, such as estimating intervertebral flexion-extension by measuring interspinous distances [10], and axial rotation by tracking changes in the position of spinous processes [11]. However, a recent review study indicated that existing methods have been limited to 2D measurements [12] due to the absence of the application of 3D reconstruction techniques. Meanwhile, several techniques such as tracked and sensorless methods, have demonstrated strong potential for 3D reconstruction from 2D ultrasound imaging. In the context of lumbar spine imaging, high validity has been reported for 3D ultrasound reconstructions when compared to CT-based models, with a mean error

of 0.44 ± 0.24 mm [13]. Furthermore, this in-vitro approach has also been validated for determining 3D lumbar kinematics, with a slight overestimation of 0.23° ± 0.20° in the measured range of motion (ROM) compared to CT-derived results [14].

Despite recent advances, no in-vivo study has yet determined 3D lumbar spine kinematics using ultrasound imaging. To address this gap, we designed the present study with three main objectives: first, to assess the validity of the current method by comparing it with CT imaging in an in-vitro setting; second, to verify the reliability of the method when applied in an in-vivo context; and finally, to define detailed normative ROM values on L4-L5 and L5–S1 kinematics during full flexion in a population aged between 20 to 60 years.

5.5 Methods

5.5.1 In-vitro validation

Specimens preparation: Two thawed human cadavers (79.5 ± 3.5 years old) were dissected to isolate the entire lumbar spine (T12–S1) while preserving the posterior structures intact. Orthopedic Schanz screws, each equipped with a cluster of four reflective markers (⌀ = 5 mm), were inserted anteriorly into the vertebral bodies. The specimens were fixed within a computer-assisted mechanical (CAM) frame using external fixation tools (Figure 1A).

CT scan imaging: A CT scanner (Revolution EVO, GE Healthcare, USA) was used to acquire DICOM images of the specimens in their neutral position, with a reconstruction slice thickness of 0.5 mm and an inter-slice spacing of 0.625 mm. The vertebrae and reflective markers were segmented using 3D Slicer software (www.slicer.org) to generate 3D models from the CT images.

Applying motion: Discrete motions, including maximum flexion-extension, maximum right and left lateral bending, and maximum right and left axial rotation, were applied to the specimens within the CAM frame. At each position, the specimens were locked in place, and the coordinates of the reflective markers were recorded using an optoelectronic tracking system (PrimeX22, OptiTrack, NaturalPoint Inc., Corvallis, OR, USA).

Ultrasound imaging: A linear ultrasound probe (SonoSite ST, FUJIFILM, USA; probe: L15-4; mode: musculoskeletal; frequency: 8.0 MHz; depth: 6 cm; frame rate: 30 fps), equipped with a cluster of four reflective markers, was used for ultrasound imaging and tracked by the same optoelectronic system. In order to match the ultrasound images with the tracking data and place them in the correct position in 3D space for reconstruction, the following calibration steps were performed:

Temporal calibration was carried out to synchronize the timing between ultrasound image acquisition and the tracking system, ensuring that the positional data from the tracker corresponded to the correct ultrasound frames. For this step, the temporal offset between the two hardware systems was calculated in the FCal software and applied in the image acquisition configuration code [14] (Fig 1).

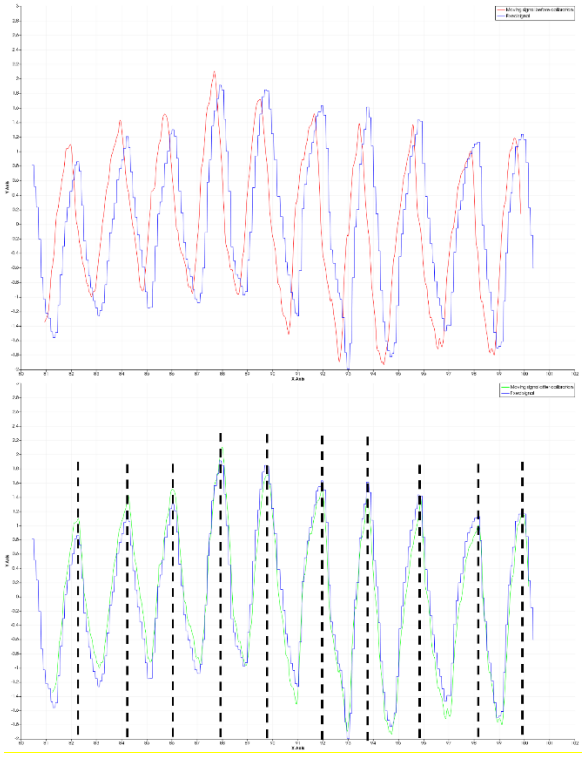

Fig 1. Temporal calibration of the tracking and ultrasound devices. In this method, the ultrasound pixel data and the tracking data were converted into two separately normalized signals, and the time offset was obtained from the X-values (time in seconds) of the signal peaks. The Y-axis represents the normalized signal amplitude. The upper graph shows the latency between the

signals before calibration, and the lower graph shows the signal positions after calibration. The dashed lines indicate the positions on the time axis used for latency calculation.

Pivot calibration was used to determine the spatial position of the tip of a tracked tool (a specifically designed stylus) relative to its tracking markers. The stylus was pivoted around its fixed tip while recording the position and orientation of the markers. These data were then used to calculate the coordinates of the tip within the tracking system's coordinate frame. The result was a fixed transformation matrix, referred to as *StylusTipToStylus* (Fig. 2), which was later used to calculate the ultrasound image position [15].

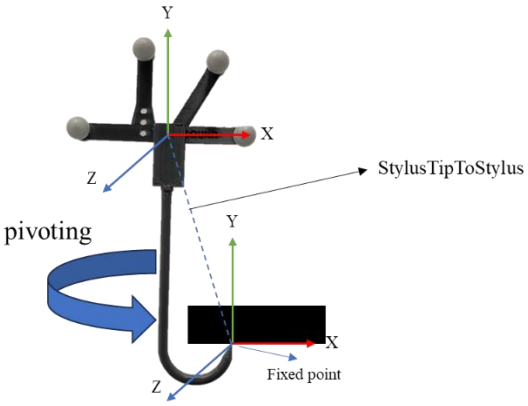

Fig 2. A calibration stylus with the definition of the local reference frame and a transformation matrix between them (*StylusTipToStylus*) from the pivot calibration.

Spatial calibration was performed to determine the spatial relationship between the ultrasound probe's image plane and its attached tracking sensor. Using the stylus, its tip was placed at various positions within the probe's field of view. The coordinates of these positions were recorded both in the ultrasound image space (pixel coordinates) and in the tracking system space (3D coordinates). A transformation matrix was then computed to map the image-space coordinates to the global coordinate system defined by the tracking sensor. This matrix integrated the probe-to-tracker transformation and the stylus tip localization based on its known geometry and tracked coordinates. The result of this calibration step was a fixed transformation matrix, referred to as *ImageToProbe* [15].

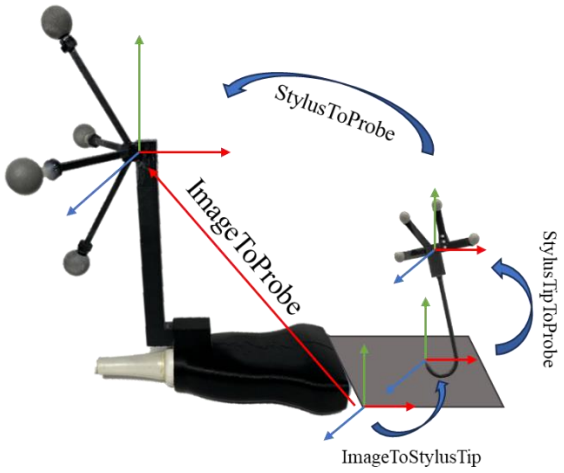

Fig 3. The procedure of calculation of ImageToProbe transformation matrix using a spatial calibration technique

After calibration, at each position, tracked ultrasound imaging was performed on the posterior aspect of the specimens (Figure 4B). The images and the trajectory data were synchronously merged and streamed through the PLUS Toolkit (www.PlusToolkit.org) and the SlicerIGT module [15] within the 3D Slicer software, with each position recorded as a separate sequence. The entire calibration procedures were repeated before any acquisition.

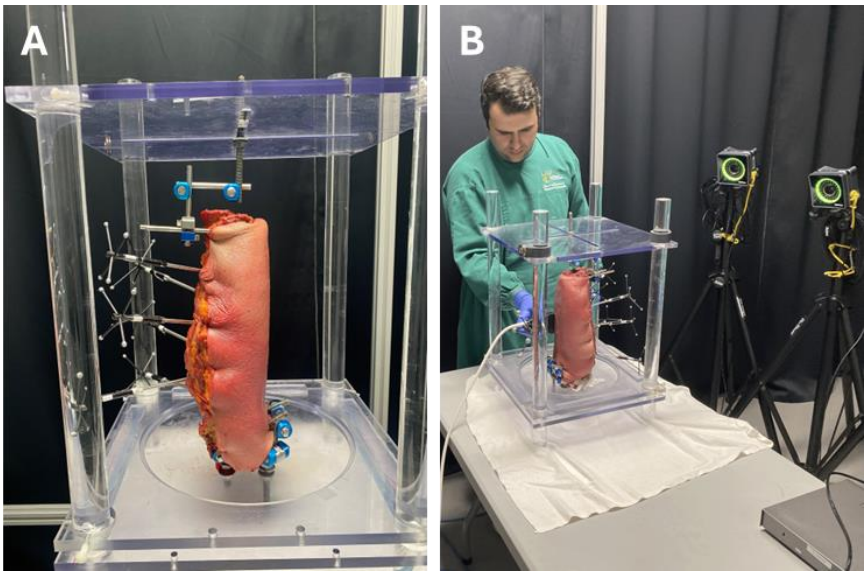

Fig 4. (A) Lateral view of one of the specimens installed within the CAM frame. (B) Process of recording ultrasound images, along with the collection of motion data from vertebrae-fixed and probe-fixed markers for motion analysis and tracked imaging.

To create the 3D model of each position, recorded ultrasound images were manually segmented using the ultrasound module of 3D slicer. For this purpose, only the hyperechoic regions above the acoustic shadow were segmented to generate posterior view of the vertebrae (Figure 5).

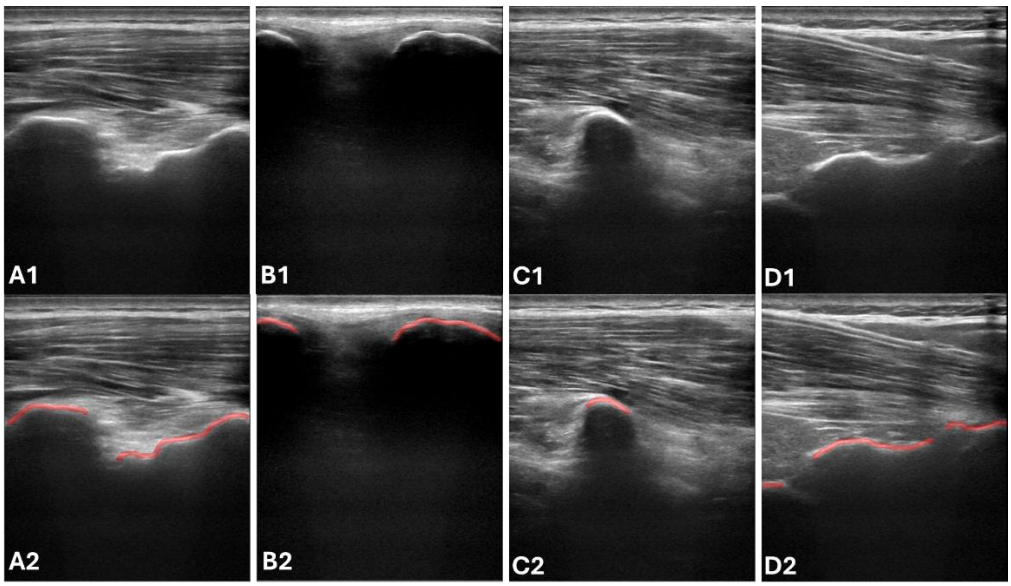

Fig 5. Manual segmentations performed on ultrasound images. The top row shows the raw images, and the bottom row shows the corresponding segmented regions. From A to D, the segmented structures include a portion of a facet joint, two spinous processes, a costiform process, and part of the sacrum, respectively

Motion visualization: To visualize the discrete motions on the CT-derived 3D models, the transformation matrices of the marker clusters' reference frames, recorded for each vertebra using the OptiTrack system, were registered onto the local reference frames defined by the segmented markers on each vertebra in the 3D models [17]. This procedure, known as motion representation, was implemented using the LhpFusionBox software (ULB, Belgium).

Intervertebral kinematics: A custom Python-based interface was developed to determine the 3D intervertebral kinematics. In this method, the 3D models were virtually

palpated to localize anatomical landmarks [18]. For vertebrae L1 to L5, ALs were defined at the most distal ends of the costiform processes and the superior, posterior ends of the spinous processes. For S1, ALs were placed at the posterior ends of the median crests and the most protruding points of the lateral crests. The anatomical reference frames were then established in accordance with the guidelines of the International Society of Biomechanics (ISB) [18]. The Z-axis was oriented between the ALs on the right and left costiform processes, while the X-axis was set as an orthogonal axis to the Z-axis, intersecting the AL on the spinous process. The Y-axis was defined as the third axis, perpendicular to both the X- and Z-axes (Figure 6).

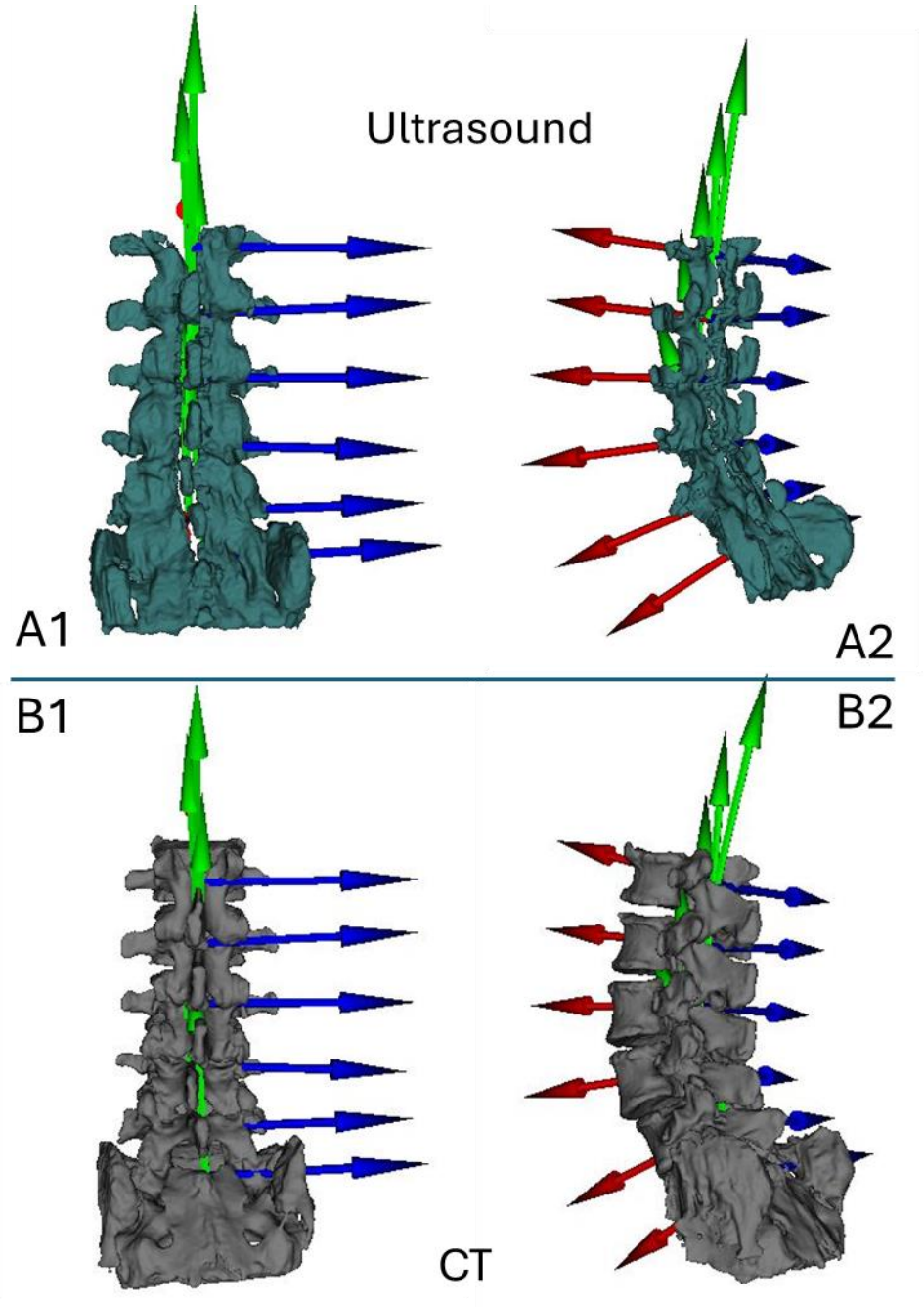

Fig 6. 3D models of one of the specimens reconstructed from ultrasound (A1: Posterior and A2: postero-lateral view) and CT images (B1: posterior and B2: postero-lateral view). Anatomical reference frames were established on each vertebra and used for ROM measurements

Validity: To confirm the validity of the ultrasound-based kinematics determinations, mean ROMs were compared to those obtained from the CT scan, and the

limits of agreement were calculated between the two methods, with the CT scan serving as the gold standard.

5.5.2 In-vivo protocol

Participants: After receiving approval from the Institutional Research Ethics Committee of the Université du Québec à Trois-Rivières (CER-24-315-07.05), a total of 56 individuals were recruited through a locally published advertisement circulated via collaborator research groups and the university's staff and student community from January 2025 to April 2025. Through the recruitment process, equal representation across four predefined age groups (20–30, 31–40, 41–50, and 51–60 years) and both sexes was ensured, with each group comprising 14 participants (7 females and 7 males). The mean ± SD ages for the respective groups were 24.07 ± 2.36, 33.85 ± 2.93, 46.07 ± 2.84, and 56.92 ± 2.64 years.

Inclusion criteria required participants to have no history of low back issues and a body mass index (BMI) below 25. The mean ± SD BMI values for the four age groups (20–30, 31–40, 41–50, and 51–60 years) were 21.43 ± 1.75, 21.61 ± 2.53, 23.34 ± 1.35, and 22.73 ± 2.17 kg/m², respectively. Exclusion criteria included any history of lumbar surgery or medical conditions that could affect the study outcomes, such as ankylosing spondylitis, rheumatoid arthritis, spondyloarthritis, or other forms of arthropathy.

All potential participants completed a consent and detailed questionnaire covering their medical history, current health status, and any prior surgical or non-surgical interventions related to the lower back.

Ultrasound imaging: Tracked ultrasound imaging was performed to scan the L4–S1 vertebrae of all participants in both standing and full-flexion positions using the same ultrasound probe as in the in-vitro step. Ultrasound gel was applied to ensure proper acoustic coupling. The probe position was tracked using five OptiTrack cameras. To facilitate the scanning process, minimize participant motion and standardized the acquisition procedure, a custom-built frame was specifically designed for this study (Figure 7A). The frame restricted lower limb movements, provided hand support for upper body comfort, and enabled participants to achieve full flexion without requiring additional

movements. An adjustable-height chest support was also integrated, allowing participants to lean forward comfortably while in the flexed position.

All participants were scanned barefoot and wore loose shorts to allow proper access to the lumbar region. After exposing the scanning area, the L4 spinous process was manually palpated by the same evaluator for all participants, using the line connecting the superior iliac crests as a reference to approximate the L4 level, and this point was marked on the skin. From this mark, the ultrasound scan was initiated approximately 5 cm cranial to L4 and then continued caudally, in longitudinal sweeps, to ensure full coverage of the costiform processes, with the probe held vertically in a sagittal orientation.

The approximate S2 level was also identified by manual palpation, using the line connecting the posterior superior iliac spines (PSIS) and the sacral midline as references, and marked on the skin. The scanning was then extended beyond the S2 mark in the caudal direction so that the S1 level was clearly visualized, with horizontal sweeps performed while maintaining sufficient image overlap and covering both PSIS. For final verification and optimal visualization of the spinous processes, a vertical sweep from top to bottom was performed directly along the midline. Throughout the entire scanning process, the primary focus was on visualizing the bony elements. When necessary, the procedure was repeated, or the probe orientation was adjusted to ensure the best possible depiction of bone contours.

Regarding the flexion test, it was performed immediately after the standing test without changing or moving the participant's body position as much as possible. Participants were asked and encouraged to reach their maximum flexion position while still feeling comfortable. Since the scanning procedure lasted approximately 2–3 minutes, measures were taken to ensure stability throughout the test. To assist in achieving maximum flexion, the knees were kept straight using an aluminum bar placed in front of the femurs to restrict forward movement. An additional aluminum bar was positioned behind the buttocks and locked onto the frame to prevent backward motion. Once in the desired flexed posture, the hinged hand supports were adjusted to match the participant's preferred arm position for comfort. The height-adjustable chest support was also positioned according to the participant's chest level, allowing them to lean on it during the scan. The

same imaging procedure used for the standing posture was repeated for the flexion scan (Figure 7B).

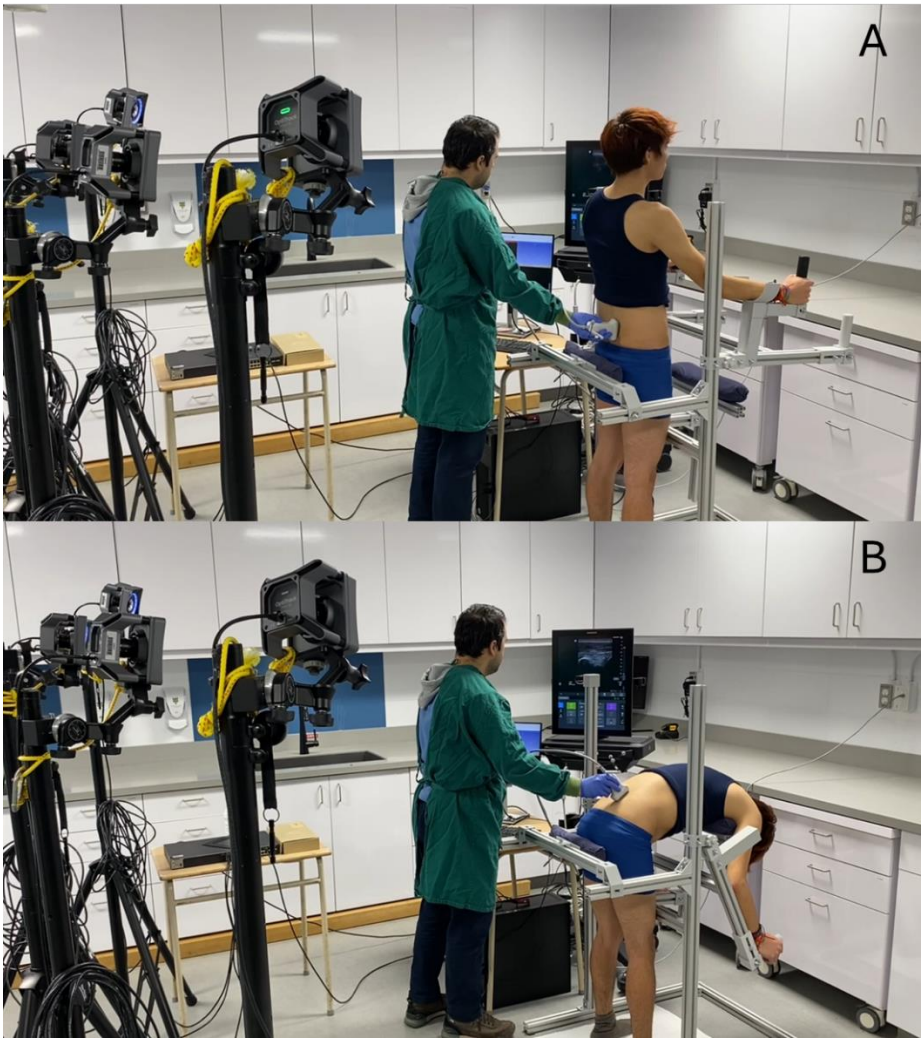

Fig 7. Imaging procedure of one of the participants in standing (A) and full flexion (B) positions.

Reliability: To verify the reliability of the procedure, the first two participants took part in within-day and between-days reliability testing. Over the course of three consecutive days, each participant performed the test three times per day, with 30-minute intervals between trials. All sessions were started at the same time of day (10:00 AM) to control for diurnal variations. To ensure consistent flexion across all sessions, both the angle of the frame and the height of the chest support were fixed to the same settings for every trial. All scans were conducted by a single operator to eliminate inter-operator

variability. Participants were asked not to engage in any strenuous or potentially influential exercise prior to testing.

3D modeling and kinematic determination: Following the same method described for the in-vitro validation, the series of tracked ultrasound images for both standing and flexion positions were manually segmented. 3D models of the vertebrae were then generated, anatomical markers were virtually palpated, reference frames were constructed, and the intervertebral ROMs, including three planar rotations and linear translations, were measured using the custom-made Python interface (Figure 8).

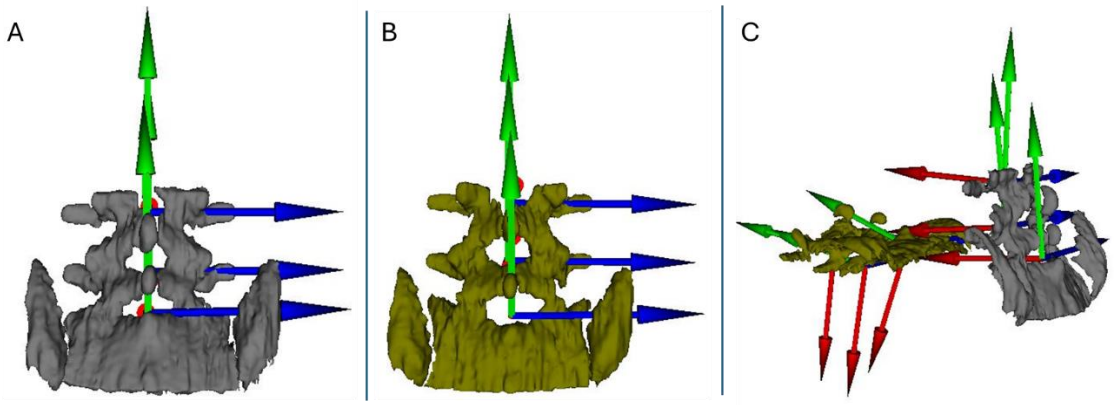

Fig 8. 3D models of the standing and flexion positions generated from ultrasound images, with anatomical reference frames established on the vertebrae. (A) Posterior view of the standing position; (B) posterior view of the flexion position; (C) postero-lateral view of both models registered

Data analysis and statistical test: To assess the agreement between ultrasound and CT measurements from the validation step, mean differences (MD) and standard deviations (SD) were calculated for each motion. The limits of agreement between the two methods were then assessed using Bland–Altman plots.

For the reliability test, the intraclass correlation coefficient (ICC 2,1; 95% CI) was calculated to evaluate the consistency of repeated ROM measurements. Within-day ICC values were computed separately for each day and each participant, and a between-day ICC was calculated using the mean ROM values across days. To provide an overall estimate of reliability, mean ± SD ICC values across sessions were also reported. Based on these ICCs and the corresponding standard deviations, the standard error of measurement (SEM) and

the minimal detectable change at 95% confidence (MDC) were derived for rotational and translational variables to quantify the smallest change exceeding measurement error. The ROM values from both participants were pooled and treated as a single data group for the reliability analysis.

For the participant-derived kinematic results, mean and SD values were calculated and compared by age group and sex. Absolute values were imported into the calculations to remove the effect of right and left motions on the mean values. Box plots were generated to visualize the results for each sex and age group at both vertebral levels. The normality of the data distributions was assessed using the Shapiro–Wilk test. Differences between age groups for each motion were assessed using the Kruskal–Wallis test (as the distribution was not normal). When significant differences were found, pairwise post-hoc comparisons were performed using Dunn's test with Bonferroni-adjusted p-values. The Mann–Whitney U test was also used to compare the results between female and male participants. Additionally, Spearman Correlation Coefficients (SCC) analysis was conducted to evaluate the strength of correlation between sagittal rotation and other motions. All statistical analyses were conducted using custom Python scripts.

5.6 Results

In-vitro validation

The mean ROM differences between ultrasound and CT across all vertebral levels (Table 1) were 0.65° ± 0.13° for flexion-extension, 0.76° ± 0.14° for lateral bending, and 0.41° ± 0.24° for axial rotation. Overall, the average difference across motions indicated an overestimation by ultrasound, with a global mean difference of 0.61° ± 0.17° compared to CT. Bland–Altman plots (Figure 9) showed that all individual differences fell within the 95% limits of agreement: 0.39° to 0.91° for flexion-extension, 0.49° to 1.03° for lateral bending, and –0.06° to 0.88° for axial rotation.

Table 1 ROMs from two specimens, Mean ± SD

	Flexion-Extension		Lateral Bending		Axial Rotation	
	US	CT	US	CT	US	CT
L1-L2	4.76±1.63	4.12±1.51	4.3±1.40	3.58±1.41	1.98±0.41	1.78±0.41
L2-L3	4.52±1.67	3.79±1.61	4.12±1.46	3.28±1.53	2.29±0.47	2.00±0.41
L3-L4	6.00±1.53	5.53±1.43	6.21±1.34	5.44±1.48	2.86±0.35	2.63±0.48
L4-L5	6.49±1.79	5.88±1.46	6.61±1.51	6.07±1.32	2.88±0.52	2.12±0.39
L5-S	3.96±1.49	3.13±1.62	4.13±1.43	3.2±1.38	1.66±0.44	1.07±0.30
MD	0.65±0.13		0.76±0.14		0.41±0.24	
Mean MD			0.61±0.17			

All values are in degree. Positive mean differences (MD) indicate higher values for ultrasound.

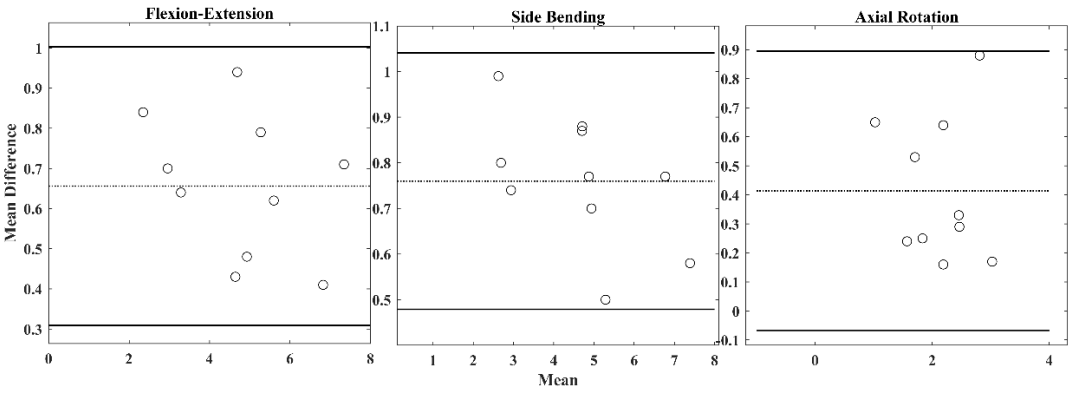

Fig 9. Bland–Altman plots showing the limits of agreement between the ultrasound and CT scan. Mean differences are represented by dotted lines, and upper and lower limits of agreement by solid lines. All values are in degrees

In-vivo measurement

Regarding the reliability test results, within-day reliability showed ICC values of 0.88 [0.77, 0.99] on Day 1, 0.92 [0.81, 1.00] on Day 2, and 0.93 [0.83, 1.00] on Day 3, resulting in an overall mean ICC of 0.91 ± 0.02. Between-day reliability, based on the mean ROM values for each day and for two participants, showed an ICC of 0.92 ± 0.01. Based on these ICC values and the corresponding standard deviations of the repeated ROM measurements, the SEM and the MDC were calculated. When pooled across the three

rotational variables, the mean MDC for rotations was 0.51 ± 0.59°, whereas for the three translational variables, the pooled mean MDC was 0.31 ± 0.21 mm.

Concerning the mean ROM for L4–L5 and L5–S1 across each motion type, age group, and sex, the values have been reported in Table 2 and visualized using box plots in Figure 10. As the primary motion was flexion, the mean flexion values were as follows: for females aged 20–30, 10.84 ± 1.77°, for males aged 20–30, 9.68 ± 2.09°, for females aged 30–40, 10.14 ± 1.92°, for males aged 30–40, 9.28 ± 2.35°, for females aged 40–50, 8.17 ± 1.85°, for males aged 40–50, 8.69 ± 1.44°, for females aged 50–60, 7.86 ± 2.03°, and for males aged 50–60, 8.46 ± 1.89°.

Table 2 ROMs of the participants, Mean ± SD

			20-30		30-40		40-50		50-60	
			Female	Male	Female	Male	Female	Male	Female	Male
L4-L5	Rotation	Fx	10.84±1.77	9.68±2.09	10.14±1.92	9.28±2.35	8.17±1.85	8.69±1.44	7.86±2.03	8.46±1.89
		LB	0.79±0.21	0.86±0.18	0.91±0.33	0.77±0.49	1.17±0.50	0.54±0.44	1.17±0.27	0.68±0.42
		AR	1.88±0.19	1.73±0.43	1.51±0.44	1.22±0.39	1.74±0.67	1.71±0.78	1.90±0.41	1.50±0.85
	Translation	PD	3.22±0.74	3.30±0.46	3.33±0.66	3.05±0.61	2.76±0.56	2.80±0.52	2.66±0.65	2.86±0.49
		ML	0.36±0.22	0.82±0.57	0.66±0.45	0.74±0.48	0.84±0.76	0.39±0.33	0.78±0.39	0.85±0.62
		AP	4.29±0.79	4.02±0.78	3.93±0.78	3.74±0.64	3.49±0.63	3.72±0.79	2.96±0.95	3.30±0.57
L5-S1	Rotation	Fx	8.21±1.82	7.94±1.37	7.85±1.78	7.12±1.65	6.41±1.21	6.96±1.29	5.80±1.76	6.00±1.03
		LB	0.61±0.10	0.78±0.27	0.89±0.38	0.76±0.38	0.83±0.19	1.45±0.76	0.47±0.31	0.82±0.54
		AR	1.54±0.93	1.04±0.46	1.80±0.80	1.68±0.63	1.74±0.63	1.44±0.47	1.12±0.82	1.60±0.57
	Translation	PD	2.94±0.52	2.74±0.37	2.67±0.49	2.53±0.47	2.32±0.39	2.58±0.53	2.13±0.49	2.21±0.66
		ML	0.82±0.34	0.84±0.41	1.00±0.39	0.91±0.41	0.89±0.71	0.76±0.37	0.83±0.76	0.48±0.40
		AP	3.23±0.57	3.41±0.68	3.34±0.68	2.84±0.78	2.91±0.59	3.00±0.49	2.52±0.48	2.44±0.64

Mean values for rotations and translations in three anatomical planes related to the L4-L5 and L5-S1 vertebral levels. Fx stands for flexion, LB stands for lateral bending, AR stands for axial rotation, PD stands for Proximodistal translation, ML stands for mediolateral translation, and AP stands for anteroposterior translation. Rotations are in degree and translations are in mm.

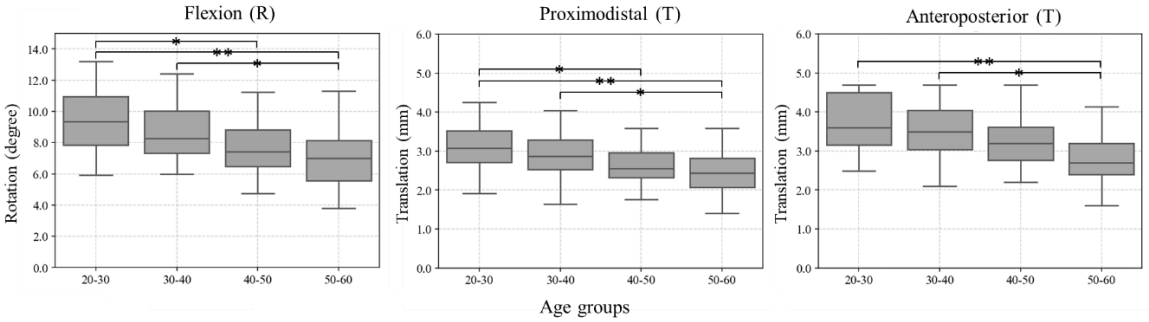

Fig 10. Box plots of lumbar range of motion (ROM) across age groups. Only conditions with statistically significant differences between age groups are shown. Horizontal lines indicate significant pairwise differences between age groups, with single and double asterisks denoting stronger differences. Rotational (R) values are expressed in degrees and translational (T) values in millimetres.

Regarding sex-related differences, the mean difference in flexion between female and male participants was $0.78 \pm 2.33°$ for the 20–29 age group, $0.72 \pm 2.59°$ for 30–40, $-0.53 \pm 2.09°$ for 40–50, and $-0.39 \pm 2.03°$ for 50–60. However, the Mann–Whitney U test revealed no statistically significant differences between males and females in any age group or for any motion variable.

Regarding kinematic differences between age groups, the Kruskal–Wallis test revealed significant differences ($p < 0.05$) in proximodistal translation, anteroposterior translation, and flexion at both vertebral levels. Post-hoc analysis indicated that for flexion, significant differences were observed between the 20–30 vs 40–50 age groups ($1.64 \pm 2.12°$, $p = 0.02$), 20–30 vs 50–60 groups ($2.17 \pm 2.39°$, $p<0.01$), and 30–40 vs 50–60 groups ($1.70 \pm 2.71°$, $p = 0.21$). For proximodistal translation, significant differences were found between the 20–30 vs 40–50 groups (0.44 ± 0.57mm, $p = 0.03$), 20–30 vs 50–60 groups (0.58 ± 0.65mm, $p<0.01$), and 30–40 vs 50–60 groups (0.43 ± 0.78mm, $p = 0.04$). As for anteroposterior translation, significant differences were detected between the 20–30 vs 50–60 groups (0.92 ± 0.83mm, $p<0.01$) and between the 30–40 vs 50–60 groups (0.66 ± 0.95mm, $p<0.01$).

Regarding the correlation (SCC) between motion variables, flexion showed a correlation of –0.07 (*p = 0.46*) with lateral bending, 0.11 (*p = 0.26*) with axial rotation, –

0.08 (*p = 0.39)* with mediolateral translation, 0.86 ($p<0.01$) with proximodistal translation, and 0.61 ($p<0.01$*)* with anteroposterior translation.

5.7 Discussion

The 3D reconstruction of medical images is essential for determining intervertebral 3D kinematics. Ultrasound imaging, being a non-ionizing, portable, and cost-effective modality, offers a promising possibility for this purpose. In this study, a tracked ultrasound imaging and 3D segmentation technique was employed to evaluate the validity of this approach by comparing it with CT scan data. The method was then applied to measure the intervertebral ROM of the lumbar spine (L4-S1) in human participants. Additionally, the reliability of the method was assessed to further demonstrate its potential for both clinical and research applications, including the estimation of the SEM and mean MDC.

Concerning validity, the ROMs (Table 1) measured using 3D models generated from ultrasound were overestimated by a mean value of 0.61±0.17° compared to those obtained from CT. A similar overestimation was reported in a previous in-vitro study on intervertebral kinematic measurement using ultrasound-based 3D reconstruction, with a mean difference of 0.23±0.20° [14]. This overestimation is likely due to the system's tendency to produce bone boundaries with greater thickness [19], leading to segmentation errors and an extended reconstructed volume. In previous comparisons with CT, mean reconstruction errors of 0.44 ± 0.63 mm [20] and 0.44 ± 0.24 mm [13] were reported for lumbar vertebrae. Despite this slight overestimation, Bland–Altman plots (Figure 9) showed a good agreement between the two imaging techniques, with all differences falling within the limits of agreement for flexion–extension, lateral bending, and axial rotation.

Following the in-vitro validation, kinematic tests were conducted on participants. As for the reliability analysis, this test demonstrated excellent consistency in both within-day (0.91 ± 0.02) and between-days (0.92 ± 0.01) assessments. Based on these ICC values and the variability of the repeated ROM measurements, the mean MDC for rotations was 0.51 ± 0.59°, whereas the mean MDC for translations was 0.31 ± 0.21 mm. These values indicate that changes smaller than about 0.51° in rotation or 0.31 mm in translation at a given segment are likely attributable to measurement error rather than true changes in

mobility, whereas changes exceeding these thresholds can be interpreted with greater confidence as reflecting real biomechanical differences. In ROM measurements, reliability is inherently influenced by several external factors, such as recent physical activity, time of day, or even participants' natural tendency toward greater or lesser flexion. To minimize such variability, we ensured that the setup remained fixed in the same configuration for each session, conducted tests at the same time of day, and used the same operator throughout. This approach was specifically designed to isolate and assess the reliability of the measurement method itself.

Regarding differences between age groups, no significant differences were observed for lateral bending and axial rotations, as well as for mediolateral translation ($p > 0.05$ for all comparisons). However, the impact of age was evident in the range of flexion. The 20–30 age group demonstrated greater flexion compared to both the 40–50 and 50–60 groups, with MD of $1.64 \pm 2.12°$ and $2.17 \pm 2.39°$, respectively. Similarly, the 30–40 group showed greater flexion than the 50–60 group, with a mean difference of $1.70 \pm 2.71°$. For proximodistal translation, the 20–30 group also demonstrated higher values compared to both the 40–50 and 50–60 groups, with MD of 0.44 ± 0.57mm and 0.58 ± 0.65mm, respectively. Likewise, the 30–40 group showed greater values than the 50–60 group, with a mean difference of 0.43 ± 0.78mm. In terms of anteroposterior translation, both the 20–30 and 30–40 groups exhibited higher values compared to the 50–60 group, with mean differences of 0.92 ± 0.83mm and 0.66 ± 0.95mm, respectively. When interpreted relative to the MDC thresholds, these age-related differences in flexion and in proximodistal and anteroposterior translations are several times larger than the corresponding MDC values, supporting the conclusion that the observed decline in segmental mobility with age reflects true biomechanical changes rather than measurement noise.

The decline in lumbar flexion with increasing age has been well documented in several in vivo studies using various motion measurement techniques. Russell et al. (1993) measured lumbar spine range of motion in standing participants using radiographic analysis and reported no significant difference between the 20–29 and 30–39 age groups but observed a significant reduction of 3.5° in the 40–49 group compared to the youngest group

[21]. Similarly, McGregor et al. (1995), using an electromagnetic tracking system during upright flexion tasks, found a decrease of 5.9° in flexion for the 40–49 group and 6.2° for the 50–59 group when compared to the 30–39 reference group [22]. Dvorák et al. (1995), in an in vivo radiographic study conducted during active flexion-extension, also confirmed an age-dependent decrease in motion [23]. Van Herp et al. (2000) analyzed three-dimensional lumbar kinematics in 100 healthy subjects using a motion capture system during standardized trunk movements. Their findings indicated a reduction of 7.0° in flexion in the 50–59 age group compared to the 20–29 group, and reductions of 3.1° and 5.1° for the 40–49 and 50–59 groups, respectively, relative to the 30–39 group [24]. Milosavljevic et al. (2005), using an inclinometer in an occupational setting, confirmed similar age-related reductions in lumbar sagittal motion [25]. Troke et al. (2005) compiled a normative database using dual inclinometer and reported progressive declines across age groups during controlled forward bending tests in standing posture [26]. These consistent findings across studies using different methods and testing protocols demonstrate a clear and progressive reduction in lumbar flexion with advancing age.

To further analyze the significant and non-significant differences between age groups, correlations were assessed between flexion, the primary motion, and the other motion directions. The results showed that, consistent with the group comparisons, there were no significant correlations between flexion and lateral bending ($r_s = –0.07$, $p = 0.46$), axial rotation ($r_s = 0.11$, $p = 0.26$), or mediolateral translation ($r_s = –0.08$, $p = 0.39$). On the other hand, proximodistal and anteroposterior translations demonstrated strong ($r_s = 0.86$, $p<0.01$) and moderate-to-strong ($r_s = 0.61$, $p<0.01$) correlations with flexion, respectively. Altogether, these findings, consistent with previous studies on lumbar coupled motions [27,28], confirm that the observed inter-motion correlations are not dependent on age.

Concerning the differences between female and male participants, no statistically significant differences were observed in ROMs, either overall or within any specific motion plane. Nonetheless, a slight overestimation of flexion was noted in younger females (20–40 years) compared to males, with mean differences of 0.78 ± 2.33° for the 20–30 group and 0.72 ± 2.59° for the 30–40 group. In contrast, in older participants, flexion was slightly overestimated in males compared to females, with mean differences of 0.53 ± 2.09° for the

40–50 group and 0.39 ± 2.03° for the 50–60 group. Given that these sex-related differences in flexion are small and mostly close to the rotational MDC, and none reached statistical significance, they are unlikely to represent clinically meaningful differences in segmental lumbar mobility at the individual level.

Reports from the literature on sex-related differences in lumbar ROM vary considerably and lack consistency. Some in-vivo studies using radiographic or motion tracking techniques have reported no significant differences between male and female participants. For example, Dvorák et al. (1995), using lateral radiographs during controlled flexion-extension tasks in standing posture, found no significant sex-based differences in lumbar mobility across age groups [23]. Similarly, Wong et al. (2004), who assessed 100 healthy volunteers using surface markers and motion capture during upright forward bending, reported similar lumbar flexion between sexes [29]. In contrast, other in-vivo studies have reported higher lumbar range of motion (ROM) in males. Dreischarf et al. (2014) analyzed upright spinal postures and movements using biplanar X-ray imaging in asymptomatic adults and observed greater lumbar mobility in males compared to females, particularly in younger age groups [30]. Egwu et al. (2012), employing dual inclinometer during standing trunk flexion, also reported higher average ROM values for males [31]. Conversely, some studies have found greater lumbar flexion in females. Cook et al. (2015) conducted an in-vitro study on cadaveric lumbar spine segments under standardized loading and reported greater flexion range in female specimens [32]. Apti et al. (2023), using a goniometric assessment in healthy young adults during active flexion in standing, also observed significantly greater lumbar ROM in females [33]. These discrepancies may stem from variations in sample characteristics, measurement techniques, or the definition of flexion endpoints across studies.

Multiple in-vivo studies have reported high reliability (intraclass correlation coefficient, ICC > 0.90) for both within-day and between-days spinal ROM assessments using various standardized measurement techniques. For example, Hani et al. (2022) used a wearable inertial measurement unit (IMU) system to assess dynamic lumbar spine motion in a clinical setting and reported excellent reliability for repeated measurements over multiple sessions [34]. Similarly, Matheve et al. (2018) evaluated lumbopelvic flexion

kinematics during functional control tasks in healthy adults using optical motion capture and found strong within- and between-session reliability of segmental motion patterns [35]. In addition to these motion capture studies; the reliability of ultrasound-based 3D reconstruction methods has also been demonstrated. For instance, one study reported an ICC (2,1) of 0.97 ± 0.03 for repeated reconstructions of a single lumbar vertebra using tracked ultrasound in-vitro [20]. Another in-vitro study by our group showed an ICC (2,1) of 0.93 ± 0.01 for repeated full-lumbar spine reconstructions using the same protocol [13]. Furthermore, a related study reported an ICC of 0.92 for full spinal reconstructions using freehand 3D ultrasound with electromagnetic tracking [37]. Together, these findings support the feasibility of achieving consistent and reproducible spinal kinematic measurements when using well-calibrated, standardized imaging or motion tracking setups.

The main limitations of this study are methodological. Despite the implementation of temporal calibration, a residual time offset between the imaging and tracking systems may still have affected the accuracy of the reconstructed motion. In addition, the segmentation process relied on manual input, which is time-consuming and susceptible to variability across observers, both during image acquisition and segmentation. Future studies should therefore include inter-observer reliability assessments to enhance the reproducibility of the method. Furthermore, this study focused exclusively on flexion movements and analyzed only two vertebral levels (L4–S1). The applicability of the proposed method to other types of motion, such as lateral bending and axial rotation, remains to be validated. These movements involve more complex vertebral coupling patterns and may introduce additional challenges in image acquisition, tracking accuracy, and 3D model reconstruction.

In conclusion, this study demonstrates that ultrasound imaging combined with motion tracking can determine 3D lumbar spine kinematics and provides normative measurements of segmental range of motion and translations across age and sex under a standardized protocol. Together with the geometric validation of the 3D ultrasound models and the high repeatability of the kinematic outputs, these results support the clinical use of this non-ionizing, portable approach for lumbar kinematic assessment. The accompanying

image dataset and manual bone labels also enable development of automated segmentation, which can further streamline clinical workflows.

5.8 Acknowledgments

Author Mohammad Reza Effatparvar received research support from Fonds de recherche du Québec—Nature et Technologie (FRQNT) under the grant [319993]. Author Stephane Sobczak received research support from Natural Sciences and Engineering Research Council of Canada (NSERC) under the grant [RGPIN-2016–05717]. The authors would like to sincerely thank all the participants for their time and valuable contribution to this research.

5.9 Data Statement

The datasets and code used during the current study are available from the corresponding author upon reasonable request, provided that such sharing does not conflict with the ethical approval obtained or compromise participant confidentiality.

5.10 References

1. Roach S, San Juan JG, Suprak DN, Lyda M. Concurrent validity of digital inclinometer and universal goniometer in assessing passive hip mobility in healthy subjects. *International journal of sports physical therapy*. 2013;8(5):680.

2. Heneghan NR, Balanos GM. Soft tissue artefact in the thoracic spine during axial rotation and arm elevation using ultrasound imaging: a descriptive study. *Manual therapy*. 2010;15(6):599-602.

3. Cuesta-Vargas AI. Development of a new ultrasound-based system for tracking motion of the human lumbar spine: reliability, stability and repeatability during forward bending movement trials. *Ultrasound in medicine & biology*. 2015;41(7):2049-2056.

4. Pearson AM, Spratt KF, Genuario J, et al. Precision of lumbar intervertebral measurements: does a computer-assisted technique improve reliability? *Spine*. 2011;36(7):572-580.

5. Breen A, Hemming R, Mellor F, Breen A. Intrasubject repeatability of in vivo intervertebral motion parameters using quantitative fluoroscopy. *European spine journal*. 2019;28:450-460.

6. Dugailly P-M, Beyer B, Sobczak S, Salvia P, Feipel V. Global and regional kinematics of the cervical spine during upper cervical spine manipulation: a reliability analysis of 3D motion data. *Manual therapy*. 2014;19(5):472-477.

7. Daniel ES, Lee RY, Williams JM. The reliability of video fluoroscopy, ultrasound imaging, magnetic resonance imaging and radiography for measurements of lumbar spine segmental range of motion in-vivo: A review. *Journal of Back and Musculoskeletal Rehabilitation*. 2023;36(1):117-135.

8. Melhem E, Assi A, El Rachkidi R, Ghanem I. EOS® biplanar X-ray imaging: concept, developments, benefits, and limitations. *Journal of children's orthopaedics*. 2016;10(1):1-14.

9. Adler RS. What is the place of ultrasound in MSK imaging? *Skeletal Radiology*. 2024;53(9):1699-1709.

10. Chleboun GS, Amway MJ, Hill JG, Root KJ, Murray HC, Sergeev AV. Measurement of segmental lumbar spine flexion and extension using ultrasound imaging. *journal of orthopaedic & sports physical therapy*. 2012;42(10):880-885.

11. McKinnon CD, Callaghan JP. The relationship between external thoracopelvic angle and lumbar segmental axial twist angle using an ultrasound imaging technique. *Human Movement Science*. 2021;78:102824.

12. Effatparvar MR, Sobczak S. Application of ultrasound in spine kinematic determination: A systemic review. *Journal of Medical Ultrasound*. 2022;30(1):6-10.

13. Effatparvar MR, Pierre M-OS, Sobczak S. Assessment and improvement of a novel ultrasound-based 3D reconstruction method: Registered for lumbar spine. *Journal of Medical and Biological Engineering*. 2022;42(6):790-799.

14. Effatparvar MR, St-Pierre M-O, Lavoie F-A, Sobczak S. Application of Musculoskeletal Ultrasound in Lumbar Spine 3D Kinematics Visualization and

Determination: An In Vitro Study. *Journal of Medical and Biological Engineering*. 2025:1-10.

15. Ungi T, Lasso A, Fichtinger G. Open-source platforms for navigated image-guided interventions. *Medical image analysis*. 2016;33:181-186.

16. Lasso A, Heffter T, Rankin A, Pinter C, Ungi T, Fichtinger G. PLUS: open-source toolkit for ultrasound-guided intervention systems. *IEEE transactions on biomedical engineering*. 2014;61(10):2527-2537.

17. Dugailly P-M, Sobczak S, Sholukha V, et al. In vitro 3D-kinematics of the upper cervical spine: helical axis and simulation for axial rotation and flexion extension. *Surgical and radiologic anatomy*. 2010;32:141-151.

18. Effatparvar MR, St-Pierre M-O, Lavoie F-A, Sobczak S. Application of Musculoskeletal Ultrasound in Lumbar Spine 3D Kinematics Visualization and Determination: An In Vitro Study. *Journal of Medical and Biological Engineering*. 2025;45(2):230-239.

19. Hacihaliloglu I. Ultrasound imaging and segmentation of bone surfaces: A review. *Technology*. 2017;5(02):74-80.

20. Forbes A, Cantin V, Develle Y, et al. Musculoskeletal ultrasound for 3D bone modeling: A preliminary study applied to lumbar vertebra. *Journal of back and musculoskeletal rehabilitation*. 2021;34(6):937-950.

21. Russell P, Pearcy MJ, Unsworth A. Measurement of the range and coupled movements observed in the lumbar spine. *Br J Rheumatol*. 1993;32(6):490-7. doi:10.1093/rheumatology/32.6.490

22. McGregor AH, McCarthy ID, Hughes SP. Motion characteristics of the lumbar spine in the normal population. *Spine (Phila Pa 1976)*. Nov 15 1995;20(22):2421-8. doi:10.1097/00007632-199511001-00009

23. Dvorák J, Vajda EG, Grob D, Panjabi MM. Normal motion of the lumbar spine as related to age and gender. *Eur Spine J*. 1995;4(1):18-23. doi:10.1007/bf00298413

24. Van Herp G, Rowe P, Salter P, Paul J. Three-dimensional lumbar spinal kinematics: a study of range of movement in 100 healthy subjects aged 20 to 60+ years. *Rheumatology*. 2000;39(12):1337-1340.

25. Milosavljevic S, Milburn PD, Knox BW. The influence of occupation on lumbar sagittal motion and posture. *Ergonomics*. 2005;48(6):657-667.

26. Troke M, Moore AP, Maillardet FJ, Cheek E. A normative database of lumbar spine ranges of motion. *Manual therapy*. 2005;10(3):198-206.

27. Orbach MR, Mahoney J, Bucklen BS, Balasubramanian S. In vitro coupled motions of the whole human thoracic and lumbar spine with rib cage. *JOR spine*. 2023;6(3):e1257.

28. Huijbregts P. Lumbar spine coupled motions: A literature review with clinical implications. *Orthopaedic Division Review*. 2004:21-25.

29. Wong KW, Leong JC, Chan M-k, Luk KD, Lu WW. The flexion–extension profile of lumbar spine in 100 healthy volunteers. *Spine*. 2004;29(15):1636-1641.

30. Dreischarf M, Albiol L, Rohlmann A, et al. Age-related loss of lumbar spinal lordosis and mobility–a study of 323 asymptomatic volunteers. *PloS one*. 2014;9(12):e116186.

31. Egwu M, Mbada C, Olowosejeje D. Normative values of spinal flexibility for Nigerians using the inclinometric technique. *Journal of exercise science and physiotherapy*. 2012;8(2):93-104.

32. Cook DJ, Yeager MS, Cheng BC. Range of motion of the intact lumbar segment: a multivariate study of 42 lumbar spines. *International journal of spine surgery*. 2015;9

33. Apti A, Çolak T, Akçay B. Normative values for cervical and lumbar range of motion in healthy young adults. *Journal of Turkish Spinal Surgery*. 2023;34(3)

34. Hani H, Souchereau R, Kachlan A, Harris H, Dufour J, Aurand A, Mageswaran P, Hyer M, Marras W. Reliability of a Wearable motion system for clinical

evaluation of dynamic lumbar spine function. *Advances in complementary & alternative medicine*. 2022;7(2):672.

35. Matheve T, De Baets L, Rast F, Bauer C, Timmermans A. Within/between-session reliability and agreement of lumbopelvic kinematics in the sagittal plane during functional movement control tasks in healthy persons. *Musculoskeletal Science and Practice*. 2018;33:90-98.

36. Hidalgo B, Gilliaux M, Poncin W, Detrembleur C. Reliability and validity of a kinematic spine model during active trunk movement in healthy subjects and patients with chronic non-specific low back pain. Journal of rehabilitation medicine. 2012;44(9):756-63.

37. Jiang W, Chen X, Yu C. A real-time freehand 3D ultrasound imaging method for scoliosis assessment. Journal of applied clinical medical physics. 2022;23(8):e13709.

Chapter 6 – Feasibility of Ultrasound Imaging for Determining Shoulder 3D Kinematics: A Pilot Study

6.1 Original Contribution of the Student and Co-authors

The sixth chapter of the thesis presents an article entitled *Feasibility of Ultrasound Imaging for Determining Shoulder 3D Kinematics: A Pilot Study.* This article, co-authored by Mohammad Reza Effatparvar, Mickaël Begon, Nicola Hagemeister, and Stéphane Sobczak, was submitted to the *Journal of Ultrasound* in July 2025.

Feasibility of Ultrasound Imaging for Determining Shoulder 3D Kinematics: A Pilot Study

Mohammad Reza Effatparvar [a, b*], Mickaël Begon [c, d], Nicola Hagemeister [e, f] Stéphane Sobczak [a, b, g]

[a] *Département d'anatomie, Université du Québec à Trois-Rivières, Trois-Rivières, Québec, Canada.*

[b] *Groupe de Recherche sur les Affections Neuromusculosquelettiques (GRAN), Université du Québec à*

Trois-Rivières, Trois-Rivières, Québec, Canada.

[c] *Laboratoire de Simulation et Modélisation du Mouvement, Université de Montréal, Montréal, QC, Canada*

[d] *CHU Sainte-Justine Azrieli Research Center, Université de Montréal, Montreal, QC, Canada*

[e] *Laboratoire d'Innovation Ouverte en technologies de la santé (LIO-ÉTS), Centre de Recherche du Centre Hospitalier de l'université de Montréal (CRCHUM), 900 St-Denis, Montréal, QC H2X 0A9, Canada*

[f] *École de Technologie Supérieure, Département de génie des systèmes, 1100 rue Notre-Dame Ouest, Montréal, QC H21 2W5, Canada*

[g] *Institut National d'Anatomie (INA), Université du Québec à Trois-Rivières, Trois-Rivières, Québec, Canada.*

*Corresponding author: Mohammad.reza.effatparvar@uqtr.ca

3351, boulevard des Forges, Trois-Rivières (Québec), Canada, G8Z 4M3

Statements and Declarations

Competing Interests

The authors have no relevant financial or non-financial interests to disclose

Author Contributions

All authors contributed to the study conception and design. Material preparation, data collection and analysis were performed by Mohammad Reza Effatparvar. The first draft of the manuscript was written by Mohammad Reza Effatparvar, and all authors commented on previous versions of the manuscript. All authors read and approved the final manuscript

Funding

Author Nicola Hagemeister received research support from Fonds de recherche du Québec—Nature et Technologie (FRQNT) under the grant [2022-PR-299758]. Author Stephane Sobczak received research support from Natural Sciences and Engineering Research Council of Canada (NSERC) under the grant [RGPIN-2016–05717].

Ethics approval

This study was performed in line with the principles of the Declaration of Helsinki. Approval was granted by ‘The Ethics Subcommittee of the Anatomy Laboratory for Teaching and Research’ of Université du Québec à Trois-Rivières (Date: 2023/10/04 No: SCELERA 23 − 14).

6.2 Abstract

Purpose: Shoulder kinematics is essential for diagnosing and rehabilitating various disorders. Motion capture with skin-attached markers is a common but inaccurate measurement method due to soft tissue artefact. Personalized models using ionizing or costly imaging methods (CT or MRI) increase kinematic accuracy. Ultrasound imaging offers a non-ionizing, cost-effective alternative and has recently been used for accurate 3D modeling. This study evaluates its feasibility for 3D shoulder kinematics.

Methods: A shoulder was isolated from a human cadaver. Technical markers (TMs) were affixed to the bony segments. Bones and TMs were segmented from CT and ultrasound images to generate 3D models. The shoulder underwent discrete motions, during which the TMs were digitized. Discrete motions were visualized on 3D models by linking digitized and segmented TMs. Anatomical reference frames were defined from anatomical landmarks based on virtual palpation. Joint kinematics was calculated, and range of motions (ROM) were reported as Euler angles. The 3D models and ROM values were compared between ultrasound and CT.

Results: The ultrasound 3D model showed a mean reconstruction error of 0.66±0.06 mm compared to the CT scan, indicating larger volumes for the ultrasound models. The ROMs from ultrasound were also slightly overestimated (0.43±0.72°) compared to CT. Bland-Altman analysis confirmed agreement between the two methods.

Conclusion: Regardless of the slight overestimation for ultrasound, high agreement was observed for the ROM measurements between the two imaging methods. This agreement indicates the possibility of adequate morphological data extraction and highlights the feasibility of using ultrasound-based data for personalized shoulder kinematic determination.

Keywords: ultrasound, shoulder, kinematics, range of motion

6.3 Résumé

Objectif : La cinématique de l'épaule est essentielle pour le diagnostic et la rééducation de divers troubles. La capture du mouvement à l'aide de marqueurs cutanés est une méthode courante, mais inexacte en raison des artefacts causés par les tissus mous. Les modèles personnalisés utilisant des méthodes d'imagerie ionisantes ou coûteuses (CT ou IRM) permettent d'augmenter la précision cinématique. L'imagerie par ultrasons, non ionisante et économique, a récemment été utilisée pour la modélisation 3D précise. Cette étude évalue sa faisabilité pour l'analyse cinématique 3D de l'épaule.

Méthodes : Une épaule humaine a été isolée d'un cadavre. Des marqueurs techniques (MT) ont été fixés aux segments osseux. Les os et les MT ont été segmentés à partir d'images CT et échographiques pour générer des modèles 3D. L'épaule a subi des mouvements discrets pendant lesquels les MT ont été numérisés. Les mouvements ont été visualisés sur les modèles 3D en associant les MT numérisés aux MT segmentés. Des repères anatomiques ont été utilisés pour définir des référentiels anatomiques par palpation virtuelle. La cinématique articulaire a été calculée et les amplitudes de mouvement (ROM) ont été exprimées sous forme d'angles d'Euler. Les modèles 3D et les ROM ont été comparés entre les images échographiques et CT.

Résultats : Le modèle 3D échographique a montré une erreur moyenne de reconstruction de 0,66±0,06 mm par rapport au CT, indiquant un volume légèrement supérieur pour les modèles échographiques. Les ROM dérivées des échographies ont également été légèrement surestimées (0,43±0,72°) par rapport au CT. L'analyse de Bland-Altman a confirmé l'accord entre les deux méthodes.

Conclusion : Malgré une légère surestimation liée aux ultrasons, un fort accord a été observé pour les mesures des ROM entre les deux modalités d'imagerie. Cet accord confirme la possibilité d'extraire des données morphologiques adéquates et souligne la faisabilité de l'utilisation des données échographiques pour la détermination personnalisée de la cinématique de l'épaule.

Mots-clés : échographie, épaule, cinématique, amplitude de mouvement

6.4 Introduction

The shoulder allows a large range of motion while maintaining strength. However, this versatility also makes it prone to various disorders, such as rotator cuff tears and osteoarthritis [1]. Accurately diagnosing these conditions and developing effective rehabilitation protocols require a comprehensive understanding of shoulder kinematics. Current noninvasive methods for analyzing shoulder kinematics primarily rely on motion capture systems with skin-attached markers [2]. However, due to the shoulder's complex motion and the limited accessibility of underlying structures, multibody kinematic models are needed to complement motion-tracking methods and ensure marker trajectories align with joint components [3]. These models, however, are sensitive to geometric parameters and joint representation [4]. Although numerous generic kinematic models exist and are commonly used, studies show that incorporating personalized information (e.g., humeral head and glenoid radii, clavicle length, gliding plane) into kinematic models can greatly increase the accuracy of the estimation [5].

Personalized 3D models can be generated using medical imaging modalities such as computed tomography (CT) [6] and magnetic resonance imaging (MRI) [7]. While these methods provide high-resolution morphological data, CT involves ionizing radiation, and MRI is limited by high costs and limited availability. As an alternative, ultrasound imaging offers a non-ionizing, low-cost, and portable solution [8]. In musculoskeletal applications, ultrasound is primarily used for diagnosing soft tissue disorders, with limited application in bone imaging due to challenges such as acoustic shadowing and lower bone contrast [9]. However, advancements in image processing and 3D reconstruction techniques have improved its viability for generating 3D bone models [10]. Despite this progress, no ultrasound-based 3D shoulder model has yet to be utilized for kinematic analysis.

This study aimed to evaluate the feasibility of ultrasound imaging for generating 3D shoulder models and the potential applications of US-generated models in kinematic analysis. To achieve this, a pilot study was conducted in which a complete 3D shoulder bone model was reconstructed from ultrasound images and compared to the model reconstructed from CT. The comparison was performed using two approaches: direct 3D model comparisons to quantify reconstruction error and range of motion (ROM)

measurements derived from kinematic analysis. Through this evaluation, the study offers insights into the potential of ultrasound imaging for personalized shoulder kinematic analysis.

6.5 Material and Methods

6.5.1 Specimen preparation

A thawed human cadaver (female, 83 years old) was dissected to isolate the right shoulder complex. To preserve structural integrity between the sternum and the vertebrae, T1 and T2, along with the first rib, were retained. T1 was fixed to the sternum, and all structures above were removed. The humerus was sectioned at its proximal one-third, and the scapula was cut accordingly.

To prevent any motion in the joints during imaging, the scapula was secured to the vertebrae using two orthopedic screws. Additionally, a Schanz screw was inserted through the humeral canal to fix the humerus to the scapula, maintaining it in a 90° abduction position. This position was chosen to accommodate the specimen within the ultrasound imaging frame.

Semi-spherical holes were drilled on the anatomical segments, and technical markers (TMs) (7.14 mm metallic spheres) were affixed using cyanoacrylate glue. For subcutaneous sites, incisions were made before marker placement. The markers were distributed as follows: three on the sternum, three on the clavicle, four on the scapula, and four on the humerus, ensuring enough coverage essential for accurate 3D motion tracking.

6.5.2 Imaging

The specimen was placed inside a plastic cylinder frame (⌀ 160 mm), which was filled with porcine gelatin (Gelatine, Type A, Pork Skin, min. Bloom 225). The setup was refrigerated to allow the gelatin to harden. Once set, DICOM images were acquired using a CT scanner (GE Healthcare, Revolution EVO) with a reconstruction slice thickness of 0.5 mm and an inter-slice spacing of 0.625 mm.

Next, the specimen was positioned and secured at the center of a Computer-Assisted Mechanical (CAM) frame (Fig. 1-A). Ultrasound imaging was performed using a

linear probe (NextGen LOGIQ e, GE Healthcare, USA) set to musculoskeletal mode (Frequency = 8 MHz, Depth = 8 cm, Gain = 60). The probe was mounted on a mobile plate inside the CAM, which moved along the specimen at a velocity of 0.5 mm/s using a stepper motor. This low speed was chosen to minimize inter-image gaps. After each longitudinal (up-down) scan, the plate was manually rotated at 30-degree intervals to ensure complete rotational coverage of the specimen [10].

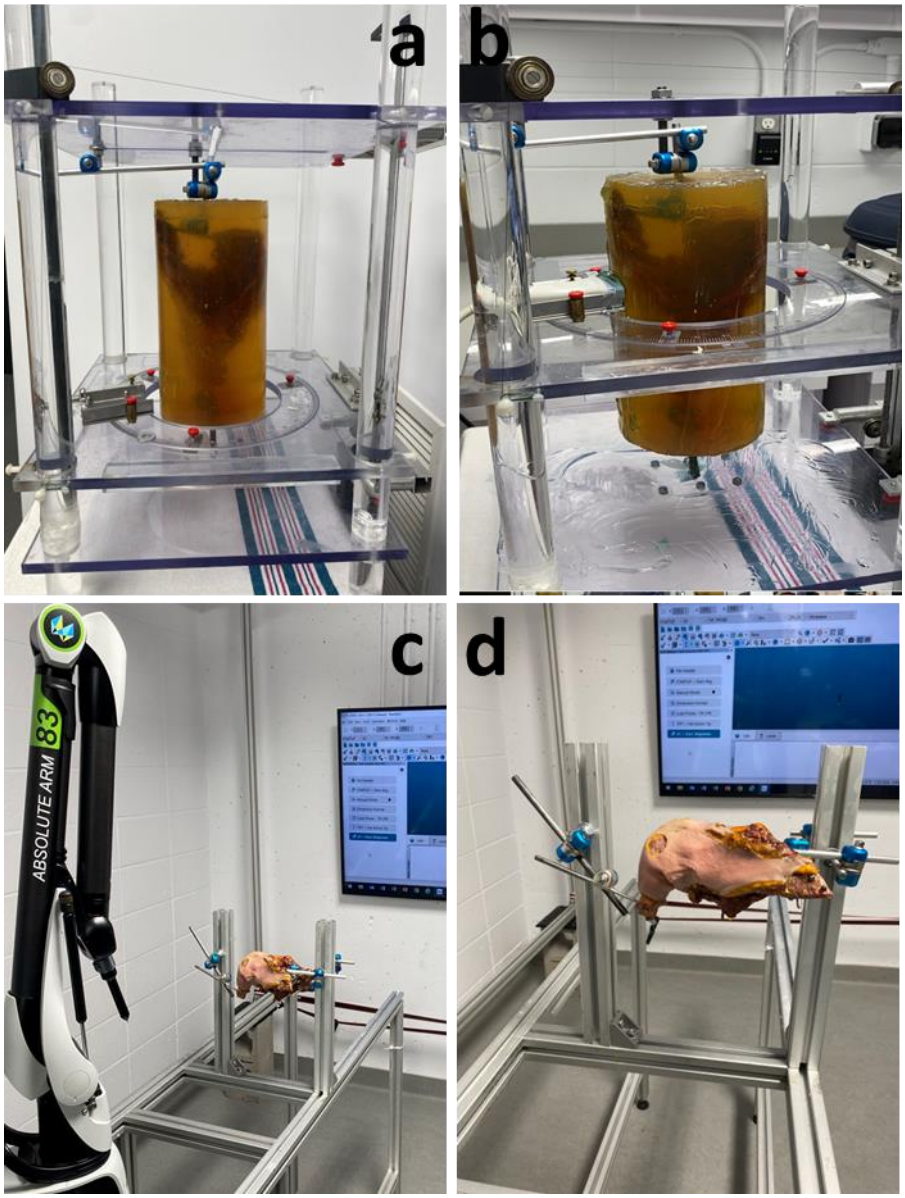

Fig.1 a The specimen embedded in gelatin and fixed within the CAM frame, which facilitates the ultrasound imaging procedure. b The probe, fixed on the probe holder, moving upward while

scanning the specimen. c The specimen and digitizer mounted and fixed on a table for digitizing the TMs. d A closer view of the specimen positioned in front of the digitizer

6.5.3 Applying discrete motions

After imaging, the gelatin, the Schanz screw in the humerus, and the screws securing the scapula were removed. The specimen was mounted, with the vertebrae stabilized on an aluminum extrusion. A Schanz screw was perpendicularly inserted into the humerus to help maintain the arm in various positions. Once the specimen was stabilized, it was subjected to six discrete positions, including neutral, 45 and 90° abduction, 45 and 90° flexion, and maximum elevation. At each position, the joint was immobilized using external fixation clamps, and TMs were digitized using a 3D digitizer (Hexagon Absolute Arm, measurement error: 0.008 mm) (Fig. 1-B).

6.5.4 Image processing and segmentation

Ultrasound images were first merged and converted into a 3D DICOM series using a custom MATLAB (MathWorks, R2021a) script [11]. In this process, the known position and orientation of the probe, provided by the CAM frame, allowed the 3D spatial positioning of each captured image, enabling the creation of a 3D DICOM series. Subsequently, both ultrasound and CT images were independently manually segmented (Fig. 2) using Amira software (5.2.2®, Germany) to generate 3D models (Fig. 3). In both ultrasound and CT images, the bone surfaces and TMs were segmented separately.

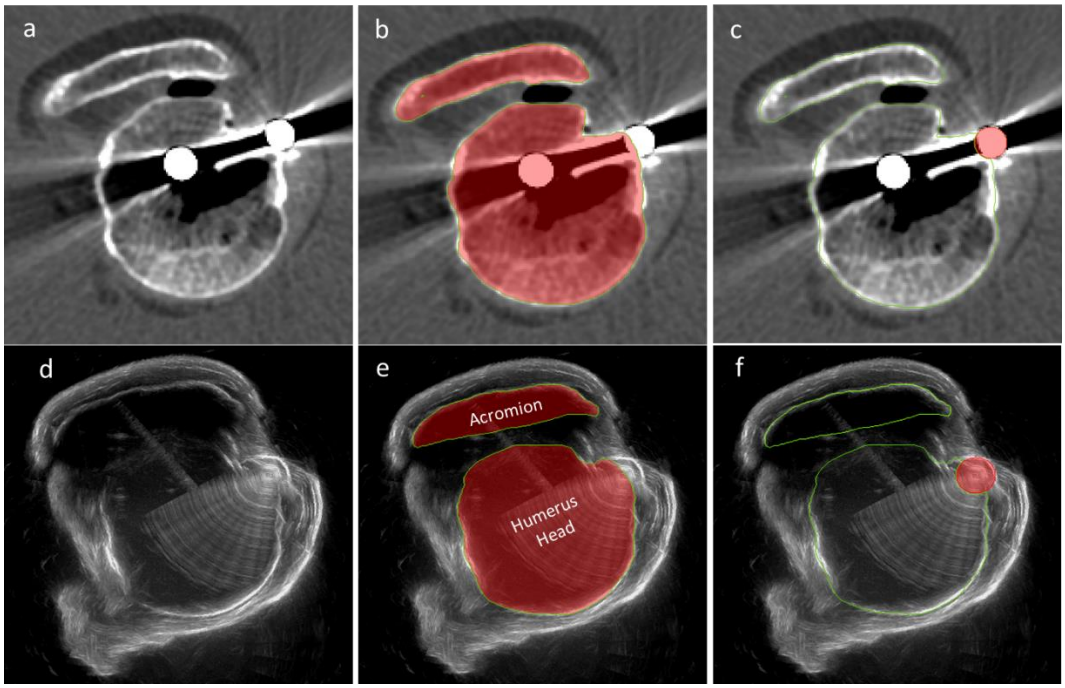

Fig.2 The segmentation of the ultrasound and CT images related to the same cross-section. a, b, and c show a CT image before segmentation, after bone and a TM segmentation highlighted. d, e, f show an ultrasound image before segmentation, after bone and a TM segmentation highlighted.

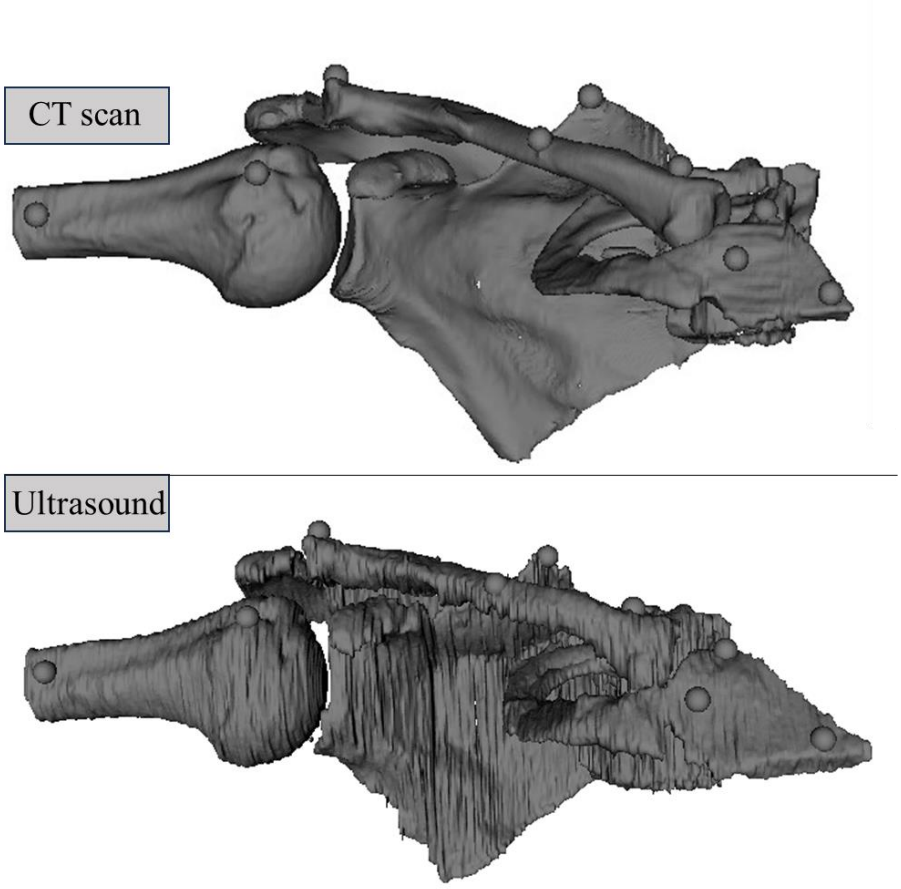

Fig.3 3D reconstructed models from CT scan (up) and ultrasound (down).

6.5.5 Motion representation

TMs digitization provided their centroid coordinates in each position to establish local reference frames and calculate rotation matrices representing the motions. These frames are referred to as technical reference frames (TRFs). Additionally, segmenting the markers from the images allowed for the calculation of their centroid coordinates within each imaging coordinate system, enabling the establishment of TRFs on the 3D models. The real discrete motions were represented on 3D models after applying the transformation matrices to the TRFs of the 3D models. The entire procedure was implemented in LhpFusionBox software (ULB, Belgium) [29].

6.5.6 Definition of anatomical reference frames

After motion representation, anatomical landmarks (ALs) were digitally palpated, in line with the recommendations of the International Society of Biomechanics (ISB) (Wu

et al., 2002) and anatomical reference frames (ARFs) were established for each component within LhpFusionBox software (Fig. 4).

The defined landmarks included:

- Thorax (3 landmarks): End of the corner of the sternum, most ventral point on the sternocostal joint of the first rib, and the spinous process of T1.
- Clavicle (2 landmarks): Most ventral point on the sternoclavicular joint and most dorsal point on the acromioclavicular joint.
- Scapula (4 landmarks): Midpoint of the triangular surface on the medial border of the scapula in line with the scapular spine (Trigonum Spinae Scapulae), most caudal point of the scapula (Angulus Inferior), most laterodorsal point of the scapula (Angulus Acromialis), and most ventral point of the processus coracoideus.
- Humerus (3 landmarks): Glenohumeral rotation center, most caudal point on the lateral side of the shaft, and most caudal point on the medial side of the shaft.

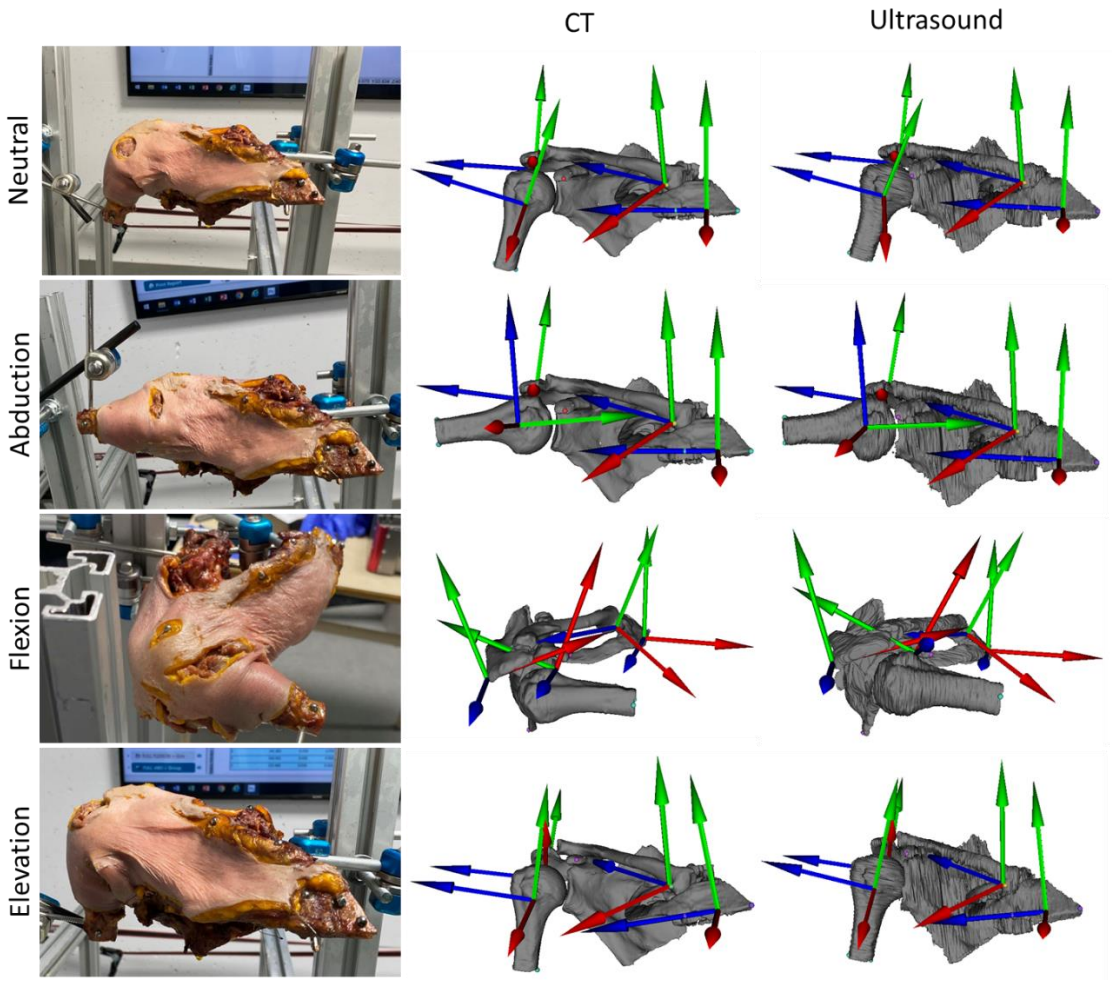

Fig.4 Applied discrete motions and their corresponding representation on the CT scan and ultrasound 3D models. The left column shows the positions, the middle column shows the motion representation on the CT models, and the right column the ultrasound models. From the first to the fourth row, the represented positions are neutral, abduction, flexion, and elevation, respectively. The TMs were removed from the models after motion representation. Markers on the segments indicate anatomical ALs. In the ARFs, the red, green, blue vectors represent the X-, Y-, and Z-axes, respectively.

6.5.7 Joint Kinematics, 3D models comparison and statistical analysis

The joint kinematics was determined, and the ROMs were measured from Euler angles for the sternoclavicular (SC), acromioclavicular (AC), and glenohumeral (GH) joints according to the ISB recommendations. Concerning the reconstruction errors, each anatomical 3D segment from ultrasound was compared with the corresponding segment from CT scan [10]. Briefly, after automatic registration of the 3D models in CloudCompare

software (v2.12 Beta, France), the mesh-to-mesh distances between the ultrasound and CT scan models were calculated and considered as the reconstruction error.

Mean reconstruction errors, mean differences (MD), standard deviation (SD) and Bland-Altman plots were used to compare the means and the limits of agreement between ultrasound and CT scan using MATLAB software.

6.6 Results

The computed reconstruction errors for each anatomical segment were 0.57±0.35 mm for the humerus, 0.68±0.52 mm for the scapula, 0.71±0.41 mm for the thorax, and 0.69±0.24 mm for the clavicle. The errors were normally distributed (Fig. 5) and indicate a general overestimation of ultrasound-derived 3D models, with a mean error of 0.66±0.06 mm.

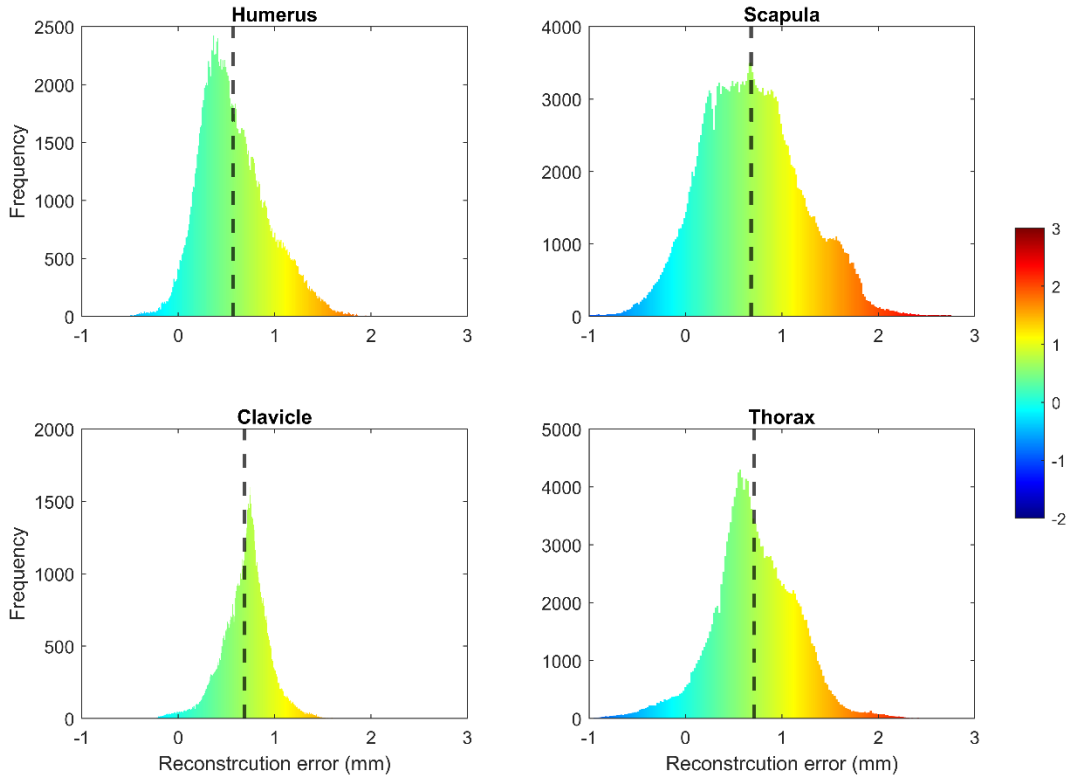

Fig.5 Distribution of data points (frequency) for ultrasound 3D models compared to CT. Colors range from green to red, indicating higher reconstruction errors, and from green to blue, indicating lower reconstruction errors. Most of data points fall on the positive side, suggesting

that ultrasound 3D models overestimate volumes compared to CT. Dashed vertical lines represent mean values.

A similar trend was observed for joint kinematics, where ROM values derived from ultrasound images were slightly higher (0.43±0.72°) (Table 1). The Bland-Altman analysis (Fig. 6) confirmed the agreement between the two methods, as most of the ROM differences remained within the limits of agreement (95% CI, ±1.96 SD).

Table 1. The ROMs values from ultrasound and CT related to the primary motion of each joint. SC stands for the sternoclavicular joint, AC stands for the acromioclavicular joint, and GH stands for the glenohumeral joint.

Applied motion to the arm	Joint	Measured Motion	CT	Ultrasound
Half abduction	SC	Elevation	1.12°	1.19°
	AC	Upward rotation	0.83°	0.96°
	GH	Abduction	31.29°	32.28°
Abduction	SC	Elevation	2.16°	2.20°
	AC	Upward rotation	1.50°	1.65°
	GH	Abduction	63.47°	65.77°
Half flexion	SC	Elevation	5.63°	5.85°
	AC	Upward rotation	4.06°	4.47°
	GH	Flexion	49.50°	50.99°
Flexion	SC	Elevation	10.20°	10.56°
	AC	Upward rotation	7.32°	8.04°
	GH	Flexion	78.25°	78.65°
Elevation	SC	Elevation	12.22°	12.14°
	AC	Elevation	20.76°	20.70°
	GH	Elevation	6.59°	5.86°
Mean			**19.66°**	**20.08°**
SD			24.81°	25.28°
Mean difference			0.43° ± 0.72°	

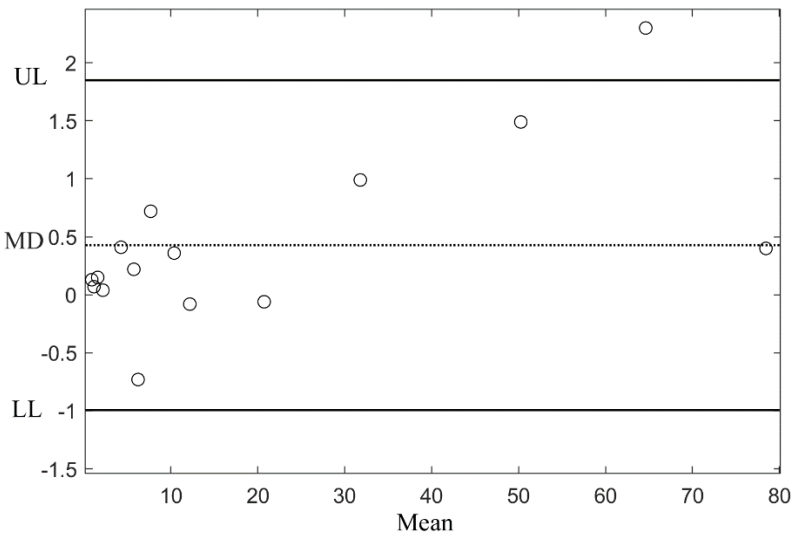

Fig.6 Bland-Altman plot showing the limits of agreement between ultrasound and CT. MD stands for mean differences and equals 0.43°, UL stands for upper limit and equals 1.84° and LL stands for lower limit and equals -0.99°. All values are in degrees.

6.7 Discussion

Incorporating personalized bone geometry (e.g., humeral head and glenoid radii, clavicle length, gliding plane) into kinematic models can greatly improve estimation accuracy [5]. Possibility of generating 3D models from ultrasound images facilitates the extraction of personalized morphological data for kinematic analysis. In this pilot study, the feasibility of this application was analyzed by comparing 3D reconstructed models from ultrasound and CT images.

CT model was considered as the reference to assess the differences between the 3D models, (Fig. 5). The ultrasound images generated slightly larger volumes 0.66±0.06 mm. This overestimation can be attributed to thicker bone boundaries in ultrasound images, which may lead to manual segmentation errors [12]. Larger 3D volumes from ultrasound images compared to CT scans have been reported in several studies across different applications, including the spine [10], kidney [13], and tumor [14].

Concerning the measured joint kinematics, joint angles were slightly overestimated by ultrasound ($0.43 \pm 0.72°$). Nonetheless, Bland-Altman analysis showed that these differences remained within the limits of agreement between the two imaging methods,

confirming the accuracy of ultrasound-based reconstructions for identifying anatomical landmarks and computing joint angles. This level of precision underscores the advantage of using subject-specific morphological data for kinematic analysis. In contrast, generic or scaled models often lack anatomical fidelity, leading to larger errors in joint kinematics. For instance, Lavail et al. reported angular errors ranging from 3.2° to 5.4° when using a scaled-generic shoulder model compared to MRI-based personalized geometry [15]. Similarly, Charbonnier et al. found 2–4° of orientation error in motion capture–based shoulder models [6]. In translational kinematics, Menze et al. showed that using a musculoskeletal model (AnyBody ShoulderArm) yielded median inferior–superior translation errors of 1.8 mm, reduced from 2.8 mm when compared to biplanar fluoroscopy [16]. Hammond et al. also observed an average linear positioning error of 2.8 mm when comparing generic OpenSim bone geometries to subject-specific models [17].

Compared to these values, the angular error in our ultrasound-based personalized model ($0.43 \pm 0.72°$) is significantly lower, highlighting the importance of anatomical specificity in achieving accurate 3D kinematic measurements. Although no prior studies have applied ultrasound imaging for 3D shoulder kinematics, this approach has been validated in the lumbar spine with a similarly low error ($0.23 \pm 0.20°$ compared to CT [18], reinforcing the broader applicability of personalized ultrasound-based modeling in musculoskeletal research.

These preliminary results pave the way for advancing the application of ultrasound imaging in shoulder 3D modeling, with potential for use in personalized kinematic models for more accurate measurements. The use of ultrasound images in in-vivo cases, combined with new artificial intelligence-based auto-reconstruction, will enable real-time 3D modeling and make the extraction of the necessary morphological data highly accessible. However, it's important to acknowledge the inherent challenges of accurately visualizing bone contours in vivo with ultrasound, particularly in complex anatomical regions like the shoulder due to overlying soft tissues and the varying bone curvatures. In conclusion, the ultrasound-based shoulder model shows strong potential for enabling accurate in-vivo kinematic reconstruction with an angular precision of approximately 1°, making it a viable tool for clinical and research applications.

6.8 References:

1. Sarquis LM, Coggon D, Ntani G, Walker-Bone K, Palmer KT, Felli VE, et al. (2016) Classification of neck/shoulder pain in epidemiological research: a comparison of personal and occupational characteristics, disability, and prognosis among 12,195 workers from 18 countries.Pain;157(5):1028-36.

2. Ceglia A, Facon K, Begon M, Seoud L (2024) Real-time, accurate, and open source upper-limb musculoskeletal analysis using a single RGBD camera.arXiv preprint arXiv:240610007.

3. Jackson M, Michaud B, Tétreault P, Begon M (2012) Improvements in measuring shoulder joint kinematics.Journal of biomechanics;45(12):2180-3.

4. Dumas R, Duprey S (2022) Subject-specific model-derived kinematics of the shoulder based on skin markers during arm abduction up to 180-assessment of 4 gleno-humeral joint models.Journal of Biomechanics;136:111061.

5. El Habachi A, Duprey S, Cheze L, Dumas R (2013) Global sensitivity analysis of the kinematics obtained with a multi-body optimisation using a parallel mechanism of the shoulder.Computer methods in biomechanics and biomedical engineering;16(sup1):61-2.

6. Charbonnier C, Chagué S, Kolo FC, Chow JC, Lädermann A (2014) A patient-specific measurement technique to model shoulder joint kinematics.Orthopaedics & Traumatology: Surgery & Research;100(7):715-9.

7. Špička J, Vychytil J, Ryba T, Havelková L (2018) Development of a personalized musculoskeletal human shoulder.

8. Effatparvar MR, Sobczak S (2022) Application of ultrasound in spine kinematic determination: A systemic review.Journal of Medical Ultrasound;30(1):6-10.

9. Romero-Morales C, Bravo-Aguilar M, Ruiz-Ruiz B, Almazán-Polo J, López-López D, Blanco-Morales M, et al. (2021) Current advances and research in ultrasound

imaging to the assessment and management of musculoskeletal disorders. Disease-a-Month;67(3):101050.

10. Effatparvar MR, Pierre M-OS, Sobczak S (2022) Assessment and improvement of a novel ultrasound-based 3D reconstruction method: Registered for lumbar spine.Journal of Medical and Biological Engineering;42(6):790-9.

11. Forbes A, Cantin V, Develle Y, Dubé Y, Bertrand-Grenier A, Ménard-Lebel C, et al. (2021) Musculoskeletal ultrasound for 3D bone modeling: A preliminary study applied to lumbar vertebra.Journal of back and musculoskeletal rehabilitation;34(6):937-50.

12. Hacihaliloglu I (2017) Ultrasound imaging and segmentation of bone surfaces: A review.Technology;5(02):74-80.

13. Dai JC, Dunmire B, Sternberg KM, Liu Z, Larson T, Thiel J, et al. (2018) Retrospective comparison of measured stone size and posterior acoustic shadow width in clinical ultrasound images.World journal of urology;36:727-32.

14. Makouei F, Ewertsen C, Agander TK, Olesen MV, Pakkenberg B, Todsen T (2022) 3D Ultrasound versus Computed Tomography for Tumor Volume Measurement Compared to Gross Pathology—A Pilot Study on an Animal Model.Journal of imaging;8(12):329.

15. Lavaill M, Martelli S, Gilliland L, Gupta A, Kerr G, Pivonka P (2022) The effects of anatomical errors on shoulder kinematics computed using multi-body models.Biomechanics and Modeling in Mechanobiology;21(5):1561-72.

16. Menze J, Croci E, Andersen MS, Hess H, Lund ME, De Pieri E, et al. (2025) Advancing musculoskeletal shoulder modeling: reflecting glenohumeral translation with bony, ligamentous, and muscular stability constraints.Frontiers in Bioengineering and Biotechnology;13:1441530.

17. Hammond CV, Henninger HB, Fregly BJ, Gustafson JA (2024) Personalization of Closed-Chain Shoulder Models Yields High Kinematic Accuracy for Multiple Motions.bioRxiv:2024.12. 19.629415.

18. Effatparvar MR, St-Pierre M-O, Lavoie F-A, Sobczak S (2025) Application of Musculoskeletal Ultrasound in Lumbar Spine 3D Kinematics Visualization and Determination: An In Vitro Study.Journal of Medical and Biological Engineering;45(2):230-9.

Chapter 7 - General discussion

Low back pain (LBP) is among the leading cause of disability worldwide and one of the most common reasons for seeking rehabilitation care (Gianola et al., 2019). In most cases, no single structural lesion can be identified and the pain is classified as non-specific or mechanical, arising from the vertebrae, intervertebral discs, and surrounding soft tissues (Will et al., 2018). Among the many contributing factors, altered lumbar spine kinematics, such as segmental hyper- or hypomobility, aberrant coupling, and impaired load sharing, has been repeatedly associated with subgroups of patients with LBP and may help explain why individuals with similar static imaging findings can present very different symptoms and clinical courses (Abd Rahman et al., 2023). Accurately determining lumbar spine kinematics is therefore crucial for understanding spinal biomechanics, identifying motion-related dysfunctions, and developing targeted rehabilitation strategies.

Currently Imaging modalities such as computed tomography (CT) (Vania et al., 2019), magnetic resonance imaging (MRI) (Li et al., 2009), and biplanar radiographies (Melhem et al., 2016) are the gold standards for 3D kinematics assessments. However, their drawbacks, including ionizing radiation, high costs, and being limited to supine position, have prompted researchers to seek alternative methods. Among these, ultrasound has emerged as a promising solution due to its affordability, portability, and safety. The primary objective of this thesis was to advance the application of ultrasound in lumbar spine kinematic analysis through a series of studies that progressively addressed gaps in existing literature and finally verify its feasibility when being transferred to the shoulder joint complex.

As a preliminary step in this thesis, we systematically reviewed and critically evaluated the existing literature concerning the application of ultrasound imaging for spinal kinematic measurements. The review addressed two specific objectives: (1) identify methodological gaps in ultrasound-based spinal kinematics; and (2) determine whether current evidence supports moving from 2D surrogates to fully 3D assessments. The review was structured along the imaging pipeline with predefined outcomes (reliability, validity, standard method, anatomical references). The primary aim was to identify methodological gaps and outline the limitations that hinder clinical translation. Its role within the thesis is

to justify the development and validation of a 3D ultrasound pipeline and to define the specifications that the experimental chapters address.

The review first revealed that all existing studies remain restricted to 2D measurements, typically focusing on changes in interspinous distances (Chleboun et al., 2012) or the linear displacement of superficial landmarks (McKinnon & Callaghan, 2019). While these approaches are accessible, they are inherently limited in capturing the full complexity of 3D kinematics. The importance of 3D assessment lies in the fact that lumbar intervertebral motion often includes subtle but clinically relevant components of other motions (Panjabi et al., 1994; Pearcy et al., 1984).

Moreover, several studies lacked standardization in image acquisition protocols (Zheng et al., 2013), tracking techniques (Zheng et al., 2016), and motion analysis algorithms (Heneghan et al., 2009). This methodological variability contributes to inconsistent reliability and validity outcomes across the literature. For instance, discrepancies in the anatomical landmarks used as reference points significantly affect reproducibility and comparisons between studies. Plus, only a limited number of investigations attempted to validate ultrasound-derived measurements against gold-standard imaging modalities (Chleboun et al., 2012), and none employed 3D reconstruction techniques.

Building upon the findings of the systematic review, the second objective of this thesis was to validate a method for 3D reconstruction of the lumbar spine using ultrasound imaging. As 3D reconstruction is a fundamental prerequisite for determining spinal kinematics in three dimensions, developing a robust and accurate technique was essential. Such a method allows for high accessibility to key morphological structures and facilitates the identification of anatomical landmarks necessary for motion tracking.

To achieve this, a motorized rotational scanning protocol was implemented on complete lumbar specimens. In this system, analogous to how CT acquires images, the ultrasound probe was rotated around the specimen and, at each angular position, translated longitudinally along it. For the longitudinal sweeps, the starting point, translation speed, and travel distance were kept constant, allowing the interslice distance to be calculated from the number of acquired images. This distance was then used as the third (z)

dimension, in addition to the in-plane x and y dimensions (image width and height), which enabled each image to be positioned in 3D space. This technique produced a 360° series of images with known x, y, and z coordinates for each slice. Following image fusion and manual segmentation, 3D models were reconstructed.

The core validation strategy consisted of comparing the ultrasound-based models with those generated from CT scans, considered the clinical gold standard. For this purpose, three anatomical landmarks were defined on each vertebra to enable an initial coarse alignment of the models. Fine registration was then performed automatically in CloudCompare (Paris, France). These anatomical landmarks were used exclusively for alignment, and their potential impact on motion measurements was reserved for later studies, as it requires a more comprehensive analysis. This method, in addition to registering the models, also enabled the registration of their associated coordinate systems. Geometric congruency between the models was then quantitatively assessed using the Iterative Closest Point (ICP) algorithm.

Overall, the ultrasound-based reconstructions showed a slight overestimation in surface distance, with a maximum mean error of 0.44 ± 0.24 mm compared to CT models. This overestimation is primarily attributed to the intrinsic characteristics of ultrasound imaging, in which highly reflective structures such as the bony cortex appear several millimeters thick. Similar findings have been reported in the literature, such as an error of 0.44 ± 0.63 mm for dry vertebra reconstructions (Forbes et al., 2021) and 3.8 ± 2.4 mm for kidney stone surface modeling (Dai et al., 2018).

Agreement between modalities was further supported by Bland-Altman analysis, with all differences falling within the calculated limits of agreement. To evaluate the method's reliability, repeated reconstructions were performed, demonstrating excellent consistency with an ICC of 0.93 ± 0.01.

In addition to quantitative metrics, visual comparisons between ultrasound and CT-based models revealed strong morphological similarity. The ultrasound-based reconstructions clearly identified key posterior bony elements, including the spinous and costiform processes, which are critical for vertebral motion analysis as they serve as the primary anatomical landmarks for kinematic tracking.

Another important aspect of this study was the evaluation of soft tissue effects on reconstruction accuracy. A linear regression analysis was conducted to examine the relationship between posterior fat pad thickness and reconstruction error at posterior landmarks. For the full dataset (n = 30), the regression yielded a slope of 0.0252 error/mm, an intercept of 0.1008, and a correlation coefficient of r = 0.33, indicating a weak association. After removing a single extreme observation near ~6 mm (negative error), the results remained similar (n = 29; slope = 0.0279, intercept = 0.1169, r = 0.37). These findings suggest that posterior soft tissues do not substantially affect reconstruction accuracy for posterior landmarks; even when accounting for the outlier, any effect, if present, appears small.

Together, these findings confirmed that ultrasound imaging can reliably generate 3D models of lumbar vertebrae with high anatomical fidelity. The ability to visualize and localize key posterior landmarks, even in the presence of soft tissue, supported the feasibility of this method for future motion analysis applications. Accordingly, the logical next step in this thesis was to investigate whether these models could effectively capture intervertebral motion. The purpose here was to test kinematic outputs under controlled conditions by comparing motions computed from ultrasound-derived geometry with those from CT-derived geometry rigidly attached to the same specimens; in principle, motions should match, and discrepancies isolate geometric/landmark sources of error.

This step was crucial for determining the feasibility of extending ultrasound-based kinematic measurements to in-vivo settings. The study was designed so that a series of identical motions were imposed on the specimens, and the same motions were then quantified using both ultrasound- and CT-based models, thereby enabling an evaluation of measurement accuracy. Since reconstruction and segmentation had already been validated in the previous step, the primary focus here was on the definition of anatomical landmarks, the establishment of anatomical reference frames, and the computation of motion. Because the only varying element between the two models was the localization of these anatomical landmarks, this step essentially evaluated the ability of ultrasound-based models to provide reliable anatomical markers for kinematic analysis. The in-vitro comparison with CT-based measurements provided a controlled and rigorous context for this validation.

Regarding the reliability, good reliability (ICC = 0.89 ± 0.01) and low MDC (3.23% ± 1.52%) values underscored the method's precision, aligning well with previous work in ultrasound-based vertebral modeling (Forbes et al., 2021). These low MDC values indicated that ultrasound could reliably measure intervertebral ROM with minimal error, supporting its value in clinical diagnosis and treatment planning.

The strong agreement with CT-derived kinematics, as shown by t-tests and Bland–Altman analyses (−0.23° ± 0.20°, p = 0.57), further supported the validity of the ultrasound approach. Importantly, the study demonstrated that the positional and orientational accuracy of anatomical landmarks, rather than image resolution alone, was a key determinant of kinematic fidelity. The observed correlation between AL orientation errors and ROM differences (r = −0.85) emphasized the need for robust and consistent landmark identification protocols. It worth to mention that normality of specimen-level paired differences (Shapiro–Wilk) was assessed prior to t-tests and Pearson correlations; given n = 7 independent specimens, distribution-free confirmatory analyses and effect sizes with confidence intervals are encouraged for future work.

Direct comparisons with previous studies were limited by methodological differences, as most prior work relied on 2D techniques. In contrast, this study employed a 3D approach, enabling a more comprehensive measurement of vertebral motion. This distinction is particularly relevant for the lumbar spine, where movements often include subtle but clinically significant coupled motions. By capturing motion across all three planes, the method used here provided a clearer picture of these complex patterns than conventional 2D techniques.

Overall, this study demonstrated that musculoskeletal ultrasound, when combined with 3D reconstruction, could reliably quantify intervertebral motion in the lumbar spine. The method yielded accurate results compared to CT imaging and effectively captured coupled kinematic behavior across vertebral levels. By validating both the reliability and accuracy of this technique in an in-vitro setting, the next phase of the thesis focused on evaluating the method in in-vivo conditions, where physiological loading and tissue variability introduce new challenges for ultrasound-based motion analysis.

To this end, a tracked ultrasound acquisition protocol was first implemented, and the necessary calibrations, temporal, pivot, and spatial, were performed. For the temporal calibration (Moult et al., 2017), the pixel intensities of the ultrasound images and the tracking data were independently normalized and converted into separate signals. The time points corresponding to the peaks of each signal (x-values) were then identified, and the differences between them were taken as the latency between the two systems (0.311 ± 3.81 ms). This latency was subsequently added as a delay to the imaging frames in the acquisition configuration code. In addition, pivot and spatial calibrations were carried out to define the transformation matrix between the ultrasound image and the center of the reflective-marker cluster attached to the probe.

For the main test, two isolated human lumbar spines were imaged, and 3D models were reconstructed and used for ROM measurements. The resulting intervertebral ROM measurements were then validated against CT-based reference values. On average, ultrasound-derived ROMs were slightly overestimated by $0.61 \pm 0.17°$. This overestimation is likely due to segmentation inaccuracies introduced by the high echogenicity of bone boundaries, which can result in thicker-than-actual representations of cortical structures.

Despite this minor discrepancy, Bland–Altman analyses confirmed good agreement between modalities across all motion planes (flexion–extension, side bending, and axial rotation), supporting the validity of ultrasound-based kinematic assessments in-vivo.

After the initial validation, the study continued with applying the imaging in an in-vivo setting and with healthy participants aging from 20–60-year-old. Age-related comparisons revealed a clear decline in lumbar flexion with increasing age, particularly between the youngest (20–30 years) and oldest (50–60 years) participant groups. The most notable differences occurred in flexion and proximodistal translation, with statistically significant reductions in motion seen in older participants. These findings align with existing literature, which consistently reports age-associated declines in lumbar mobility.

Furthermore, correlation analyses demonstrated strong relationships between flexion and coupled translations, especially proximodistal ($\rho = 0.86$) and anteroposterior ($\rho = 0.61$), highlighting the value of 3D measurement for capturing complex lumbar spine

kinematics. Notably, these correlations were not significantly influenced by age, suggesting that the observed inter-motion dependencies reflect fundamental biomechanical behavior rather than demographic variability.

Sex-based comparisons revealed no statistically significant differences in ROMs across motion planes, although minor variations were observed between age subgroups. These results contribute to ongoing discussions in the literature, where findings remain inconsistent due to differences in sample size, motion capture methods, and operational definitions of movement endpoints.

As for the reliability analysis, this test demonstrated excellent consistency, with within-day reliability of 0.91 ± 0.02 and between-day reliability of 0.92 ± 0.01. As specific considerations were taken into account to minimize variability related to external factors, these reliability results demonstrate the precision of the measurement technique. Observed between-group differences exceeded the previously established MDC from the in-vitro validation, indicating that the effects were larger than pipeline noise and supporting the substantive interpretation of the in-vivo findings.

Beyond absolute ROM values, an important contribution of the 3D approach is to allow us to describe how flexion is accompanied by proximodistal and anteroposterior translations, how individual motion segments contribute to the global lumbar motion, and how these coupled behaviours remain relatively consistent across ages in healthy adults. Such pattern-level information is clinically relevant because patients with low back pain are often distinguished less by the magnitude of their ROM than by aberrant or asymmetric motion patterns (e.g., hinge behaviour at a single segment, altered coupling, or disrupted contribution of specific levels). The normative patterns reported here therefore provide a reference framework for future studies aiming to detect pathological movement patterns in LBP populations.

The study successfully demonstrated that ultrasound imaging, when coupled with an appropriate tracking strategy, is a valid and reliable method for assessing 3D lumbar intervertebral kinematics in-vivo. This represents a significant step toward establishing musculoskeletal ultrasound as a viable alternative to CT or MRI for motion analysis in both clinical and research settings.

7.1 Toward Practical Applications

7.1.1 Clinical Relevance for Low Back Pain

Low back pain remains one of the most prevalent musculoskeletal disorders worldwide and is often associated with altered or reduced segmental mobility. A major challenge in current clinical practice is the difficulty of assessing vertebral-level motion non-invasively, which limits the ability to identify whether movement restrictions or instabilities are localized to specific segments. The method developed in this thesis provides an opportunity to bridge this gap by offering a radiation-free, segmental assessment of lumbar kinematics.

From a rehabilitation perspective, such detailed evaluation alongside other dimensions of a comprehensive assessment could help distinguish whether a patient would benefit more from a hands-on intervention (e.g., manual therapy techniques targeting specific vertebrae) or from a hands-off approach (e.g., exercise-based programs focused on global stability). By quantifying intervertebral motion with high precision, the technique could ultimately support a more individualized rehabilitation strategy, ensuring that therapeutic choices are guided by objective biomechanical evidence. In addition, future clinical protocols will need to account for the practical constraints of low back pain management, particularly the difficulty some patients may have in maintaining static postures. Optimizing acquisition duration, selecting clinically relevant postures, and, where possible, incorporating functional tasks will be essential to maximize both patient comfort and clinical relevance.

7.1.2 Transferability of the Method to Other Joints

The transition from laboratory-based research to practical application requires demonstrating that the developed method is adaptable to other anatomical regions. In this context, Chapter 6 was dedicated to assessing the feasibility of applying the ultrasound-based 3D reconstruction technique to the shoulder joint. Although the 3D models reconstructed from ultrasound images showed a slight overestimation of bone volume (0.66 ± 0.06 mm), the joint kinematics demonstrated strong agreement with CT-based measurements, with an angular error of $0.43 \pm 0.72°$, remaining within the limits of

agreement in the Bland-Altman analysis. The quality of the 3D models and the level of precision highlight the method's potential for use in other joints. Moreover, the integration of tracked ultrasound acquisition can further enhance the method's applicability by facilitating imaging in in-vivo scenarios.

Beyond joint-specific transferability, the question of continuous movement is context-dependent. In an in-vitro setting, it is feasible to record continuous motion and register it onto an existing 3D model, enabling time-resolved kinematic analysis. In an in-vivo setting, however, continuous acquisition is not supported within the present workflow because accurate 3D model generation requires the region of interest to remain stable during scanning; thus, quasi-static postures are used for model creation, after which kinematics is derived. Consequently, the current method provides discrete intervertebral ROM values between selected postures rather than full time-resolved kinematic trajectories, which limits its direct use for clinicians who wish to analyze continuous movement cycles (e.g., gait or repeated lifting tasks).

7.1.3 Segmentation Challenges

Regardless of the successful experimental results, such as the demonstrated validity and reliability of the technique, one major challenge remains when applying tracked ultrasound imaging (Cai et al., 2023); a large number of ultrasound images must be acquired during scanning to minimize inter-image gaps and improve the quality of the reconstructed 3D model (Orlando et al., 2022). These numerous images then require manual segmentation to enable accurate 3D reconstruction. While manual segmentation can yield highly precise results (results of the chapter 5), it is time-consuming and operator-dependent, thereby limiting the method's scalability and potential for clinical adoption. This limitation is particularly pronounced as the number of frames grows during continuous acquisitions.

To overcome this limitation, recent advances in artificial intelligence (Biswas & Banik, 2022), particularly in medical image segmentation, offer promising avenues for automation. Among these, U-Net (Ronneberger et al., 2015), a convolutional neural network architecture specifically designed for biomedical image segmentation, has emerged as a leading solution. U-Net uses a symmetric encoder-decoder structure that

captures both spatial and contextual features, making it highly effective for segmenting structures with varying shapes (Li et al., 2022), such as vertebrae in ultrasound images.

As the final component of this thesis, we are currently developing an automatic segmentation pipeline for lumbar spine ultrasound images using a U-Net architecture implemented with Tensorflow Keras library. After manually segmenting all the collected images, we have built a large labeled dataset that serves as the foundation for training the U-Net model. For training and evaluation, 70% of the participant data is being used for training, 10% for validation, and the remaining 20% is reserved for testing (Karimi et al., 2021). Notably, our testing procedure goes beyond traditional model evaluation: in addition to computing standard segmentation metrics (e.g., Dice coefficient) (Seghier, 2024), the segmented test images will be used to generate full 3D models from the recorded ultrasound sequences. These automatically reconstructed 3D models will then be compared with those generated from the manually segmented ground truth in order to assess both reconstruction fidelity and joint kinematics accuracy. The full workflow of this process is illustrated in Figure 16, which outlines the sequence recording, segmentation pipeline, model training, and the final evaluation steps involving 3D reconstruction and comparison.

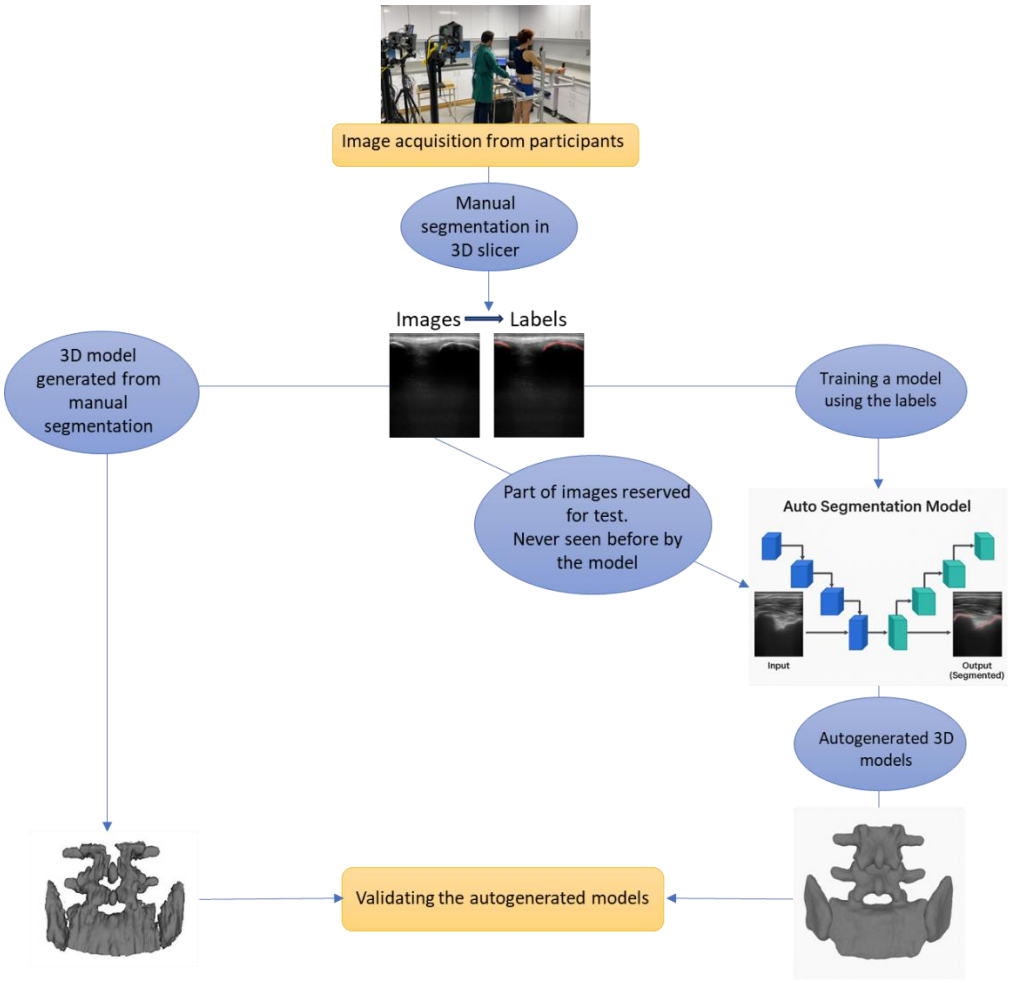

Figure 12. Workflow illustrating how the acquired images are used for training and fully automatic 3D model generation. In this procedure, 70% of the segmented images obtained from participants in Chapter 5 will be used to train a U-Net–based auto-segmentation model. This trained model is then will be applied to a separate set of previously unseen images to generate 3D models automatically. These automatically reconstructed models will be subsequently compared with corresponding models generated using manual segmentation.

It is important to emphasize that these auto-segmentation developments represent a methodological extension initiated at the end of the thesis, rather than a primary objective of the experimental chapters. The current results are therefore exploratory and mainly serve to demonstrate feasibility and to prepare more comprehensive future studies. Regarding these developments, the initial training has already been done, and a U-Net model with promising visual results has been obtained; its trained weights, inference code, and quantitative segmentation metrics, as well as its full integration into 3D reconstructions and subsequent kinematic evaluations, are explicitly defined as future work. Thus, the main

deliverables associated with auto-segmentation—complete pipeline integration, systematic assessment of kinematic accuracy, and testing in pathological cohorts—are deliberately positioned as perspectives rather than core outcomes of the present thesis. In addition, after the integration of automatic segmentation, the surface quality will be addressed explicitly: any smoothing will be quantified by measuring landmark displacement and reporting ROM sensitivity with and without smoothing.

7.2.3 Importance of 3D Model Quality

The quality of the 3D models used throughout this study has been crucial in achieving high accuracy and precision in both validity and reliability assessments. A key factor influencing model quality is the number of ultrasound images used during the reconstruction process. Increasing the number of images helps minimize inter-slice gaps, leading to smoother and more anatomically accurate reconstructions (Orlando et al., 2022). While such image volume can become overwhelming for manual segmentation, due to time and user dependency, it poses no difficulty for automated methods. The use of automatic segmentation techniques enables processing a larger volume of images efficiently, thus enhancing model quality without compromising scalability. Additionally, surface smoothing requires caution: smoothing may bias cortical edges and shift anatomical landmarks. Therefore, when smoothing is applied, landmark placement should be performed on unsmoothed models or after constrained/low-bias smoothing, and the effect of smoothing on landmark location should be quantified (e.g., report landmark shift with/without smoothing).

High-quality 3D models are particularly essential in the context of kinematic analysis. They directly affect the accuracy of AL identification and marker placement, both of which influence the definition of ARFs (Gunderson et al., 2025). Errors in marker selection or anatomical mapping can significantly distort the computed kinematics (Adhia et al., 2013). Therefore, generating precise and detailed 3D models is not only beneficial for visualization but also foundational for producing accurate and reliable kinematic measurements.

Beyond purely anatomical landmarks, geometric approaches for marker localization, such as fitting simple primitives (e.g., spheres or cylinders) or using principal

axes of inertia, offer an alternative way to define bony reference frames from the 3D models (Conconi et al., 2021). These geometric methods can reduce the influence of local segmentation noise and provide mathematically well-conditioned axes, which may improve the robustness of marker localization. In this thesis, we primarily relied on anatomically defined ALs and ARFs, but future developments should systematically compare anatomical and geometric frames to determine the most reliable strategy for clinical use.

7.2.4 Kinematic Measurement Challenges

In addition to the progress made in ultrasound-based 3D reconstruction, the process of kinematic measurement was a major challenge. In line with the overarching goal of this thesis to develop a clinically applicable solution, a Python-based interface was created to streamline spine kinematics measurement.

Traditional kinematic software is often time-consuming and technically complex, involving manual reference frame definition and data extraction. In contrast, the developed interface simplifies the entire process. As illustrated in Figure 17, the user imports two 3D models (e.g., standing and flexion positions), selects the desired vertebral level, and performs marker selection. The system then automatically constructs local reference frames based on the ISB recommendations and computes the flexion-extension, lateral bending, and axial rotation, using Euler angles. This approach significantly reduces the time and complexity associated with kinematic calculations.

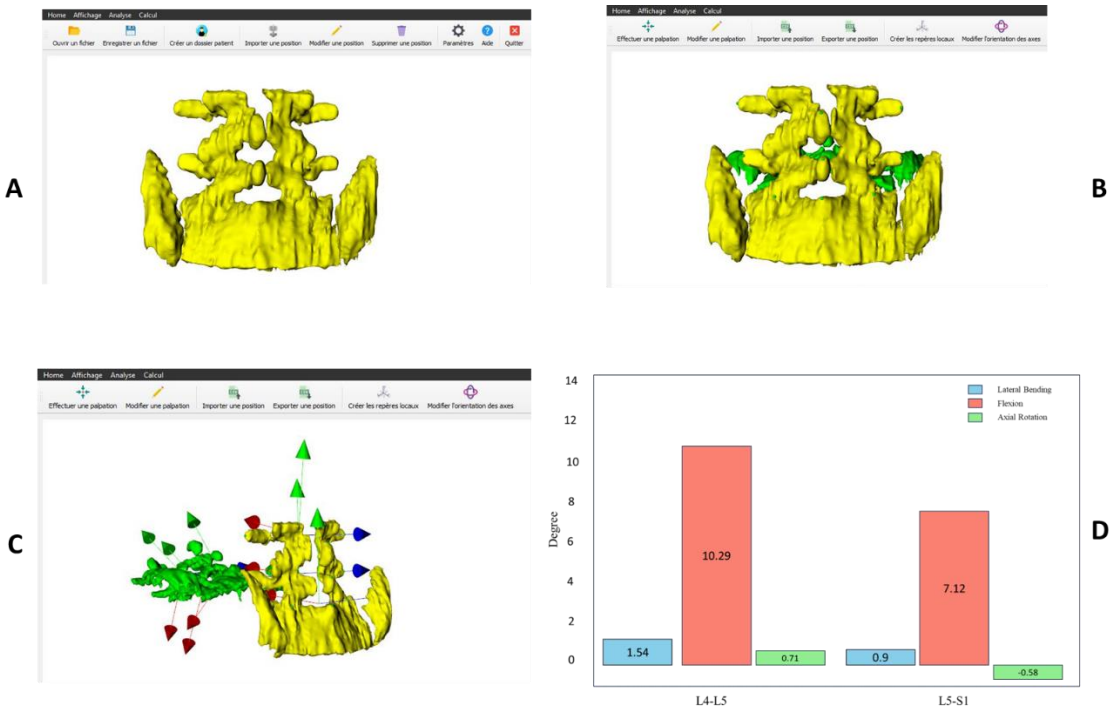

Figure 13. The newly developed kinematic measurement interface
(A) the 3D models are imported; (B) ALs are selected; (C) ARFs are automatically constructed; and (D) the 3D intervertebral ROMs are computed and reported.

Looking ahead, one of the primary future developments will be the integration of tracked ultrasound imaging, starting from calibration through to image acquisition, within the same interface. Combined with the ongoing implementation of automatic segmentation using deep learning, this will enable full 3D model generation and kinematic computation within a unified platform. Such integration has the potential to greatly enhance usability and bring this technique closer to practical deployment in clinical environments.

7.2.5 Operator Effect on Measurement Consistency

Ultrasound is as an operator-dependent imaging modality (Ohrndorf et al., 2010), as both the acquisition and interpretation of images can require substantial experience. However, in this study, the entire imaging protocol was highly standardized and partially automated from the initial steps, which significantly minimized operator variability. All imaging was performed by the same operator using a consistent scanning protocol, ensuring uniformity in image acquisition and reducing the need for inter-observer assessment at this stage. This standardization contributed to the consistency and quality of

the resulting images, making the segmentation and 3D reconstruction process more reliable. Inter-observer evaluation was not performed in the in-vivo study because standardization and single-operator acquisition were prioritized to minimize confounds in the first validation; a dedicated inter-operator reliability study is outlined in "Future Work."

In future work, although the application of automatic segmentation will reduce operator dependency (Renard et al., 2020), it would still be valuable to assess inter-operator reliability by allowing different clinicians to perform the ultrasound scans. The trained segmentation model could then be used to generate 3D reconstructions and compute kinematic measurements. Such an evaluation would help determine the robustness and clinical readiness of the proposed method under variable real-world conditions.

7.2.6 General limitations

Despite the methodological advances and promising results, several limitations of this thesis must be acknowledged. First, the initial reconstruction method was validated in vitro on isolated lumbar specimens, and its direct use in-vivo required adapting the workflow to a tracked ultrasound protocol. This limitation was addressed within the thesis by implementing and validating the tracked method in both in-vitro and in-vivo contexts, thereby demonstrating that the reconstruction and kinematic pipeline can operate under realistic measurement conditions.

Second, the calibration procedures (temporal, pivot, spatial) are relatively long and complex, relying on multiple software tools and careful experimental setup. This complexity increases the risk of user error and may limit adoption in routine clinical environments. In this thesis, these issues were mitigated by strict standardization and by having all acquisitions performed by a single, trained operator. However, from a translational perspective, these calibration steps need to be simplified and integrated into a unified software environment.

Third, segmentation procedure was a major bottleneck. High-quality 3D reconstructions currently depend on manual segmentation of numerous ultrasound images, which is time-consuming and operator-dependent. This limitation restricts scalability and makes large clinical studies difficult. The ongoing development of an automatic

segmentation pipeline based on U-Net is specifically aimed at addressing this issue by drastically reducing manual workload and improving consistency.

Fourth, the entire workflow is operator-dependent, and this thesis did not include a inter-operator reliability study. While single-operator acquisition was a deliberate choice to minimize variability in this first validation, it also means that robustness to different users has not yet been demonstrated. A logical next step is to have multiple clinicians perform the scans using the same protocol and to use the automated segmentation and kinematic pipeline to assess inter-operator reproducibility. This will be essential before the method can be considered ready for broad clinical deployment.

Finally, the range of motions and spinal levels investigated was limited. Flexion was studied as the primary motion, and only two vertebral levels (L4–S1) were analyzed in detail. Other motion directions (lateral bending, axial rotation as primary tasks) and additional levels of the lumbar spine remain to be assessed. Addressing these limitations will help to fully exploit the potential of ultrasound-based 3D kinematic analysis for characterizing both the magnitude and the pattern of lumbar spine motion in clinical populations.

7.2.7 Future Work and Research Directions

While this thesis has demonstrated the feasibility and validity of ultrasound-based 3D reconstruction for lumbar spine kinematics, several avenues remain for future development before the method can achieve widespread clinical adoption.

First, although imaging protocols were standardized and performed by a single operator, future studies should evaluate inter-operator reliability. This step is essential to determine whether different clinicians can produce consistent reconstructions and kinematic measurements when using the same workflow. For example, intra- and inter-rater reliability studies in ultrasound-based spinal imaging have been reported (Tozawa et al., 2022), but no work has yet addressed these aspects in the context of 3D segmentation and kinematic reconstruction.

Second, to enhance clinical usability, the current system should evolve into a fully integrated platform that combines tracked ultrasound acquisition, automatic segmentation,

3D model reconstruction, and kinematic computation within a single interface. The software developed during this thesis provides a foundation, but additional improvements are needed to ensure real-time processing, intuitive design, and compatibility with clinical workflows. Comparable integration efforts exist, such as the PLUS toolkit (Lasso et al., 2014), which provides an open-source framework for tracked ultrasound imaging and data acquisition, though it is not yet tailored for spine kinematic.

Third, the application of deep learning for automatic segmentation should be extended and validated across larger, more diverse populations, including patients with spinal pathologies. This will allow testing whether pathological conditions (e.g., degenerative changes, scoliosis) affect segmentation quality and kinematic accuracy. Public datasets such as LUMINOUS (Belasso et al., 2020), which contains ultrasound images of the lumbar multifidus, have enabled algorithm development in healthy populations, but equivalent resources for pathological cohorts remain absent.

Fourth, beyond the lumbar spine, further investigations should test the transferability of this method to other joints (e.g., cervical spine, shoulder, hip). Such work will help establish the broader clinical value of ultrasound-based kinematic analysis in musculoskeletal health. For instance, exploratory applications of tracked ultrasound have been reported for knee joint kinematics (Niu et al., 2024), suggesting feasibility of adapting the method to other regions.

Finally, from a clinical translation perspective, prospective in-vivo studies are required to demonstrate the added value of this technique in patient assessment and rehabilitation. Such studies could determine whether segmental kinematic profiles derived from ultrasound can improve diagnosis, personalize treatment decisions, and monitor therapeutic outcomes in low back pain management. At present, no prospective in-vivo clinical study has tested this approach for the lumbar spine.

Together, these directions outline a roadmap for transforming the method developed in this thesis from a validated experimental technique into a robust, user-friendly clinical tool.

7.3 Conclusion

This thesis presented the development and validation of a novel ultrasound-based approach for analyzing 3D lumbar spine kinematics. The proposed method enabled the reconstruction of accurate 3D vertebral models from ultrasound images and supported precise measurement of intervertebral motion across all planes.

To enhance clinical applicability, the workflow incorporated standardized imaging protocols, a custom Python interface for kinematic analysis, and is training a U-Net–based automatic segmentation pipeline. The method demonstrated strong validity and reliability in both in-vitro and in-vivo settings, captured age-related differences in spinal mobility, and showed good agreement with CT-based reference values. Furthermore, the approach was successfully extended to the shoulder joint, demonstrating its adaptability to other anatomical regions. Overall, this work established musculoskeletal ultrasound, combined with automation and tracking technologies, as a promising alternative for 3D motion analysis in clinical and research contexts.

Reference

Abd Rahman, N. A., Li, S., Schmid, S., & Shaharudin, S. (2023). Biomechanical factors associated with non-specific low back pain in adults: A systematic review. *Physical Therapy in Sport*, *59*, 60–72.

Adams, M. A., & Dolan, P. (2005). Spine biomechanics. *Journal of biomechanics*, *38*(10), 1972–1983.

Adhia, D. B., Bussey, M. D., Ribeiro, D. C., Tumilty, S., & Milosavljevic, S. (2013). Validity and reliability of palpation-digitization for non-invasive kinematic measurement–a systematic review. *Manual therapy*, *18*(1), 26–34.

Agostini, V., Gastaldi, L., Rosso, V., Knaflitz, M., & Tadano, S. (2017). A wearable magneto-inertial system for gait analysis (H-Gait): Validation on normal weight and overweight/obese young healthy adults. *Sensors*, *17*(10), 2406.

Aiyangar, A. K., Zheng, L., Tashman, S., Anderst, W. J., & Zhang, X. (2014). Capturing three-dimensional in vivo lumbar intervertebral joint kinematics using dynamic stereo-X-ray imaging. *Journal of biomechanical engineering*, *136*(1), 011004.

Alencastre-Miranda, M., Munoz-Gomez, L., Murrieta-Cid, R., & Monroy, R. (2006). Local reference frames vs. global reference frame for mobile robot localization and path planning. 2006 Fifth Mexican International Conference on Artificial Intelligence,

Ancillao, A. (2022). The helical axis of anatomical joints: calculation methods, literature review, and software implementation. *Medical & Biological Engineering & Computing*, *60*(7), 1815–1825.

Arshad, R., Pan, F., Reitmaier, S., & Schmidt, H. (2019). Effect of age and sex on lumbar lordosis and the range of motion. A systematic review and meta-analysis. *Journal of biomechanics*, *82*, 1–19.

Balasubramanya, R., & Selvarajan, S. K. (2020). Lumbar spine imaging.

Bayartai, M.-E., Taulaniemi, A., Tokola, K., Vähä-Ypyä, H., Parkkari, J., Husu, P., Kankaanpää, M., Vasankari, T., Bauer, C. M., & Luomajoki, H. (2023). Role of the interaction between lumbar kinematics and accelerometer-measured physical activity in bodily pain, physical functioning and work ability among health care workers with low back pain. *Journal of Electromyography and Kinesiology*, *69*, 102744.

Belasso, C. J., Behboodi, B., Benali, H., Boily, M., Rivaz, H., & Fortin, M. (2020). LUMINOUS database: lumbar multifidus muscle segmentation from ultrasound images. *BMC musculoskeletal disorders*, *21*(1), 703.

Benoit, D. L., Ramsey, D. K., Lamontagne, M., Xu, L., Wretenberg, P., & Renström, P. (2006). Effect of skin movement artifact on knee kinematics during gait and cutting motions measured in vivo. *Gait & posture*, *24*(2), 152–164.

Betsch, M., Wild, M., Johnstone, B., Jungbluth, P., Hakimi, M., Kühlmann, B., & Rapp, W. (2013). Evaluation of a novel spine and surface topography system for dynamic spinal curvature analysis during gait. *PloS one*, *8*(7), e70581.

Biswas, A., & Banik, R. (2022). Advancements in medical image analysis: A comprehensive method of AI-based classification and segmentation technique. Artificial Intelligence and Applications,

Bogduk, N. (2016). Functional anatomy of the spine. *Handbook of clinical neurology*, *136*, 675–688.

Breen, A., & Breen, A. (2016). Accuracy and repeatability of quantitative fluoroscopy for the measurement of sagittal plane translation and finite centre of rotation in the lumbar spine. *Medical Engineering & Physics*, *38*(7), 607–614.

Breen, A., & Breen, A. (2018). Uneven intervertebral motion sharing is related to disc degeneration and is greater in patients with chronic, non-specific low back pain: an in vivo, cross-sectional cohort comparison of intervertebral dynamics using quantitative fluoroscopy. *European spine journal*, *27*(1), 145–153.

Brehler, M., Islam, A., Vogelsang, L., Yang, D., Sehnert, W., Shakoor, D., Demehri, S., Siewerdsen, J. H., & Zbijewski, W. (2019). Coupled active shape models for automated segmentation and landmark localization in high-resolution CT of the foot and ankle. Proceedings of SPIE--the International Society for Optical Engineering,

Byrne, R. M., Zhou, Y., Zheng, L., Chowdhury, S. K., Aiyangar, A., & Zhang, X. (2018). Segmental variations in facet joint translations during in vivo lumbar extension. *Journal of biomechanics*, *70*, 88–95.

Cai, L., Li, Q., Zhang, J., Zhang, Z., Yang, R., & Zhang, L. (2023). Ultrasound image segmentation based on Transformer and U-Net with joint loss. *PeerJ Computer Science*, *9*, e1638.

Camomilla, V., Cereatti, A., Cutti, A. G., Fantozzi, S., Stagni, R., & Vannozzi, G. (2017). Methodological factors affecting joint moments estimation in clinical gait analysis: a systematic review. *Biomedical engineering online*, *16*(1), 106.

Chèze, L. (2014). *Kinematic analysis of human movement*. John Wiley & Sons.

Chleboun, G. S., Amway, M. J., Hill, J. G., Root, K. J., Murray, H. C., & Sergeev, A. V. (2012). Measurement of segmental lumbar spine flexion and extension using ultrasound imaging. *journal of orthopaedic & sports physical therapy*, *42*(10), 880–885.

Conconi, M., Pompili, A., Sancisi, N., Leardini, A., Durante, S., & Belvedere, C. (2021). New anatomical reference systems for the bones of the foot and ankle complex: definitions and exploitation on clinical conditions. *Journal of foot and ankle research*, *14*(1), 66.

Cook, C., Brismée, J.-M., & Sizer Jr, P. S. (2006). Subjective and objective descriptors of clinical lumbar spine instability: a Delphi study. *Manual therapy*, *11*(1), 11–21.

Cuesta-Vargas, A. I. (2015). Development of a new ultrasound-based system for tracking motion of the human lumbar spine: reliability, stability and repeatability during forward bending movement trials. *Ultrasound in medicine & biology*, *41*(7), 2049–2056.

Dai, J. C., Dunmire, B., Sternberg, K. M., Liu, Z., Larson, T., Thiel, J., Chang, H. C., Harper, J. D., Bailey, M. R., & Sorensen, M. D. (2018). Retrospective comparison of measured stone size and posterior acoustic shadow width in clinical ultrasound images. *World journal of urology*, *36*(5), 727–732.

Daniel, E. S., Lee, R. Y., & Williams, J. M. (2023). The reliability of video fluoroscopy, ultrasound imaging, magnetic resonance imaging and radiography for measurements of lumbar spine segmental range of motion in-vivo: A review. *Journal of back and musculoskeletal rehabilitation*, *36*(1), 117–135.

DeSai, C., Reddy, V., & Agarwal, A. (2018). Anatomy, back, vertebral column.

Dickey, J. P., Pierrynowski, M. R., Bednar, D. A., & Yang, S. X. (2002). Relationship between pain and vertebral motion in chronic low-back pain subjects. *Clinical Biomechanics*, *17*(5), 345–352.

Dixon, L., Lim, A., Grech-Sollars, M., Nandi, D., & Camp, S. (2022). Intraoperative ultrasound in brain tumor surgery: A review and implementation guide. *Neurosurgical Review*, *45*(4), 2503–2515.

Drakonaki, E. (2012). Ultrasound elastography for imaging tendons and muscles. *Journal of ultrasonography*, *12*(49), 214.

Dugailly, P.-M., Sobczak, S., Moiseev, F., Sholukha, V., Salvia, P., Feipel, V., Rooze, M., & Jan, S. V. S. (2011). Musculoskeletal modeling of the suboccipital spine: kinematics analysis, muscle lengths, and muscle moment arms during axial rotation and flexion extension. *Spine*, *36*(6), E413–E422.

Dugailly, P.-M., Sobczak, S., Sholukha, V., Van Sint Jan, S., Salvia, P., Feipel, V., & Rooze, M. (2010). In vitro 3D-kinematics of the upper cervical spine: helical axis and simulation for axial rotation and flexion extension. *Surgical and radiologic anatomy*, *32*, 141–151.

Ebraheim, N. A., Hassan, A., Lee, M., & Xu, R. (2004). Functional anatomy of the lumbar spine. Seminars in pain medicine,

Effatparvar, M. R., & Sobczak, S. (2022). Application of ultrasound in spine kinematic determination: A systemic review. *Journal of Medical Ultrasound*, *30*(1), 6–10.

Errabity, A., Calmels, P., Han, W.-S., Bonnaire, R., Pannetier, R., Convert, R., & Molimard, J. (2023). The effect of low back pain on spine kinematics: A systematic review and meta-analysis. *Clinical Biomechanics*, 106070.

Evans, P. R. (2001). Rotations and rotation matrices. *Acta Crystallographica Section D: Biological Crystallography*, *57*(10), 1355–1359.

Flash, T., Meirovitch, Y., & Barliya, A. (2013). Models of human movement: Trajectory planning and inverse kinematics studies. *Robotics and Autonomous Systems*, *61*(4), 330–339.

Forbes, A., Cantin, V., Develle, Y., Dubé, Y., Bertrand-Grenier, A., Ménard-Lebel, C., & Sobczak, S. (2021). Musculoskeletal ultrasound for 3D bone modeling: A preliminary study applied to lumbar vertebra. *Journal of back and musculoskeletal rehabilitation*, *34*(6), 937–950.

Fraeulin, L., Holzgreve, F., Brinkbäumer, M., Dziuba, A., Friebe, D., Klemz, S., Schmitt, M., Theis A, A.-L., Tenberg, S., & van Mark, A. (2020). Intra-and inter-rater reliability of joint range of motion tests using tape measure, digital inclinometer and inertial motion capturing. *PloS one*, *15*(12), e0243646.

Fritz, J. M., Piva, S. R., & Childs, J. D. (2005). Accuracy of the clinical examination to predict radiographic instability of the lumbar spine. *European spine journal*, *14*, 743–750.

García-Jaén, M., Sebastia-Amat, S., Sanchis-Soler, G., & Cortell-Tormo, J. M. (2024). Lumbo-Pelvic Rhythm Monitoring Using Wearable Technology with Sensory Biofeedback: A Systematic Review. Healthcare,

Gianola, S., Castellini, G., Andreano, A., Corbetta, D., Frigerio, P., Pecoraro, V., Redaelli, V., Tettamanti, A., Turolla, A., & Moja, L. (2019). Effectiveness of treatments for acute and sub-acute mechanical non-specific low back pain: protocol for a systematic review and network meta-analysis. *Systematic reviews*, *8*(1), 196.

Grood, E. S., & Suntay, W. J. (1983). A joint coordinate system for the clinical description of three-dimensional motions: application to the knee.

Gruber, D. (2000). The mathematics of the 3D rotation matrix. Xtreme game developers conference,

Gunderson, N., Chen, P., Ruthberg, J. S., Bly, R. A., Seibel, E. J., & Abuzeid, W. M. (2025). High-fidelity 3D reconstruction for accurate anatomical measurements in endoscopic sinus surgery. Medical Imaging 2025: Image-Guided Procedures, Robotic Interventions, and Modeling,

Haynes, W. (2003). New strategies in the treatment and rehabilitation of the lumbar spine. *Journal of Bodywork and Movement Therapies*, *7*(2), 117–130.

Heneghan, N. R., & Balanos, G. M. (2010). Soft tissue artefact in the thoracic spine during axial rotation and arm elevation using ultrasound imaging: a descriptive study. *Manual therapy*, *15*(6), 599–602.

Heneghan, N. R., Hall, A., Hollands, M., & Balanos, G. M. (2009). Stability and intra-tester reliability of an in vivo measurement of thoracic axial rotation using an innovative methodology. *Manual therapy*, *14*(4), 452–455.

Hindle, B. R., Keogh, J. W., & Lorimer, A. V. (2021). Inertial-Based Human Motion Capture: A Technical Summary of Current Processing Methodologies for Spatiotemporal and Kinematic Measures. *Applied Bionics and Biomechanics*, *2021*(1), 6628320.

Hosseinian, S., & Arefi, H. (2015). 3D Reconstruction from Multi-View Medical X-ray images–review and evaluation of existing methods. *The international archives of the photogrammetry, remote sensing and spatial information sciences*, *40*, 319–326.

Kai, L., & Qun, X. (2011). Assessing validation of dual fluoroscopic image matching method for measurement ofin vivospine kinematics. *Chinese Medical Journal*, *124*(11), 1689–1694.

Kanayama, M., Abumi, K., Kaneda, K., Tadano, S., & Ukai, T. (1996). Phase Lag of the Intersegmental Motion in Flexion-Extension of the Lumbar and Lumbosacral Spine: An: In Vivo: Study. *Spine*, *21*(12), 1416–1422.

Karimi, D., Warfield, S. K., & Gholipour, A. (2021). Transfer learning in medical image segmentation: New insights from analysis of the dynamics of model parameters and learned representations. *Artificial intelligence in medicine*, *116*, 102078.

Kecskemethy, A. (2011). Integrating efficient kinematics in biomechanics of human motions. *Procedia IUTAM*, *2*, 86–92.

Kim, G.-U., Chang, M. C., Kim, T. U., & Lee, G. W. (2020). Diagnostic modality in spine disease: a review. *Asian Spine Journal*, *14*(6), 910.

Lasso, A., Heffter, T., Rankin, A., Pinter, C., Ungi, T., & Fichtinger, G. (2014). PLUS: open-source toolkit for ultrasound-guided intervention systems. *IEEE transactions on biomedical engineering*, *61*(10), 2527–2537.

Leardini, A., Chiari, L., Della Croce, U., & Cappozzo, A. (2005). Human movement analysis using stereophotogrammetry: Part 3. Soft tissue artifact assessment and compensation. *Gait & posture*, *21*(2), 212–225.

Leitner, C., Hager, P. A., Penasso, H., Tilp, M., Benini, L., Peham, C., & Baumgartner, C. (2019). Ultrasound as a tool to study muscle–tendon functions during locomotion: A systematic review of applications. *Sensors*, *19*(19), 4316.

Lemos, T. V., Albino, A. C. G., Matheus, J. P. C., & de Melo Barbosa, A. (2014). The effect of kinesio taping in forward bending of the lumbar spine. *Journal of physical therapy science*, *26*(9), 1371–1375.

Leone, A., Guglielmi, G., Cassar-Pullicino, V. N., & Bonomo, L. (2007). Lumbar intervertebral instability: a review. *Radiology*, *245*(1), 62–77.

Li, G., Wang, S., Passias, P., Xia, Q., Li, G., & Wood, K. (2009). Segmental in vivo vertebral motion during functional human lumbar spine activities. *European spine journal*, *18*, 1013–1021.

Li, Y., Yao, Q., Yu, H., Xie, X., Shi, Z., Li, S., Qiu, H., Li, C., & Qin, J. (2022). Automated segmentation of vertebral cortex with 3D U-Net-based deep convolutional neural network. *Frontiers in Bioengineering and Biotechnology*, *10*, 996723.

Lin, H., Seerden, S., Zhang, X., Fu, W., & Vanwanseele, B. (2020). Inter-segmental coordination of the spine is altered during lifting in patients with ankylosing spondylitis: A cross-sectional study. *Medicine*, *99*(5), e18941.

Littlewood, C., & May, S. (2007). Measurement of range of movement in the lumbar spine—what methods are valid? A systematic review. *Physiotherapy*, *93*(3), 201–211.

Lund, T., Nydegger, T., Schlenzka, D., & Oxland, T. R. (2002). Three-dimensional motion patterns during active bending in patients with chronic low back pain. *Spine*, *27*(17), 1865–1874.

Ma, Y., Mithraratne, K., Wilson, N. C., Wang, X., Ma, Y., & Zhang, Y. (2019). The validity and reliability of a kinect v2-based gait analysis system for children with cerebral palsy. *Sensors*, *19*(7), 1660.

Mahadevan, V. (2018). Anatomy of the vertebral column. *Surgery (Oxford)*, *36*(7), 327–332.

Mahesh, M. (2001). Fluoroscopy: patient radiation exposure issues. *Radiographics*, *21*(4), 1033–1045.

Maken, P., & Gupta, A. (2023). 2D-to-3D: a review for computational 3D image reconstruction from X-ray images. *Archives of Computational Methods in Engineering*, *30*(1), 85–114.

Masharawi, Y., Rothschild, B., Dar, G., Peleg, S., Robinson, D., Been, E., & Hershkovitz, I. (2004). Facet orientation in the thoracolumbar spine: three-dimensional anatomic and biomechanical analysis. *Spine*, *29*(16), 1755–1763.

McGregor, A. H., McCarthy, I. D., & Hughes, S. P. (1995). Motion characteristics of the lumbar spine in the normal population. *Spine*, *20*(22), 2421–2428.

McKinnon, C. D., & Callaghan, J. P. (2019). Validation of an ultrasound protocol to measure intervertebral axial twist during functional twisting movements in isolated functional spinal units. *Ultrasound in medicine & biology*, *45*(3), 642–649.

McKinnon, C. D., & Callaghan, J. P. (2021). The relationship between external thoracopelvic angle and lumbar segmental axial twist angle using an ultrasound imaging technique. *Human movement science*, *78*, 102824.

Melhem, E., Assi, A., El Rachkidi, R., & Ghanem, I. (2016). EOS® biplanar X-ray imaging: concept, developments, benefits, and limitations. *Journal of children's orthopaedics*, *10*(1), 1–14.

Mhaskar, V. A., Agrahari, H., & Maheshwari, J. (2023). Ultrasound guided arthroscopic meniscus surgery. *Journal of Ultrasound*, *26*(2), 577–581.

Michelini, G., Corridore, A., Torlone, S., Bruno, F., Marsecano, C., Capasso, R., Caranci, F., Barile, A., Masciocchi, C., & Splendiani, A. (2018). Dynamic MRI in the evaluation of the spine: state of the art. *Acta Bio Medica: Atenei Parmensis*, *89*(Suppl 1), 89.

Mohokum, M., Schülein, S., & Skwara, A. (2015). The validity of rasterstereography: a systematic review. *Orthopedic reviews*, *7*(3), 5899.

Moran, M., & Myers, M. (2022). Use of ultrasonography for identification of long bone fractures. *Visual Journal of Emergency Medicine*, *28*, 101381.

Moult, E. M., Lasso, A., Ungi, T., Pinter, C., Welch, M., & Fichtinger, G. (2017). Improved temporal calibration of tracked ultrasound: An open-source solution. *Journal of Medical Robotics Research*, *2*(04), 1750008.

Niu, K., Sluiter, V., Lan, B., Homminga, J., Sprengers, A., & Verdonschot, N. (2024). A method to track 3D knee kinematics by multi-channel 3D-tracked A-mode ultrasound. *Sensors*, *24*(8), 2439.

Ohrndorf, S., Naumann, L., Grundey, J., Scheel, T., Scheel, A. K., Werner, C., & Backhaus, M. (2010). Is musculoskeletal ultrasonography an operator-dependent method or a fast and reliably teachable diagnostic tool? Interreader agreements of three ultrasonographers with different training levels. *International journal of rheumatology*, *2010*(1), 164518.

Orlando, N., Gyacskov, I., Gillies, D. J., Guo, F., Romagnoli, C., D'Souza, D., Cool, D. W., Hoover, D. A., & Fenster, A. (2022). Effect of dataset size, image quality, and image type on deep learning-based automatic prostate segmentation in 3D ultrasound. *Physics in Medicine & Biology*, *67*(7), 074002.

Pakeloğlu, A. C., Koç, M., Yılmaz, A. S., Bayar, B., & Bayar, K. (2023). Comparing the reliability of the Goniometer Pro application and flexicurve for measuring thoracic kyphosis: a cross-sectional study. *International Journal of Therapy And Rehabilitation*, *30*(11), 1–9.

Panjabi, M. M. (1992). The stabilizing system of the spine. Part II. Neutral zone and instability hypothesis. *Clinical Spine Surgery*, *5*(4), 390–397.

Panjabi, M. M., Oxland, T., Yamamoto, I., & Crisco, J. J. (1994). Mechanical behavior of the human lumbar and lumbosacral spine as shown by three-dimensional load-displacement curves. *JBJS*, *76*(3), 413–424.

Panjabi, M. M., & White III, A. A. (1980). Basic biomechanics of the spine. *Neurosurgery*, *7*(1), 76–93.

Papi, E., Koh, W. S., & McGregor, A. H. (2017). Wearable technology for spine movement assessment: A systematic review. *Journal of biomechanics*, *64*, 186–197.

Pearcy, M., Portek, I., & Shepherd, J. (1984). Three-dimensional x-ray analysis of normal movement in the lumbar spine. *Spine*, *9*(3), 294–297.

Pearson, A. M., Spratt, K. F., Genuario, J., McGough, W., Kosman, K., Lurie, J., & Sengupta, D. K. (2011). Precision of lumbar intervertebral measurements: does a computer-assisted technique improve reliability? *Spine*, *36*(7), 572–580.

Pope, M. H. (1989). Biomechanics of the lumbar spine. *Annals of medicine*, *21*(5), 347–351.

Pourahmadi, M. R., Takamjani, I. E., Jaberzadeh, S., Sarrafzadeh, J., Sanjari, M. A., Bagheri, R., & Jannati, E. (2018). Test-retest reliability of sit-to-stand and stand-

to-sit analysis in people with and without chronic non-specific low back pain. *Musculoskeletal Science and Practice*, *35*, 95–104.
Raastad, J., Reiman, M., Coeytaux, R., Ledbetter, L., & Goode, A. P. (2015). The association between lumbar spine radiographic features and low back pain: a systematic review and meta-analysis. Seminars in Arthritis and Rheumatism,
Renard, F., Guedria, S., Palma, N. D., & Vuillerme, N. (2020). Variability and reproducibility in deep learning for medical image segmentation. *Scientific Reports*, *10*(1), 13724.
Roach, S., San Juan, J. G., Suprak, D. N., & Lyda, M. (2013). Concurrent validity of digital inclinometer and universal goniometer in assessing passive hip mobility in healthy subjects. *International journal of sports physical therapy*, *8*(5), 680.
Robertson, D. G. E., Caldwell, G. E., Hamill, J., Kamen, G., & Whittlesey, S. (2013). *Research methods in biomechanics*. Human kinetics.
Ronneberger, O., Fischer, P., & Brox, T. (2015). U-net: Convolutional networks for biomedical image segmentation. International Conference on Medical image computing and computer-assisted intervention,
Rousseau, M.-A., Laporte, S., Dufour, T., Steib, J.-P., Lazennec, J.-Y., & Skalli, W. (2011). Three-dimensional assessment of the intervertebral kinematics after Mobi-C total disc replacement at the cervical spine in vivo using the EOS stereoradiography system. *SAS journal*, *5*(3), 63–68.
Rozumalski, A., Schwartz, M. H., Wervey, R., Swanson, A., Dykes, D. C., & Novacheck, T. (2008). The in vivo three-dimensional motion of the human lumbar spine during gait. *Gait & posture*, *28*(3), 378–384.
Rubin, D. I. (2007). Epidemiology and risk factors for spine pain. *Neurologic clinics*, *25*(2), 353–371.
Sassack, B., & Carrier, J. D. (2023). Anatomy, back, lumbar spine. In *StatPearls [Internet]*. StatPearls Publishing.
Schultz, B., Fogel, N., Finlay, A., Collinge, C., Githens, M. F., Higgins, T., Mehta, S., O'Toole, R. V., Summers, H., & Bishop, J. A. (2019). Orthopedic surgeons have inadequate knowledge of the cost of trauma-related imaging studies. *Orthopedics*, *42*(5), e454–e459.
Sedrez, J. A., de Mesquita, P. V., Gelain, G. M., & Candotti, C. T. (2019). Kinematic characteristics of sit-to-stand movements in patients with low back pain: A systematic review. *Journal of Manipulative and Physiological Therapeutics*, *42*(7), 532–540.
Seghier, M. L. (2024). Image Segmentation Evaluation With the Dice Index: Methodological Issues. In (Vol. 34, pp. e23203): Wiley Online Library.
Severijns, P., Overbergh, T., Schmid, S., Moke, L., & Scheys, L. (2021). Spinal palpation error and its impact on skin marker-based spinal alignment measurement in adult spinal deformity. *Frontiers in Bioengineering and Biotechnology*, *9*, 687323.
Shapiro, J. (2020). Surgical Biomechanics: Principles of Procedure Choice. *Clinics in Podiatric Medicine and Surgery*, *37*(1), 101–116.
Siciliano, B., Sciavicco, L., Villani, L., & Oriolo, G. (2009). Kinematics. *Robotics: Modelling, Planning and Control*, 39–103.
Slabaugh, G. G. (1999). Computing Euler angles from a rotation matrix. *Retrieved on August*, *6*(2000), 39–63.

Song, Y., Wen, W. q., Xu, J., Zhang, Z. p., Han, Y., Li, K. p., Wang, X. d., Xu, H. x., Liu, J., & Miao, J. (2021). Kinematic characteristics and biomechanical changes of lower lumbar facet joints under different loads. *Orthopaedic Surgery*, *13*(3), 1047–1054.

Stahl, C. M., Meisinger, Q. C., Andre, M. P., Kinney, T. B., & Newton, I. G. (2016). Radiation risk to the fluoroscopy operator and staff. *American Journal of Roentgenology*, *207*(4), 737–744.

Steffensen, E. A., Magalhães, F., Knarr, B. A., & Kingston, D. C. (2023). Comparison of markerless and marker-based motion capture of gait kinematics in individuals with cerebral palsy and chronic stroke: A case study series. *Research Square*, rs. 3. rs–2557403.

Tavana, S., Davis, B., Canali, I., Scott, K., Leong, J., Freedman, B., & Newell, N. (2023). A novel tool to quantify in vivo lumbar spine kinematics and 3D intervertebral disc strains using clinical MRI. *Journal of the Mechanical Behavior of Biomedical Materials*, *140*, 105730.

Teu, K. K., Kim, W., Tan, J., & Fuss, F. K. (2005). Using dual Euler angles for the analysis of arm movement during the badminton smash. *Sports Engineering*, *8*, 171–178.

Tojima, M., Ogata, N., Yozu, A., Sumitani, M., & Haga, N. (2013). Novel 3-dimensional motion analysis method for measuring the lumbar spine range of motion: repeatability and reliability compared with an electrogoniometer. *Spine*, *38*(21), E1327–E1333.

Tousignant, M., Poulin, L., Marchand, S., Viau, A., & Place, C. (2005). The Modified–Modified Schober Test for range of motion assessment of lumbar flexion in patients with low back pain: A study of criterion validity, intra-and inter-rater reliability and minimum metrically detectable change. *Disability and rehabilitation*, *27*(10), 553–559.

Tozawa, R., Katoh, M., Kawasaki, T., Aramaki, H., Kumamoto, T., & Fujinawa, O. (2022). Reliability of ultrasound to measure the distance between lumbar interspinous processes. *Medical Engineering & Physics*, *99*, 103740.

Triantafyllou, A., Papagiannis, G., Stasi, S., Gkrilias, P., Kyriakidou, M., Kampouroglou, E., Skouras, A.-Z., Tsolakis, C., Georgoudis, G., & Savvidou, O. (2023). Lumbar Kinematics Assessment of Patients with Chronic Low Back Pain in Three Bridge Tests Using Miniaturized Sensors. *Bioengineering*, *10*(3), 339.

Valstar, E. R., De Jong, F., Vrooman, H., Rozing, P., & Reiber, J. (2001). Model-based Roentgen stereophotogrammetry of orthopaedic implants. *Journal of biomechanics*, *34*(6), 715–722.

van den Hoorn, W., Coppieters, M. W., van Dieën, J. H., & Hodges, P. W. (2016). Development and validation of a method to measure lumbosacral motion using ultrasound imaging. *Ultrasound in medicine & biology*, *42*(5), 1221–1229.

Van Hooren, B., Teratsias, P., & Hodson-Tole, E. F. (2020). Ultrasound imaging to assess skeletal muscle architecture during movements: a systematic review of methods, reliability, and challenges. *Journal of Applied Physiology*, *128*(4), 978–999.

Van Tulder, M., Becker, A., Bekkering, T., Breen, A., del Real, M. T. G., Hutchinson, A., Koes, B., Laerum, E., Malmivaara, A., & Care, C. B. W. G. o. G. f. t. M. o. A. L. B. P. i. P. (2006). European guidelines for the management of acute nonspecific low back pain in primary care. *European spine journal*, *15*(Suppl 2), s169.

Vania, M., Mureja, D., & Lee, D. (2019). Automatic spine segmentation from CT images using convolutional neural network via redundant generation of class labels. *Journal of Computational Design and Engineering*, *6*(2), 224–232.

Vincent, J., Traywick, L. S., & Washburn, L. (2012). *Low Back Disorders: Injury Prevention and Risk Reduction*. Cooperative Extension Service, University of Arkansas, US Department of ….

Vladimir, M. (1988). Kinematics of human motion. *Int. J. Computer Vision*.

Waldron, K. J., & Schmiedeler, J. (2016). Kinematics. *Springer handbook of robotics*, 11–36.

Weisstein, E. W. (2003). Rotation matrix. *https://mathworld. wolfram. com/*.

Weisstein, E. W. (2009). Euler angles. *https://mathworld. wolfram. com/*.

West, J. B., Khadem, R., & Maurer Jr, C. R. (2003). Overcoming the distortion problem in image-enhanced fluoroscopy. Medical Imaging 2003: Image Processing,

Widmer, J., Fornaciari, P., Senteler, M., Roth, T., Snedeker, J. G., & Farshad, M. (2019). Kinematics of the spine under healthy and degenerative conditions: a systematic review. *Annals of biomedical engineering*, *47*, 1491–1522.

Will, J. S., Bury, D. C., & Miller, J. A. (2018). Mechanical low back pain. *American family physician*, *98*(7), 421–428.

Wittenburg, J. (2016). Kinematics. *Berlin, Heidelberg: Springer Berlin Heidelberg*, *10*, 978–973.

Wong, K. W., Leong, J. C., Chan, M.-k., Luk, K. D., & Lu, W. W. (2004). The flexion–extension profile of lumbar spine in 100 healthy volunteers. *Spine*, *29*(15), 1636–1641.

Wren, T. A., Isakov, P., & Rethlefsen, S. A. (2023). Comparison of kinematics between Theia markerless and conventional marker-based gait analysis in clinical patients. *Gait & posture*, *104*, 9–14.

Wu, G., & Cavanagh, P. R. (1995). ISB recommendations for standardization in the reporting of kinematic data. *Journal of biomechanics*, *28*(10), 1257–1262.

Wu, G., Siegler, S., Allard, P., Kirtley, C., Leardini, A., Rosenbaum, D., Whittle, M., D D'Lima, D., Cristofolini, L., & Witte, H. (2002). ISB recommendation on definitions of joint coordinate system of various joints for the reporting of human joint motion—part I: ankle, hip, and spine. *Journal of biomechanics*, *35*(4), 543–548.

Wu, Y., Lu, R., Liao, S., Ding, X., Su, W., & Wei, Q. (2021a). Application of ultrasound in the closed reduction and percutaneous pinning in supracondylar humeral fractures. *Journal of Orthopaedic Surgery and Research*, *16*, 1–8.

Wu, Y., Lu, R., Liao, S., Ding, X., Su, W., & Wei, Q. (2021b). Application of ultrasound in the closed reduction and percutaneous pinning in supracondylar humeral fractures. *Journal of Orthopaedic Surgery and Research*, *16*(1), 588.

Xi, X., Ling, Z., Wang, C., Gu, C., Zhan, X., Yu, H., Lu, S., Tsai, T.-Y., Yu, Y., & Cheng, L. (2022). Lumbar segment-dependent soft tissue artifacts of skin markers during in vivo weight-bearing forward–Backward bending. *Frontiers in Bioengineering and Biotechnology*, *10*, 960063.

Xu, F., Lin, J., Jiang, S., Sun, Z., Zhou, S., Li, Z., Wang, S., & Li, W. (2024). In vivo segmental vertebral kinematics in patients with degenerative lumbar scoliosis. *European spine journal*, *33*(2), 571–581.

Yamamoto, I., Panjabi, M. M., Crisco, T., & Oxland, T. (1989). Three-dimensional movements of the whole lumbar spine and lumbosacral joint. *Spine*, *14*(11), 1256–1260.

Zagrevskiy, V., & Zagrevskiy, O. (2016). Spatial model of biomechanical system: Geometric transformations. *Theory and Practice of Physical Culture*(8), 27–27.

Zatsiorsky, V. (2002). Kinetics of Human Motion. *Human Kinetics*.

Zemp, R., List, R., Gülay, T., Elsig, J. P., Naxera, J., Taylor, W. R., & Lorenzetti, S. (2014). Soft tissue artefacts of the human back: comparison of the sagittal curvature of the spine measured using skin markers and an open upright MRI. *PloS one*, *9*(4), e95426.

Zheng, M., Mohamodi, A., Szabo, T., & Snyder, B. (2016). In-vivo cervical spine FSU dynamic motion measured by dual ultrasound: The effect of muscle activation. 2016 IEEE international ultrasonics symposium (IUS),

Zheng, M., Shiuan, K., Masoudi, A., Buckland, D., Szabo, T., & Snyder, B. (2013). Dynamic ultrasound imaging of cervical spine intervertebral discs. 2013 IEEE International Ultrasonics Symposium (IUS),